Synthesis, Properties, and Reactivity of Pentafluorophenyl Substituted Cyclopentadienes and Their Transition Metal Complexes

Matthew P. Thornberry

Dissertation Submitted to the Faculty of the

Virginia Polytechnic Institute and State University

in partial fulfillment of the requirements for the degree of

Doctor of Philosophy

in

Chemistry

Paul Deck, Chairman

Mark Anderson

John Dillard

Brian Hanson

Richard Gandour

August 3, 2001

Blacksburg, Virginia

Keywords: pentafluorophenyl, cyclopentadienyl, substituent effects, polymerization

Synthesis, Properties, and Reactivity of Pentafluorophenyl Substituted Cyclopentadienes and Their Transition Metal Complexes

Matthew P. Thornberry

(ABSTRACT)

Substituent effects in η^5-cyclopentadienyl (Cp) transition metal complexes have been intensely studied since the discovery of the first such complex, ferrocene. Modifications of the Cp ligand framework effect changes in the physical properties and chemical reactivity of the coordinated transition metal. This concept is useful when applied to catalysis mediated by Cp complexes, because the performance of the catalyst can be markedly improved using well-chosen ligand substituents.

Studies of electronic substituent effects ideally employ a wide range of electron-donating and electron-withdrawing groups. Unfortunately, most of the available electron-withdrawing groups suffer from problems with Cp ligand synthesis, Cp anion stability, and electron-withdrawing group stability under catalytic conditions. This dissertation shows that the pentafluorophenyl (C_6F_5) substituent is highly electron-withdrawing but avoids all of these problems.

Several new C_6F_5-substituted cyclopentadienes are prepared by the reaction of sodium cyclopentadienide and hexafluorobenzene (C_6F_6) under varying conditions. Corresponding C_6F_5-substituted cyclopentadienyl ligands (sodium salts) are obtained upon deprotonating the dienes with NaH. Complexes of Mn(I), Re(I), Fe(II), Co(II), Zr(IV) are synthesized by reacting these ligands with transition metal halides.

The acidities of several C_6F_5- and C_5F_4N-substituted cyclopentadienes and indenes are measured using ^{19}F NMR spectroscopy. The electron-withdrawing fluorinated aryl groups have a substantial acidifying effect. The identity and number of substituents (C_6F_5, C_5F_4N, CH_3, and *t*-Bu), the position of the substituents on the cyclopentadiene, and the intramolecular (vicinal) steric effects also influence acidity. The electron-withdrawing ability of the C_6F_5 group is also characterized by infrared spectroscopic analysis of substituted $CpM(CO)_3$ (M = Mn(I) and Re(I)) and electrochemical analysis of substituted ferrocenes.

X-ray crystal structures of several C_6F_5-substituted Cp complexes reveal interesting structural motifs, including pi-stacking of the C_6F_5 substituents, Cp-M bond elongation, and CO-C_6F_5 interactions. In addition, dynamic Cp-C_6F_5 and Cp-M rotational barriers are measured by variable temperature NMR spectroscopy.

Finally, ethylene polymerizations and ethylene/1-hexene copolymerizations are conducted using C_6F_5- and C_6H_5-substituted zirconocene dichlorides as catalysts. Contrary to findings published elsewhere, this study shows that substituent electronic effects induce substantial changes in comonomer incorporation.

Acknowledgements

I would like to thank the following coworkers for synthesizing and supplying several of the unpublished compounds appearing in this dissertation: Nathan Reynolds (**27**, **30**), Caleb Kroll (**9**, **14a/b**), Andrea Warren (**11a/b**, **12a/b**, **13a/b**), Mason Haneline (**8**, **7a/b**). Tom Glass provided assistance with variable temperature NMR experiments and ^{13}C NMR analysis of polymer samples. Helpful discussions with Richard Gandour, Eric Hawrelak, Xu Cheng, and Owen Lofthus are also gratefully acknowledged.

Table of Contents

List of Figures

List of Tables

Chapter 1: Overview of Cp Substituent Effects

Introduction

The cyclopentadienyl ligand (Cp) is one of the most versatile, robust, and tunable ligands available to organometallic chemists. Since the discovery of ferrocene (Cp_2Fe), Cp complexes of most of the transition metals, main group metals and metalloids, lanthanides, and several of the actinides have been prepared.[1-3] Figure 1.1 illustrates some of the common transition metal Cp structures, which are the focus of the following chapters. Complexes having two Cp ligands are classified as metallocenes, and those bearing one, two, or three additional ligands are termed bent metallocenes. Compounds having one Cp ligand but two, three, or four additional ligands are called half-sandwich or piano stool complexes.

Ferrocene and cymantrene, $CpMn(CO)_3$, are two exceptional examples of Cp-M bond stability. In these complexes it is possible to functionalize the Cp ligand without cleaving the Cp-M bond. In many other Cp complexes, various reactions at other ligand sites (nucleophilic and electrophilic attack, insertion, and substitution) can take place without disrupting the Cp-M bond. Some Cp-M bonds are also fairly labile, and substitutions of Cp ligands (in addition to

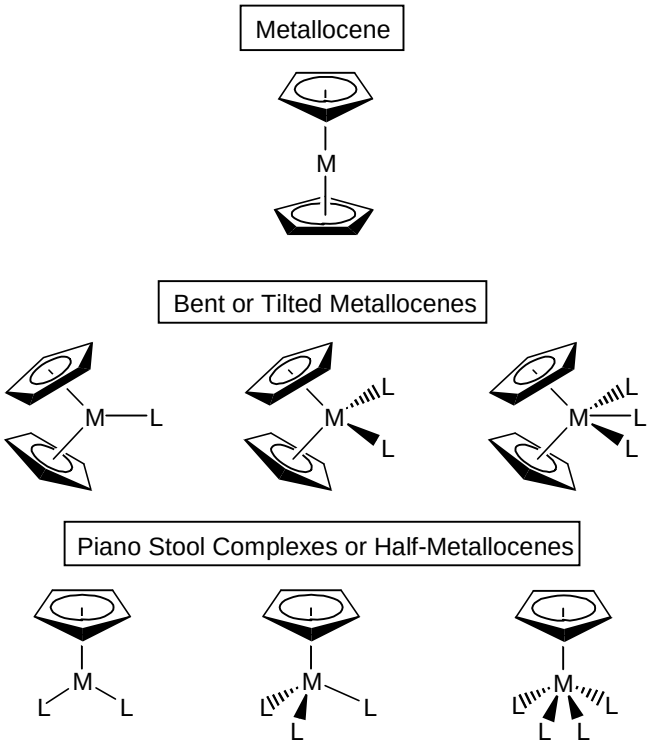

Figure 1.1. Examples of Cp complexes.

electrophilic and nucleophilic attack at Cp) are well documented. However, the strong sigma- and pi-donating character of the Cp anion is particularly well suited for bonding with vacant transition metal orbitals, which explains why Cp is so often used as an "ancillary" ligand in transition metal organometallic chemistry.

A variety of functional groups can also be attached to the Cp ligand before it is even bonded to the transition metal. The presence of Cp substituents can lead to interesting and important changes in the physical, spectroscopic, and chemical properties of the transition metal complex. The extent of these changes is limited only by the properties of the functional groups attached to the Cp ligand. The physicochemical changes and variations in reactivity that these substituents impart are commonly understood in terms of steric and electronic effects.

Steric and Electronic Effects

The study of steric effects requires substituents whose sizes vary dramatically but whose electron-donating properties remain constant. Electronic effects are measured with substituents of varying electron-donating ability but whose size does not influence the measured variable. It has been generalized that "steric effects increase exponentially while electronic effects are additive."[4]

Steric effects predominate when a bulky substituent crowds the metal coordination sphere. This often leads to altered reactivity when compared to unsubstituted Cp complexes. For example, the reaction of 2 equiv of TlCp with one equivalent of UCl_4 in DME does not give the expected Cp_2UCl_2 product. Instead a mixture of ligand redistrubution products ($CpUCl_3$(DME) and Cp_3UCl) is obtained.[5] However, when the much bulkier pentamethylcyclopentadienyl ligand (Cp^*) is used in a similar reaction, $Cp^*_2UCl_2$ is obtained selectively.[6] In this case, ligand redistribution is prevented because the Cp^* ligand sterically saturates the U(IV) coordination sphere preventing coordination of a third ligand. The Cp^* ligand has also prevented aggregation in transition metal complexes. For example, "Cp_2ZrH_2" forms the intractable dimeric complex $[Cp_2Zr(\mu\text{-}H)H]_2$ whereas the Cp^* ligand results in monomeric $Cp^*_2ZrH_2$.[7,8] Steric effects are often exploited in asymmetric synthesis and catalysis, because the sizes and locations of substituents can influence substrate orientation and transition state stability.[7,8] For example, $CpZrCl_3$ catalyzes the ortho-hydroxyalkylation of α-napthol with

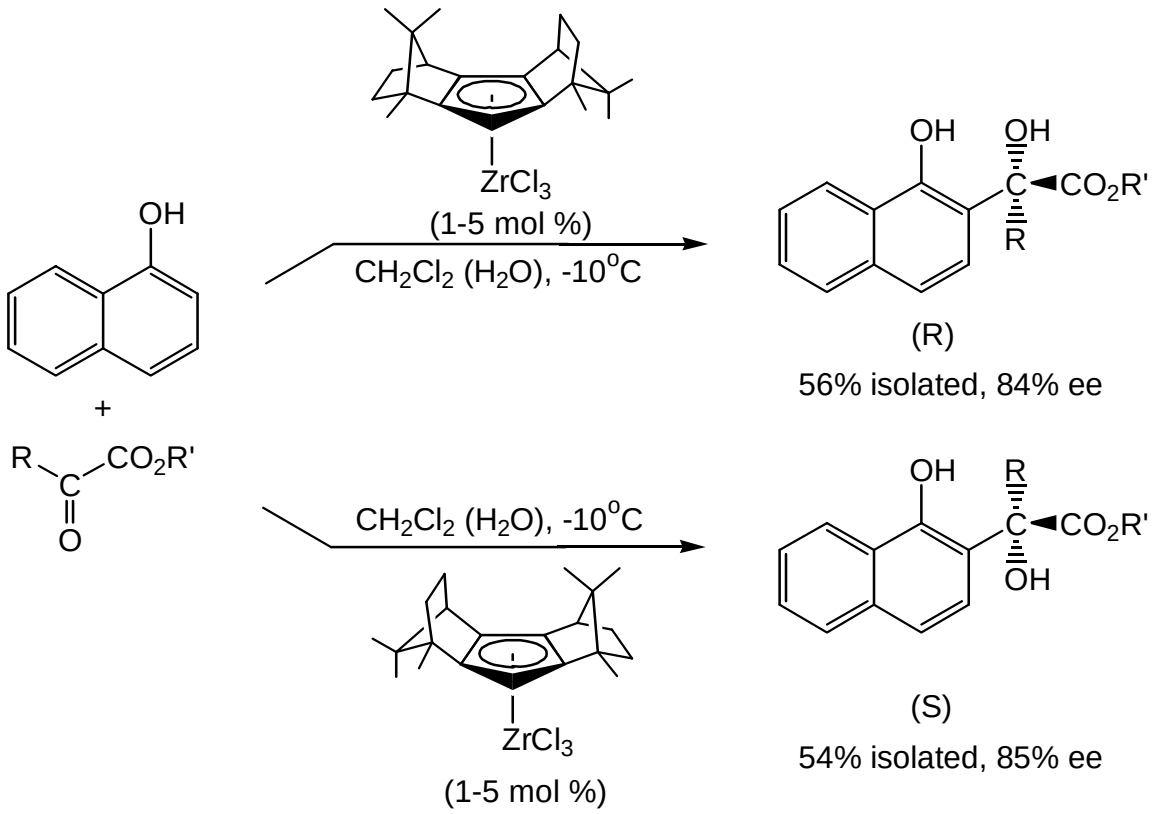

Figure 1.2. Steric effects in $CpZrCl_3$ catalysts.

pyruvate esters ($RCOCO_2R'$). When a chiral derivative of $CpZrCl_3$ is used, the catalysis is enantioselective (Figure 1.2). [9]

Electronic effects refer to the Cp ligand 's electron donating ability as a function of its substituents. Electron-donating substituents decrease the electrophilicity of the metal center by releasing electron density into the coordinated Cp ligand. An electron-withdrawing group decreases electron donation and makes the metal more electrophilic. Electronic effects are easily measured by techniques that probe the metal's local environment. Some of these techniques include XPS,[4,10,11] IR spectroscopy,[11-15] UV-Vis spectroscopy, [16] electrochemistry,[17-20] and gas-phase ionization energies.[15,21,22] ^{1}H NMR spectroscopy and several other NMR active nuclei have appeared in electronic effect studies (^{13}C NMR,[12,23] ^{31}P NMR,[14] ^{51}V NMR,[24] ^{57}Fe NMR,[25] ^{59}Co NMR,[23,26] ^{91}Zr NMR,[27] and ^{103}Rh NMR[13,15,28]). Several of the above techniques are illustrated in the following electronic effect examples and in subsequent chapters of this thesis.

By changing metal electron density, Cp substituents can influence the rates of metal-centered reactions. For example, the functionalization of CpCo(COD) (COD = cyclooctadiene) with electron-withdrawing substituents produces a measurable rate enhancement for COD

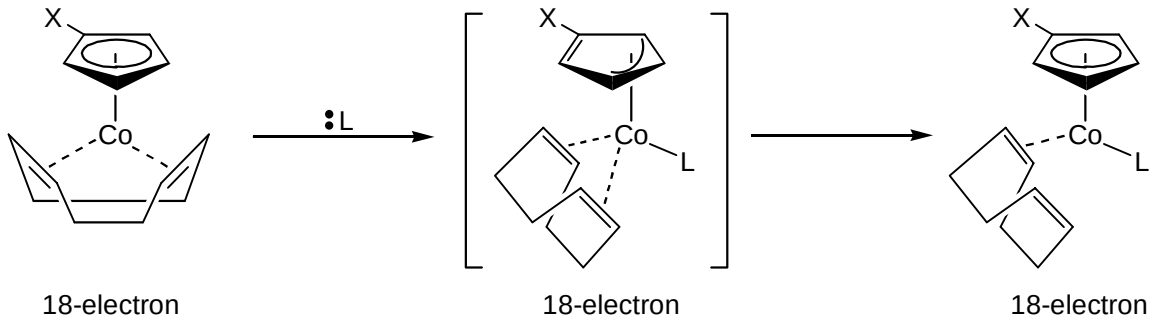

Figure 1.3. Ring slippage in (CpX)Co(COD).

displacement by solvent (acetonitrile or benzene).[12] Rate data from ^{1}H NMR spectra allowed the calculation of the activation enthalpy which was higher for Cp ($\Delta H^{\ddagger}$ = 38 kcal/mol) relative to the formyl-substituted Cp ligand ($\Delta H^{\ddagger}$ = 25 kcal/mol). The associative substitution reaction is facilitated by the Cp ring slippage ($\eta^5 \rightarrow \eta^3 \rightarrow \eta^5$) mechanism first suggested by Basolo (Figure 1.3).[29] Electron-withdrawing groups stabilize the electron-rich allylic intermediate which is necessary to prevent the formation of an unfavorable 20-electron complex. Reactions between $CpRh(CO)_2$ or (η^5-indenyl)$Rh(CO)_2$ and alkylphosphines exhibit a similar rate enhancement when electron-withdrawing substituents are incorporated.[28,30-32]

The endothermic insertion of α-olefins into niobocene hydrides was also found to depend on the Cp substituents. Bercaw showed that the Cp^* ligand lowered insertion rates and increased activation barriers relative to Cp when the olefin was ethylene.[33] This observation was rationalized by considering the insertion a reductive process where the olefin adduct is formally Nb(V) and the insertion product is Nb(III) (Figure 1.4). This assumption was supported by NMR and structural data which suggest a degree of metallacyclopropane character in the olefin adduct. The measured activation barriers showed that the strongly electron-donating Cp^* ligand ($\Delta G^{\ddagger}$ = 18.3 kcal/mol) stabilizes the Nb(V) adduct more effectively than the unsubstituted Cp ligand ($\Delta G^{\ddagger}$ = 17.2 kcal/mol). However, when a bulkier olefin (propylene) is inserted, there is a significant reversal in this trend ($\Delta G^{\ddagger}(Cp^*)$ = 14.1 kcal/mol; $\Delta G^{\ddagger}(Cp)$ = 16.5 kcal/mol) which can be explained by a steric effect. The bulky Cp^* ligand destabilizes the ground state relative to the transition state which resembles the insertion product according to the Hammond postulate.[34] This example effectively illustrates how electronic and steric effects are often simultaneously responsible for the observed reactivity of Cp complexes.

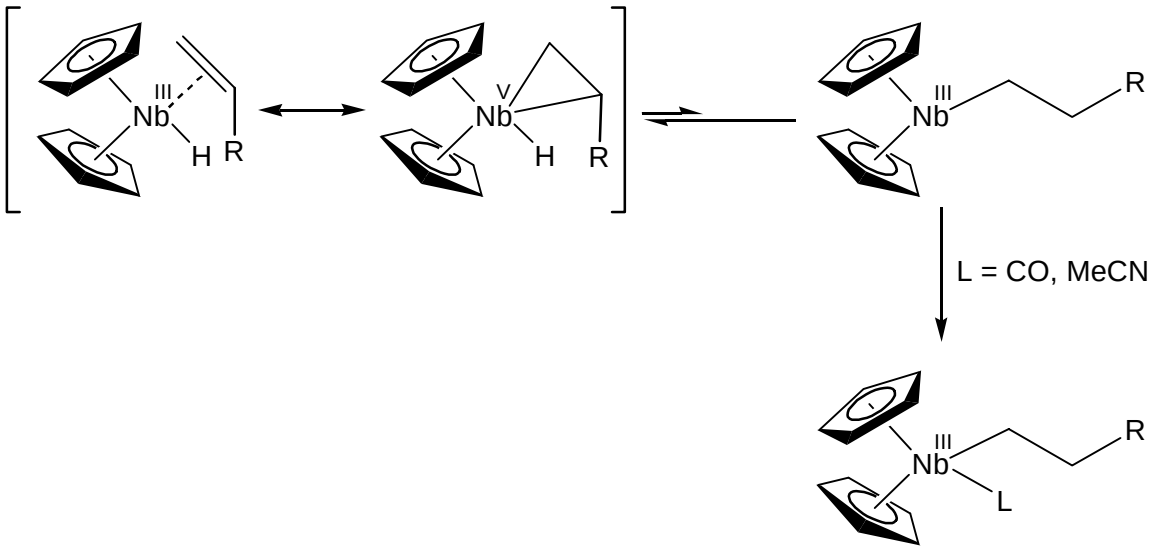

Figure 1.4. Olefin insertion in Cp_2NbH(olefin).

A similar electronic effect was observed in the reactions of titanacyclobutanes with alkynes or ketones.[16] When R = H (see Figure 1.5), reaction rates are 6 to 8 times faster than those obtained when R = CH_3. This decline in rate is attributed to the stabilization of the Ti(IV) starting material relative to the Ti(II) olefin adduct by the electron-donating methyl substituents.

Arthurs and Nelson measured electronic effects on ethylene rotation in substituted

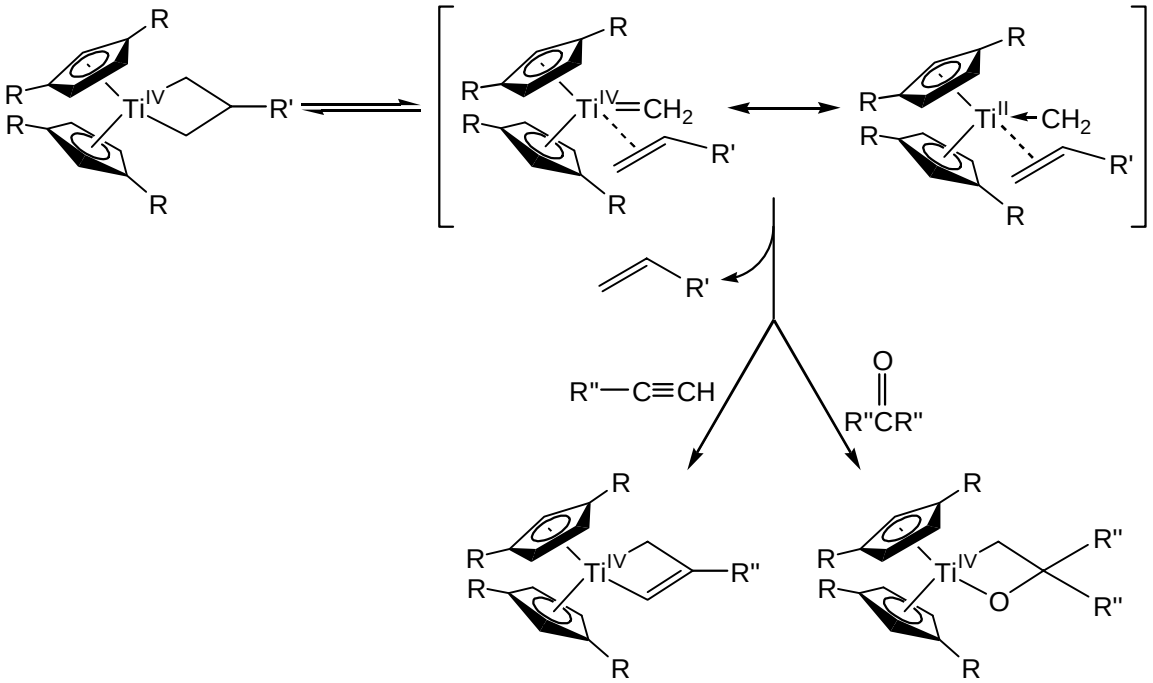

Figure 1.5. Metathesis reactions of titanacyclobutanes.

$CpRh(C_2H_4)_2$ complexes.[35] The rotational barriers were determined using ^1H NMR spectroscopy by measuring the coalesence temperature of the diastereotopic ethylene signals. $CpRh(C_2H_4)_2$ was determined to have a $\Delta G^{\ddagger}$ of 65.7 kJ/mol while the more electron rich Cp^* ligand has a value of 71.5 kJ/mol. Electron-withdrawi ng groups such as cyano ($\Delta G^{\ddagger}$ = 58.9 kJ/mol) and formyl ($\Delta G^{\ddagger}$ = 54.5 kJ/mol) exhibit higher ethylene rotation rates relative to $CpRh(C_2H_4)_2$. Electron-withdrawing groups lower the rotational barrier by diminishing metal electron donation into the C_2H_4 pi antibonding orbital and thus weakening the metal-C_2H_4 pi bond. Conversely, electron-donating substituents strengthen the pi bonding and raise the observed rotational barriers.

The impact of electronic effects on activation energies and reaction rates has sparked similar studies with Cp-based transition metal catalysts. For example, pyridine derivatives are made using CpCo(diene) catalyst precursors, which cyclotrimerize alkynes and nitriles (Figure 1.6).[12,23,26,36,37] It was previously mentioned that electron-withdrawing substituents enhance solvent coordination in CpCo(COD) complexes by facilitating ring slippage. Similarly, electron-withdrawing substituents enhance the rate of alkyne coordination which is assumed to be the rate-determining step in CpCo(COD)-catalyzed cyclotrimerizations.[12] As shown in Table 1.1, the electron-withdrawing acetyl group requires the lowest temperature (125 °C) for 65% propyne conversion but provides little regioselectivity. The electron-donating Cp^* ligand requires the highest temperature (220 °C) but gives the best regioselectivity. Catalyst precursors of the type $CpRh(C_2H_4)_2$ have also been used in pyridine derivative synthesis.[38] However, the trend in catalyst activities obtained between 60 and 100 °C differs greatly from the analogous Co catalysts. In the Rh catalysts, the electron-withdrawing substituents diminish the activity while electron-donating groups increase the activity. This trend suggests that the oxidative coupling of two alkynes to form a metallacyclopentadiene is the rate-determining step. For example, in the cyclotrimerization of 1-hexyne and propionitrile at 80 °C, a methoxycarbonyl substituent only

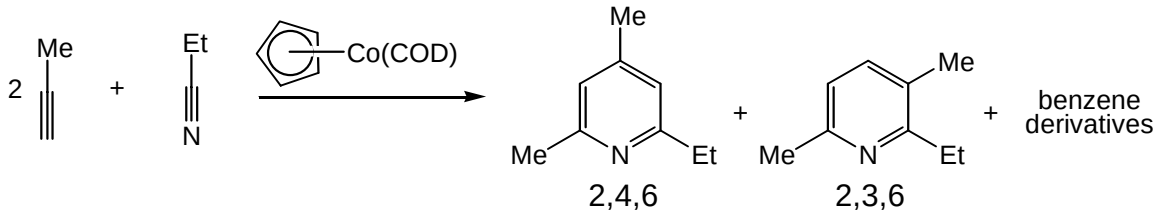

Figure 1.6. CpCo(COD)-catalyzed cyclotrimerization.

Table 1.1. Product yields in Cp'Co(COD)-catalyzed cyclotrimerizations.

Catalyst		Percent Yields[b]	
Cp' Ligand	Temp. (^{o}C)[a]	2,4,6	2,3,6
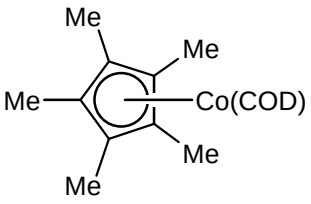	220	77.8	22.2
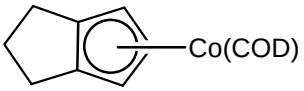	180	71.4	28.6
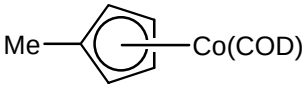	162	66.9	33.1
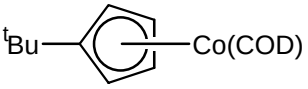	152	63.9	36.1
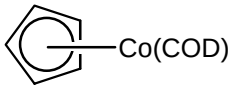	147	63.1	36.9
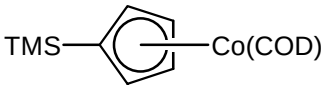	144	62.5	37.5
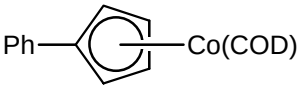	140	63.4	36.6
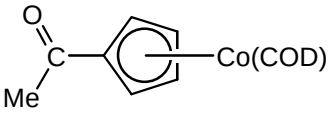	123	59.3	40.7

a. Reaction temperature for 65% alkyne conversion
b. Substrates and products are defined in Fig. 1.6

converts 0.5% of the starting alkyne while the dimethylamino substituent cyclotrimerizes 30.5% of the alkyne. These example show that substituent effects can be useful not only in optimizing catalytic reactions but also in obtaining fundamental mechanistic information.

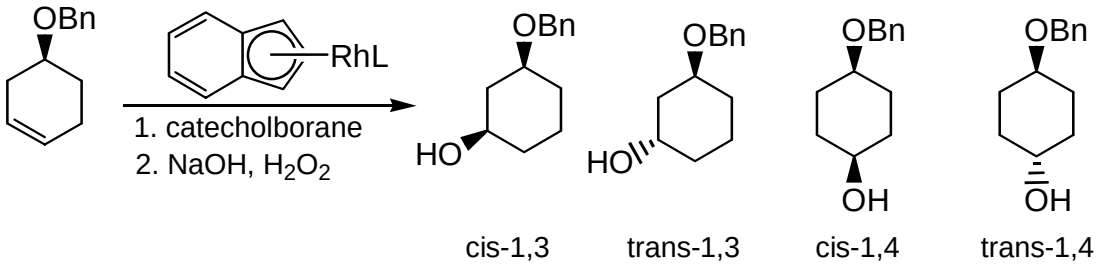

Figure 1.7. [Ind]RhL-catalyzed hydroboration

Compounds of the type (η^5-indenyl)Rh(η^2-alkene)$_2$ (alkene = C_2H_4 or COD) are catalysts for the directed hydroboration of 4-(benzyloxy)cyclohexene (Figure 1.7). The presence

Table 1.2. [Ind]RhL-catalyzed hydroboration product yields and distribution.

Catalyst	Products[c]			
Indenyl Ligand	cis-1,3	trans-1,3	cis-1,4	trans-1,4
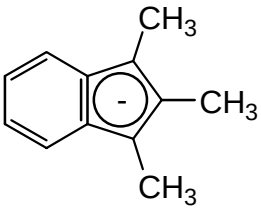	65[a]	12[a]	10[a]	13[a]
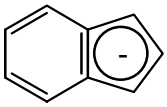	75[a] 74[b]	8[a] 9[b]	7[a] 11[b]	11[a] 6[b]
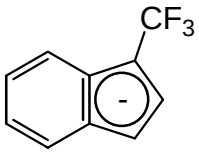	81[b]	10[b]	5[b]	4[b]
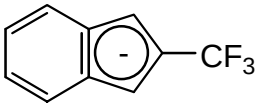	81[b]	9[b]	6[b]	4[b]
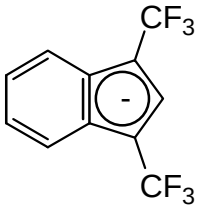	84[b]	8[b]	3[b]	5[b]

a. L = 2 C_2H_4; b. L = COD; c. Substrates and products are defined in Fig. 1.7

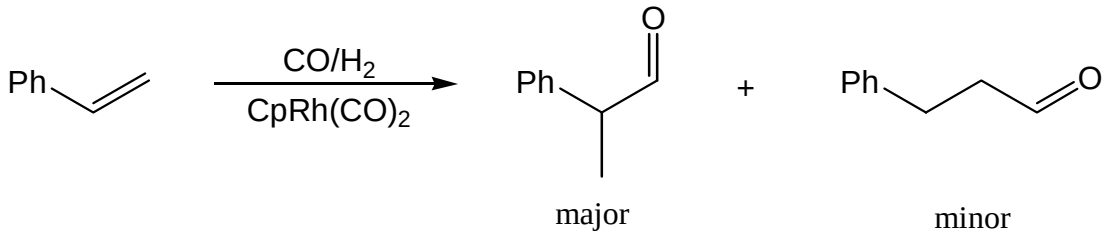

Figure 1.8. $CpRh(CO)_2$-catalyzed hydroformylation.

of electron-donating methyl substituents lowers the stereoselectivity of the reaction while electron-withdrawing trifluoromethyl substituents increase the overall stereoselectivity (Table 1.2).[39,40] The proposed mechanism requires a ring slippage of the indenyl ligand before metal-substrate coordination can occur. Again, electron-withdrawing groups facilitate ring slippage by stabilizing the η^3-allylic intermediate which is necessary for the directed hydroboration reaction.

The hydroformylation of styrene is catalyzed by $CpRh(CO)_2$ complexes in the presence of carbon monoxide and hydrogen (Figure 1.8). Costa and coworkers showed that the activity of the catalyst depends on the Cp substituents.[41] A methoxycarbonyl substituent gives nearly quantitative styrene conversion while the unsubstituted Cp ligand only converts 25% under similar conditions. Again, the electron-withdrawing substituent facilitates a Cp ring slip which is necessary to avoid the formation of a 20-electron complex.

In group 4 metallocene-catalyzed olefin polymerization, propagation involves olefin insertion into a metal-alkyl bond (Figure 1.9). Electron-donating Cp substituents with minimal steric effects are found to increase the propagation rate.[1,42,43] The electron-donating groups facilitate olefin insertion by weakening the M-R bond. Electron-withdrawing substituents lower the metal electron density and strengthen the M-R bond, making insertion more difficult. A more detailed analysis of these electronic effects is presented in Chapter 6.

As described above, substituent effects are defined in terms of electronic effects and

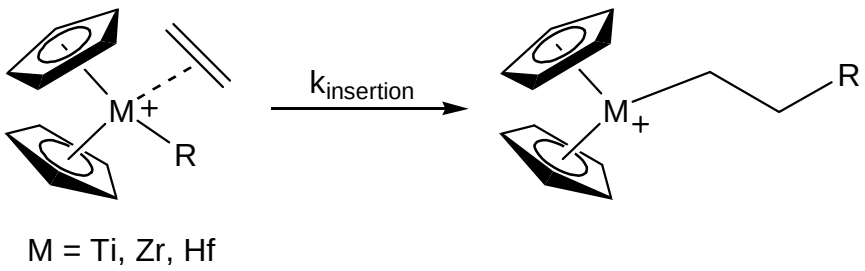

Figure 1.9. Olefin insertion into group 4 metallocenium-alkyl bonds.

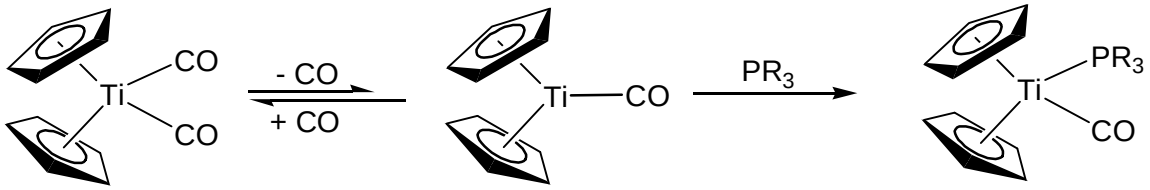

Figure 1.10. CO dissociation in $Cp_2Ti(CO)_2$.

steric effects. However, often both influence the observed reactivity. For example, reactions of $Cp_2Ti(CO)_2$ with PR_3 were found to depend on both steric and electronic factors (Figure 1.10).[11,44] Rate data obtained from UV and ^1H NMR spectra show that the initial CO dissociation is rate-limiting. The Cp^* ligand was expected to exhibit the slowest rates. The electron-donating methyl groups should slow CO dissociation by increasing Ti-CO bond strength through increased dπ-pπ back-bonding. However, the observed reaction rates contradict the above rationale presumably because the steric bulk of the Cp^* ligand also favors CO dissociation while also discouraging reassociation. This competition between steric and electronic effects must be accounted for in any study which attempts to probe the nature of substituent effects.

Electron-Withdrawing Group Complications

In general, the study of electronic effects is underdeveloped compared to the study of steric effects. This trend reflects the large number of known Cp ligands that are ideal for the study of steric effects. Many alkyl-substituted (Me, Et, ^{i}Pr, ^{t}Bu) Cp ligands have been reported and provide the size and shape variations conducive to the study of steric effects.[3,45,46] While several electron-withdrawing substituents have been reported (nitro,[47] cyano,[48,49] trialkylammonio,[50] trialkylphosphonio,[30] halo,[51,52] perfluoroalkyl,[53-56] acetyl,[57,58] and ester[58-60] functionalities), they are all limited by at least one of the following four problems.

An inefficient, multi-step Cp ligand synthesis is the first and most common problem with the current selection of electron withdrawing substituents. For example, the syntheses for pentasubstituted Cp ligands (CF_3[53] and F[61]) are multistep and require exotic reagents and harsh conditions (Figure 1.11). Other halogenated Cp ligand syntheses require inefficient reactions such as successive metalation/halogenation exchange[62-64] or flash vacuum thermolysis.[65-67] Others have reported using diazotetrahalocyclopentadienes as Cp ligand precursors but these are also difficult to synthesize.[68-70]

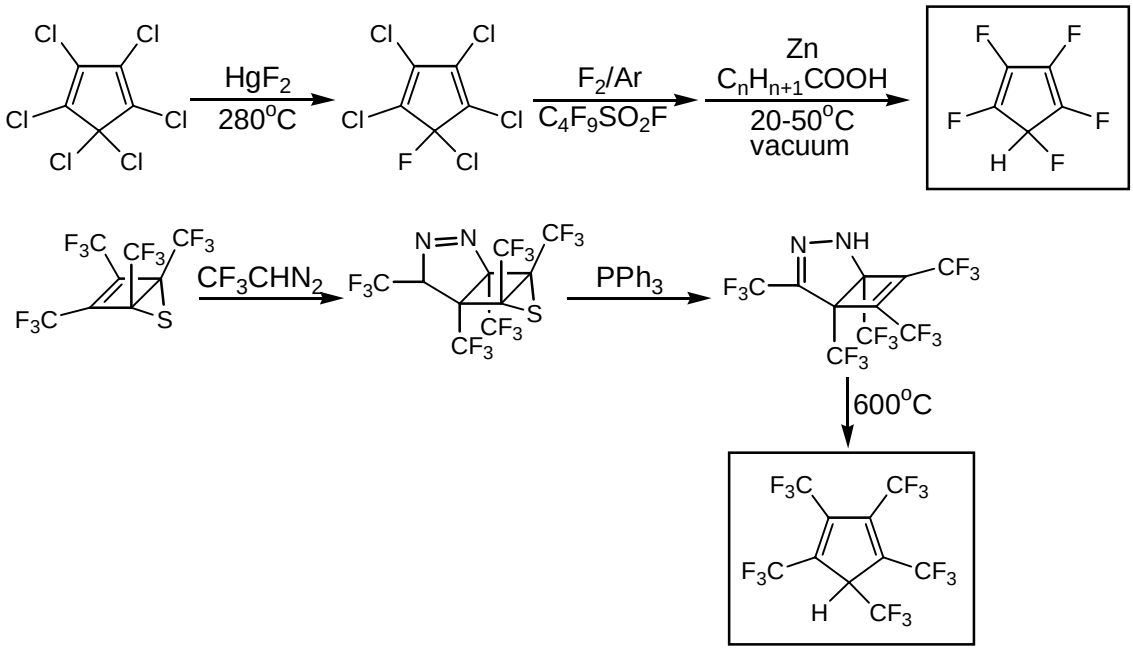

Figure 1.11. Syntheses of pentasubstituted cyclopentadienes containing electron-withdrawing groups.

Poor control over the extent of functionalization is the second limitation of Cp ligands containing electron-withdrawing groups. Typically, different synthetic pathways are necessary to obtain Cp ligands with varying numbers of the same electron-withdrawing substituent. As shown in Figure 1.12, it would be ideal if one reaction pathway produced several degrees of Cp functionalization. Additionally, controlling product distribution with reaction conditions (temperature, time, amount of reagents) is essential to limit separation difficulties and raise individual product yields. For example, several cyano-substituted cyclopentadienes are obtained upon the repetitive reaction of NaH and cyanogen chloride with NaCp.[49] More recently, Rappoport and coworkers obtained tetra-, tri-, and di(methoxycarbonyl)cyclopentadienes from the controlled hydrolysis/decarboxylation of penta(methoxycarbonyl)cyclopentadiene in the presence of KOH.[71] Unfortunately, this type of variation and control is uncommon among for many electron-withdrawing substituted cyclopentadienes. For example, the conditions for the syntheses of pentafluoro- and penta(trifluoromethyl)cyclopentadiene (Figure 1.11) cannot be modified to give mono-, di-, tri-, or tetrasubstituted cyclopentadienes. Instead, the entire synthetic scheme must be reworked from different starting materials.

The instability of electron-withdrawing groups in Cp anions is the third problem. The substitution reaction between a transition metal halide and a Cp anion is the most common and

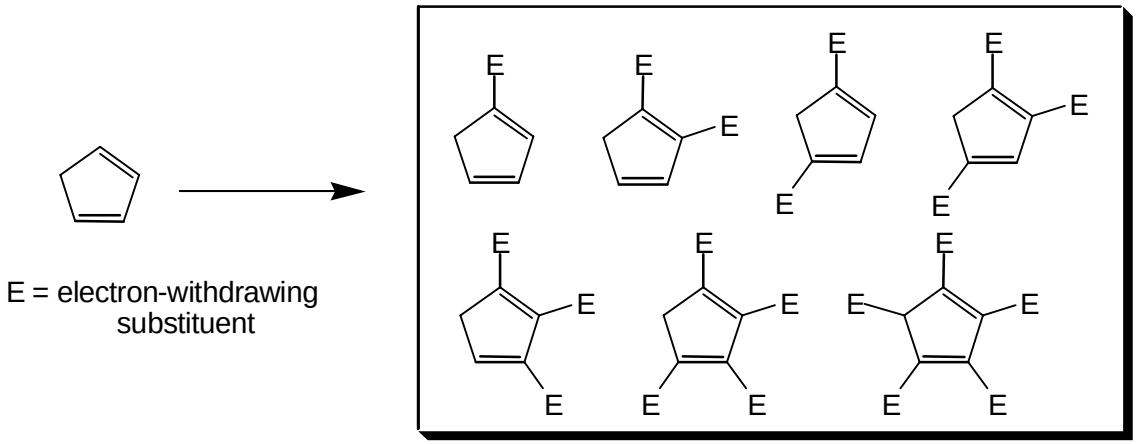

Figure 1.12. Ideal substitution products.

efficient route to a variety of transition metal complexes (Figure 1.13). This synthetic route is eliminated if the anionic Cp ligand cannot be isolated as a stable salt. The trifluoromethyl- and halo-functionalized Cp anions in Figure 1.14 demonstrate this problem. Attempts to synthesize these Cp anions resulted in immediate and irreversible decomposition to halide elimination byproducts. [52,54,55,61,72] Because of this limitation, halide substituents are usually added to the Cp framework after the ligand is covalently bound to the metal. Unfortunately, this synthetic approach is limited to the more robust Cp complexes such as Cp_2Fe and $CpMn(CO)_3$.[73-78]

The Lewis basicity of heteroatom lone pairs is the fourth and final limitation of electron-withdrawing substituents. Most electron-withdrawing groups contain heteroatoms (oxygen, nitrogen, and the halides) whose lone pairs can disrupt Cp complex synthesis. For example, Bruce and coworkers demonstrated that an ester-substituted cyclopentadienyl anion will

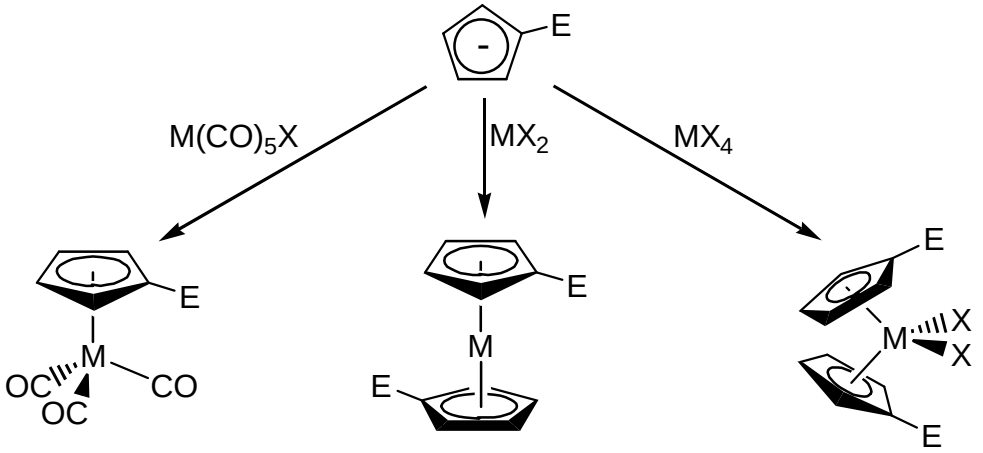

Figure 1.13. Substitution chemistry of Cp anion.

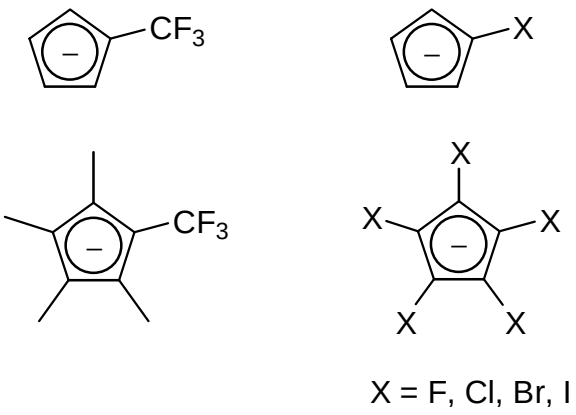

Figure 1.14. Unstable Cp anions.

coordinate to Cr(III) through the oxygen lone pairs rather than the Cp pi electrons (Figure 1.15).[79] The same ligand exhibits similar coordination in Fe(II),[80] Co(II),[80] Ru(II),[81] Rh(III),[82] and Cu(II)[80] complexes. Heteroatom lone pairs in the Cp ligand $[C_5(CN)_5]^-$ reportedly disrupt Cp coordination in Mn(I) and Re(I) complexes through multiple nitrogen lone pair coordination.[83] The disruption of Cp coordination is most common among the electrophilic early transition metals. As a result, there have been few reports of early transition metals containing electron-withdrawing functionalized Cp ligands.[52,54,84]

History of the Pentafluorophenyl Substituent

The pentafluorophenyl (C_6F_5) substituent is an electron-withdrawing group that is not limited by the four above problems. However, this was not obvious from early, scattered reports of C_6F_5-substituted Cp ligands. In 1973, (pentafluorophenyl)cyclopentadiene was obtained in a 4% yield from the reaction of $CpCu(PBu_3)$ and pentafluoroiodobenzene.[85] In 1975, Mo(V) and W(V) metallocenes containing the pentafluorophenyl group were briefly mentioned in an EPR study.[86] In 1986, (pentafluorophenyl)cyclopentadiene was identified as a byproduct from the photo-induced decomposition of bis(pentafluorophenyl)titanocene.[87,88] In 1991, the photolysis

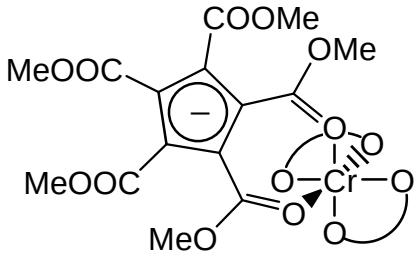

Figure 1.15. Oxygen chelation in $[C_5(CO_2Me)_5]_3Cr(III)$.

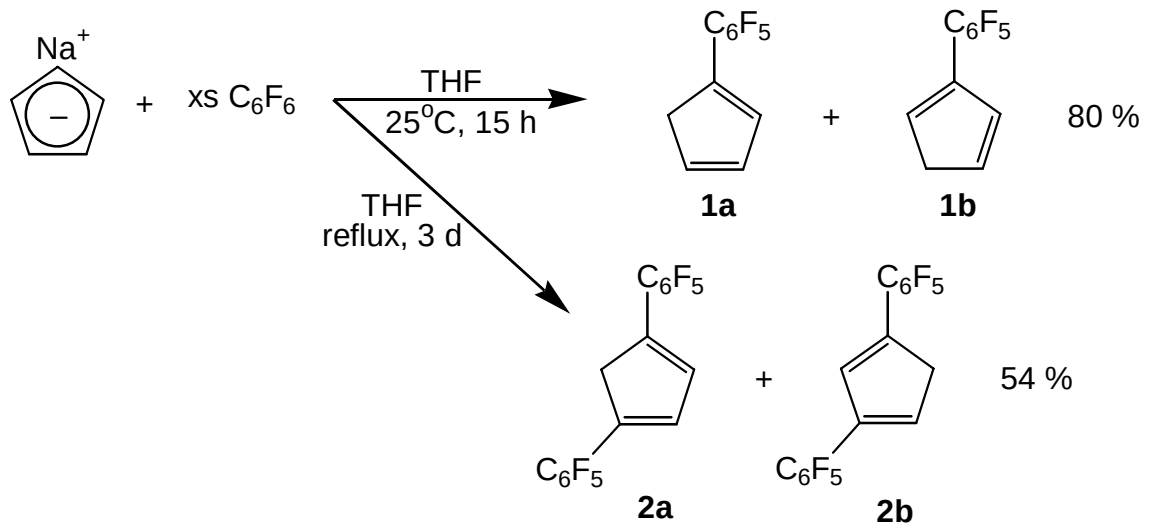

Figure 1.16. Synthesis of C_6F_5-substituted cyclopentadienes.

of iodoferrocene in the presence of hexafluorobenzene was reported to give a 32% yield of (pentafluorophenyl)ferrocene.[89] This compound was also reported in 1999 as a byproduct from the reaction of $CpFe(CO)_2^-$ with bromopentafluorobenzene.[90] It was not until 1996 that an efficient ligand synthesis for (pentafluorophenyl)cyclopentadiene (**1a/b**) and bis(pentafluorophenyl)cyclopentadiene (**2a/b**) was reported by Deck and coworkers (Figure 1.16).[91] They also showed that the corresponding Cp anions were isolable as sodium salts and could be used to make early and late transition metal complexes by simple substitution chemistry. Since this discovery, Rausch and coworkers have also demonstrated that the C_6F_5 group can be used in Cp complexes of Ti(IV).[92]

Scope of Dissertation

As outlined in Figure 1.17, the exploration of new C_6F_5-substituted Cp ligands and their transition metal complexes is investigated in the following chapters. First, the synthesis described in Figure 1.16 is extended to an entire family of homologous C_6F_5-substituted cyclopentadienes. The electronic effect of the C_6F_5 group is quantified in acidity studies of C_6F_5-containing cyclopentadienes and indenes. The anionic salts of these cyclopentadienes are then used in the efficient syntheses of transition metal complexes. The IR spectra of C_6F_5-substituted piano stool complexes and the electrochemistry of C_6F_5-substituted metallocenes is also be used to quantify the electronic effect of the C_6F_5 substituent. The influence of C_6F_5 substituents on group 4 metallocene-catalyzed olefin polymerization is also analyzed. The structural

implications of the C_6F_5 group is assessed in a series of variable temperature NMR studies which estimate rotational barriers for aryl and Cp ring rotation. Finally, molecular structures determined by X-ray crystallography illustrate several solid state motifs in C_6F_5-substituted Cp transition metal complexes.

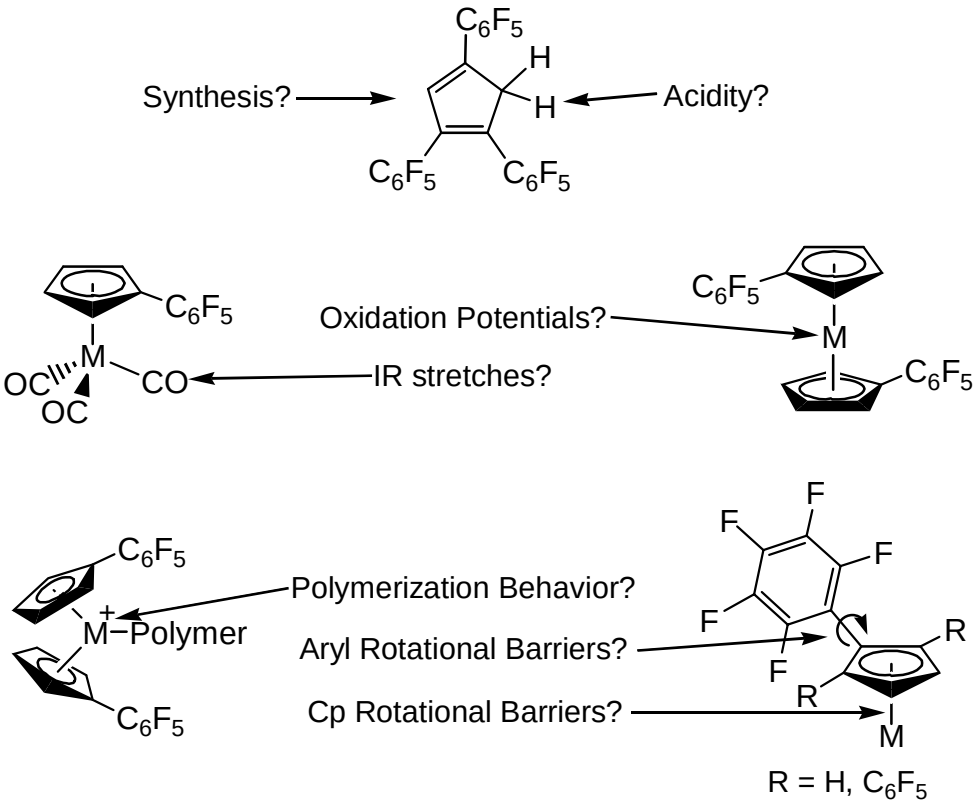

Figure 1.17. Scope of dissertation.

Chapter 2: Ligand Synthesis

Introduction

The C_6F_5 group is an ideal electron-withdrawing substituent for metallocenes because of its simple Cp ligand synthesis, tunable degree of functionalization, stable Cp anion, and unreactive lone pairs. All other known electron-withdrawing substituents lack at least one of these attributes.

It was previously shown that the reaction of C_6F_6 with NaCp yields the C_6F_5-substituted cyclopentadienes **1a**/**b** and **2a**/**b** (Figure 1.16).[91] The 1,2 and 2,3-diarylated cyclopentadienes in Figure 2.1 were isolated together as minor byproducts (approx. 1%) from the synthesis of **2a**/**b**.[93] Unpublished work involving the reaction of alkyl-substituted Cp anions with C_6F_6 also produces cyclopentadienes containing vicinal C_6F_5 substituents (Figure 2.2). This chapter describes cyclopentadienes that possess three or more C_6F_5 groups in which the vicinal placement of C_6F_5 groups is unavoidable.

As shown in Figure 2.3, the arylation of cyclopentadiene occurs by a nucleophilic aromatic substitution mechanism. First, the nucleophilic Cp anion adds to a C-F bond and forms the Meisenheimer intermediate represented by three resonance structures. The six electronegative fluorines stabilize the anionic intermediate. Fluoride anion elimination followed

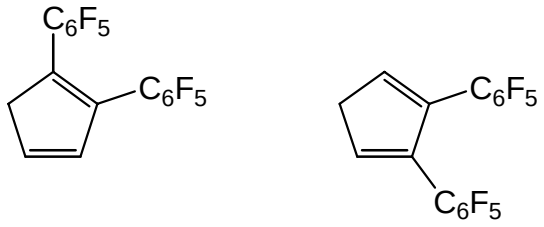

Figure 2.1. Structures of 1,2-$(C_6F_5)_2C_5H_4$ and 2,3-$(C_6F_5)_2C_5H_4$.

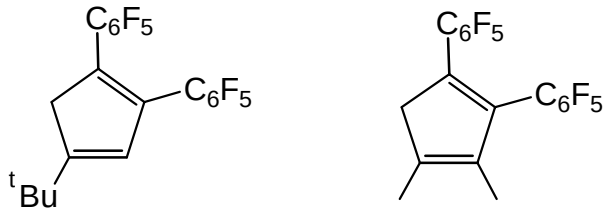

Figure 2.2. Cyclopentadienes containing alkyl and C_6F_5 groups.

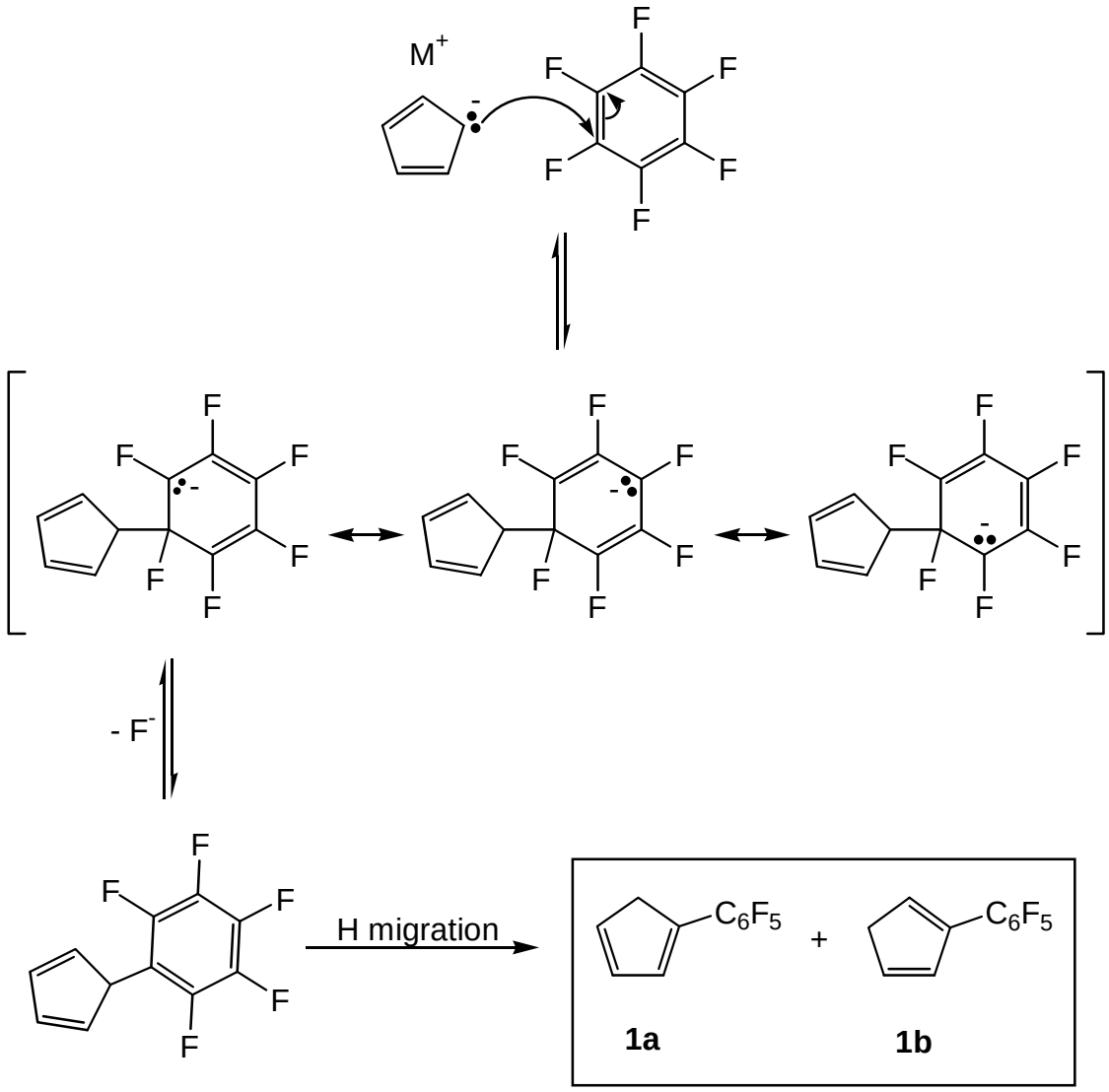

Figure 2.3. Nucleophilic aromatic substitution mechanism.

by hydrogen migration gives the cyclopentadienes **1a**/**b**. However, when excess NaH is present, immediate Cp anion formation by deprotonation probably follows fluoride elimination. Subsequent hydrolysis of the Cp anion then gives the cyclopentadienes **1a/b**.

As shown in Figure 1.16, the synthesis of C_6F_5-substituted cyclopentadienes involves a simple, one-step reaction. The reagents NaCp, C_6F_6, and NaH are cheap and readily available. In addition to the previously mentioned mono- (**1a**/**b**) and disubstituted (**2a**/**b**) cyclopentadienes, this chapter shows that tri- and tetrasubstituted cyclopentadienes can be made using the same reagents but with higher reaction temperatures and longer reaction times. Access to several degrees of substitution is a useful feature of the C_6F_5-substituted cyclopentadiene synthesis.

Cp anion stability is essential if organometallic complexes are to be obtained by well-known substitution reactions involving transition metal halides (Figure 1.13). Unfortunately, electron-withdrawing group functionalization often affords Cp anions that readily decompose. Fortunately, C_6F_5-substituted Cp anions are isolable and indefinitely stable when stored in a glovebox.[91,94] Several known C_6F_5-substituted Cp and indenyl anions are shown in Figure 2.4. These C_6F_5-substituted Cp ligands have been used in transition metal complex synthesis without any notable complications involving lone pair coordination to the metal.[91-96]

Chapter Overview

This chapter describes the synthesis of tris- and tetrakis(pentafluorophenyl)-cyclopentadienes. By varying the reaction conditions of the nucleophilic aromatic substitution reaction, the product distribution can be optimized. The corresponding Cp anions of these C_6F_5-substituted cyclopentadienes were also synthesized. The synthetic conditions and characterization of the C_6F_5-substituted Cp ligands are described below.

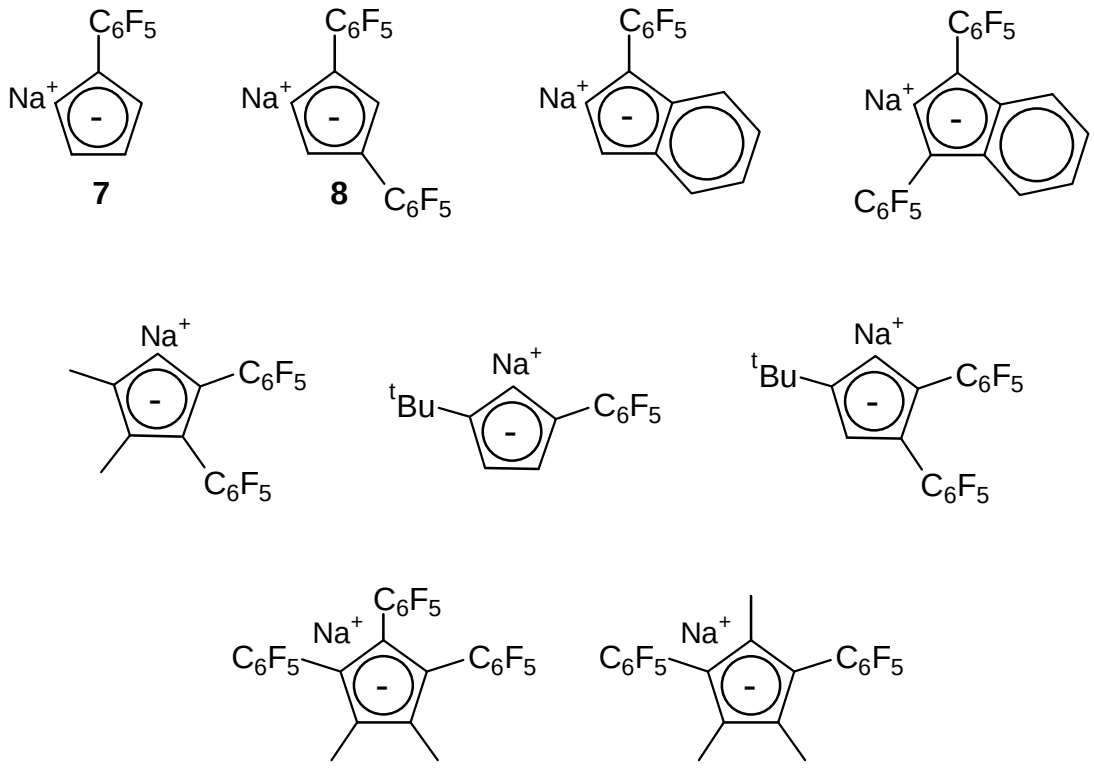

Figure 2.4. Known C_6F_5-substituted Cp and Indene anions.

Results & Discussion

Cyclopentadiene Synthesis and Characterization

As shown in Figure 2.5, MCp (M = Na^+ or Li^+) is reacted with a large excess hexafluorobenzene (C_6F_6) in the presence of NaH to yield a variety of C_6F_5-substituted

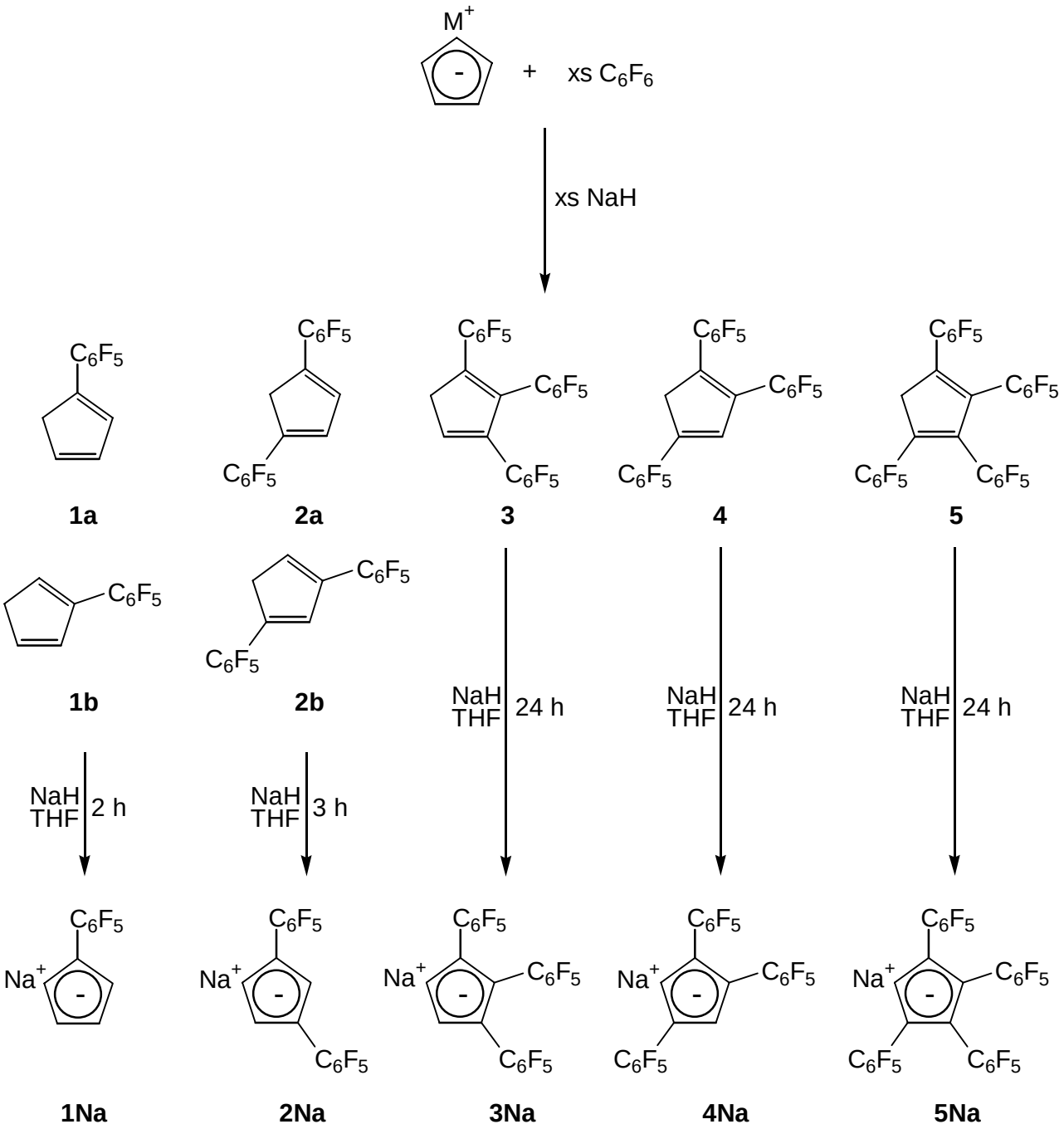

Figure 2.5. Synthesis of C_6F_5-substituted Cp ligands.

cyclopentadienes. The monosubstituted (**1a**/**b**) and disubstituted (**2a**/**b**) double bond isomer pairs were described previously.[91,93] The two trisubstituted regioisomers (**3** and **4**) and the tetrasubstituted cyclopentadiene (**5**) are new compounds. The identity of the initial Cp counterion (Li^+ or Na^+) did not significantly alter the product distributions. The effect of the solvent, temperature, and reaction time on the product yields are presented in Table 2.1. As the temperature and reaction time are increased, the yields of the more arylated products increase while the yields of the lesser arylated products decrease. There is no clear selectivity for the triarylated regioisomers **3** and **4**. The highest isolated yields of **3** and **4** are obtained using high reaction temperatures (110 °C). Yields of **5** are not reported in entries 1-7 because, if any was formed, it was unknowingly removed during the silica gel and alumina chromatography purification stages. However, later analysis of the crude product NMR spectra of entries 6 and 7 reveal that minor amounts (less than 5%) of **5** were formed.

All attempts to synthesize the pentasubstituted cyclopentadiene shown in Figure 2.6 were unsuccessful. Reactions in refluxing tetraglyme gave **5** and decomposition products with broad NMR spectral features suggesting oligomerization. Reactions carried out in a sealed autoclave with temperatures as high as 200 ºC produced similar results. It is possible that the tetrasubstituted cyclopentadiene precursor (**5**) is too crowded to allow the addition of a fifth aryl ring. Furthermore, each additional C_6F_5 group decreases the nucleophilicity of the Cp anion and thereby diminishes the probability of the nucleophilic aromatic substitution mechanism.

Table 2.1. Product distribution and yields.

	conditions			isolated yields (based on % MCp)				
entry	solvent	T (^oC)	Time (h)	**1a/b**	**2a/b**	**3**	**4**	**5**
1	DME	85	12	9	19	10	10	na[b]
2	DME	85	24	2[a]	26[a]	19[a]	22[a]	0[a]
3	DME	85	24	0	17	11	5	na[b]
4	DME	85	96	0[a]	6[a]	20[a]	32[a]	0[a]
5	DME	85	96	0	8	8	18	na[b]
6	diglyme	110	14	0	3	17	23	na[b]
7	diglyme	110	25	0	1	14	22	na[b]
8	diglyme	162	48	0	0	0	0	58

a. Crude product yields determined by NMR prior to seperation; b. If **5** was produced, it was unknowningly removed during chromatography.

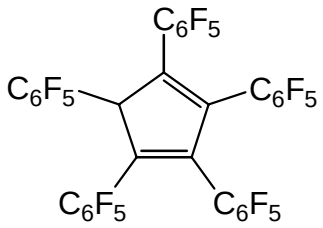

Figure 2.6. Unknown pentakis(pentafluorophenyl)cyclopentadiene.

Mixtures of **1**, **2**, **3**, and **4** are separated by silica gel chromatography using a hexanes eluant. The poor solubility of **3** provides an alternate method for its separation from product mixtures. Compound **3** is successfully separated from **1**, **2**, and **4** by washing the mixture repeatedly with hexanes followed by filtration. The filtrate contains **1**, **2**, **4**, and minor amounts of **3** and is chromatographed to complete the product separation. Compound **5** is also sparingly soluble in hexanes and does not elute appreciably on silica gel or alumina supports. However, selective formation of **5** is possible when long reaction times and high reactions temperatures are used (entry 8 in Table 2.1).

Compounds **3** and **4** are both white solids and exhibit similar NMR spectral features. Both cyclopentadienes possess one CH, one CH_2, and three unique C_6F_5 groups. The regiochemistry could not be determined by ^{19}F NMR but was deduced from their ^{1}H NMR spectra. Compound **4** is expected to have chemical shifts that are further downfield than those in **3** because the CH and CH_2 protons are adjacent to two electron-withdrawing C_6F_5 groups. Additionally, the CH-CH_2 coupling in **3** is expected to be greater than in **4** because the proton environments are separated by three bonds rather than four. As expected, the chemical shifts of **4** (7.32 and 4.14 ppm) are further downfield relative to **3** (6.97 and 3.80 ppm), and compound **4** has no measurable CH-CH_2 coupling while **3** exhibits a coupling constant of ≈1.5 Hz. Compound **5** exhibits time-averaged C_{2v} symmetry in solution. The ^{1}H NMR shows a single CH_2 resonance (4.17 ppm), only slightly downfield from the analogous resonance in **4** (4.14 ppm). The ^{19}F NMR exhibits two unique C_6F_5 rings which also indicates twofold symmetry.

Crystal Structures of Cyclopentadienes

An X-ray crystal structure for **3** was obtained and confirmed the above structural assignment. Crystal data are presented in Table 2.2, selected bond distances and angles in Table 2.3, and the crystal structure in Figure 2.7. The crystal structure shows a random positional disorder where the outer C_6F_5 groups and the CH/CH_2 groups interchange across a

Table 2.2. Crystallographic data for C_6F_5-substituted cyclopentadienes.

compound	**3**	**5**	**5**· **½C_6D_6**
empirical formula	$C_{23}H_3F_{15}$	$C_{29}H_2F_{20}$	2 $C_{29}H_2F_{20}$· C_6D_6
fw	564.26	730.31	1544.72
diffractometer	Enraf-Nonius CAD 4	Nonius Kappa CCD	Nonius Kappa CCD
cryst dimens (mm)	0.30 × 0.30 × 0.10	0.23 × 0.32 × 0.38	0.18 × 0.20 × 0.30
cryst system	tetragonal	triclinic	monoclinic
a (Å)	7.4767(9)	11.1190(2)	10.6760(4)
b (Å)	7.4767(9)	14.7360(3)	10.8820(5)
c (Å)	35.794(2)	15.6200(3)	24.4400(12)
α (deg)	90	82.1670(13)	
β (deg)	90	80.2890(11)	94.266(3)
γ (deg)	90	79.7970(15)	
V (Å)^3	2000.9(6)	2467.78(8)	2831.5(2)
space group	$P4_12_12$ (No. 92)	P-1 (No. 2)	$P2_1/n$ (No. 14)
Z	4	4	2
D_{calc} (Mg m^{-3})	1.869	1.966	1.812
abs coeff (mm^{-1})	0.199	0.221	0.199
F_{000}	1104	1424	1508
λ (Mo K_α) (Å)	0.71073	0.71073	0.71073
temp (K)	103	100	150
range for collection	0.0-31.0	1.4-27.9	2.7-27.5
no. of reflns colld	7175	18771	10584
no. of indep reflns	2070	11729	6259
abs corr method	none	none	none
data / restrs / params	1820/0/187	11729/0/884	6259/0/470
R [$I > 2\sigma(I)$]	0.047	0.068	0.036
R_w [$I > 2\sigma(I)$]	0.060	0.184	0.082
GoF on F^2	0.949	1.56	0.84
peak, hole (e Å^{-3})	0.25, -0.20	0.61, -0.44	0.21, -0.21

Table 2.3. Selected metric data for **3**.

distances (Å)		bond angles (deg)		Cp-C_6F_5 (deg)	
C1-C2	1.4113(17)	C1-C2-C3	108.94(14)	C4-C7	57.0
C2-C3	1.420(3)	C2-C3-C3a	106.58(17)	C8-C13	54.8
C3-C3a	1.486(3)	C2a-C1-C2	108.95(11)		
C1-C4	1.4761(15)	C2-C1-C4	125.52(8)		
C2-C8	1.477(2)	C1-C2-C8	124.01(13)		
		C3-C2-C8	127.05(15)		

crystallographic C_2 axis. The cyclopentadiene-C_6F_5 dihedral angles for the two crystallographically unique rings (57.0º, 54.8º) are large relative to the reported angles for the two distinct polymorphs of **2a** (13.0º, 15.4º, 10.4º, 4.5º)[93] but similar to the range of angles (40.3– 61.4º) determined for triphenyl-(2-acetyl-3,4,5-triphenylcyclopenta-2,4-dienyl)arsonium perchlorate (Figure 2.8).[97] The crowded pentacarbonyl(η^1-3-pentafluorophenyl)-1-indenyl]rhenium(I) complex also exhibits a similar dihedral angle (51.6º).[94]

An X-ray structure of **5** (Figure 2.9) was obtained from a crystal grown by evaporating a 5:95 ethyl acetate:hexanes solution. Crystal data are presented in Table 2.2; bond distances and angles are listed in Table 2.4. The unit cell contains two independent but structurally similar molecules of **5**. The cyclopentadiene-C_6F_5 dihedral angles for the outer rings range from 39.7 – 45.9º while the inner rings exhibit dihedral angles that are substantially more orthogonal to the

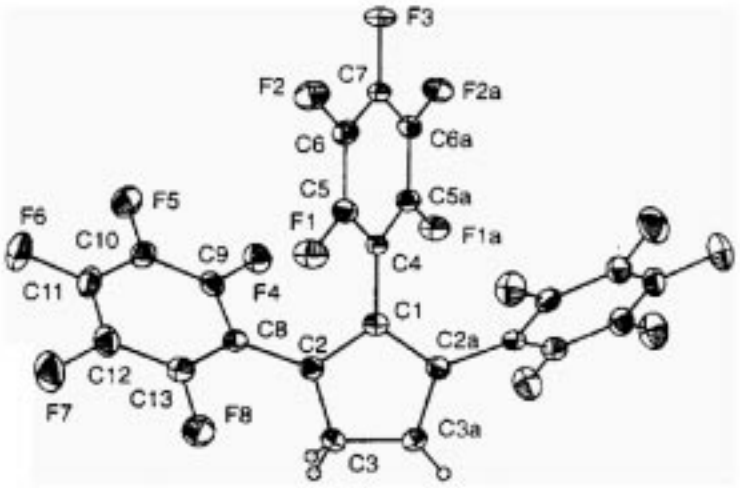

Figure 2.7. Thermal ellipsoid plot of **3** shown at 50% probability.

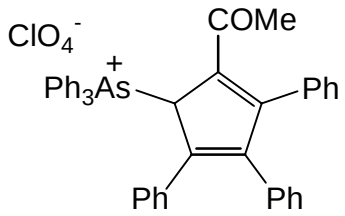

Figure 2.8. Triphenyl-(2-acetyl-3,4,5-triphenylcyclopenta-2,4-dienyl)arsonium perchlorate.

cyclopentadiene ring (53.3 – 58.5º). The outer aryl angles are larger than those measured for 1,2,3,4-tetraphenylcyclopentadiene (32.5º, 22.8º)[98] and 1,2,3,4,5-pentaphenylcyclopentadiene (32.2º, 30.8º).[99] The larger dihedral angles in **5** could be attributed to the increased crowding accompanying the larger covalent radii of fluorine (0.72 Å) compared to hydrogen (0.37 Å). However, the inner dihedral angles in **5** (53.3 – 58.5º) are generally lower than those reported for 1,2,3,4-tetraphenylcyclopentadiene (69.0º, 39.2º)[98] and 1,2,3,4,5-pentaphenylcyclopentadiene (65.2º, 70.4º).[99]

Another X-ray structure of **5** (Figure 2.10) was obtained from a crystal grown from C_6D_6. Crystal data are presented in Table 2.2; bond distances and angles are shown in Table 2.4. The unit cell exhibits a stacking interaction between a C_6D_6 molecule and two crystallographically identical C_6F_5 groups from different molecules of **5**. These two molecules are related by a crystallographic inversion center located at the C_6D_6 centroid. The stacking C_6F_5 and C_6D_6 rings are virtually coplanar with an interplanar angle of 5.2º. The stacking is defined by a C_6F_5-

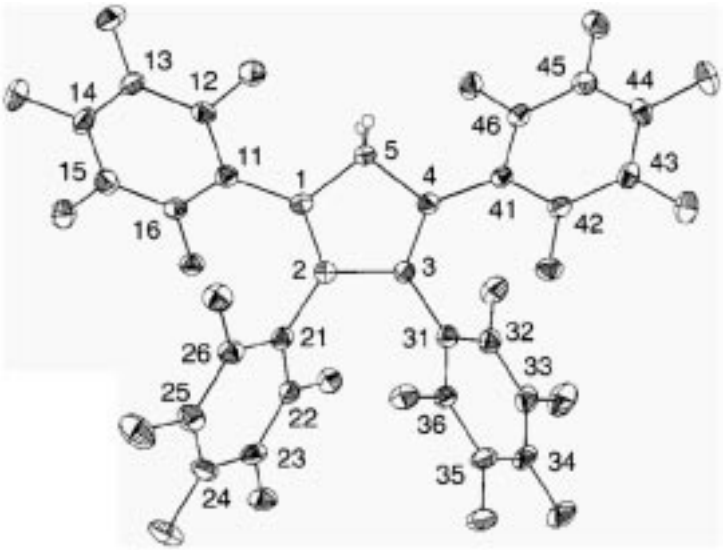

Figure 2.9. Thermal ellipsoid plot of **5** shown at 50% probability. One of two nearly identical independent molecules is shown.

Table 2.4. Selected metric data for **5**.

distances (Å)	**5**		**5·½C_6D_6**	angles (deg)	**5**		**5·½C_6D_6**
C1-C2	1.355(4)	1.349(4)	1.349(3)	C1-C2-C3	108.6(3)	109.3(3)	109.2(2)
C2-C3	1.481(5)	1.472(4)	1.476(3)	C2-C3-C4	109.8(3)	109.3(3)	109.0(2)
C3-C4	1.358(5)	1.359(4)	1.354(3)	C3-C4-C5	107.8(3)	108.6(3)	109.0(2)
C4-C5	1.499(4)	1.498(4)	1.506(3)	C4-C5-C1	104.9(3)	104.0(3)	103.5(2)
C5-C1	1.495(5)	1.505(4)	1.502(3)	C5-C1-C2	108.8(3)	108.8(3)	109.3(2)
				Cp-C_6F_5 (C11-C16)	39.7(5)	40.0(5)	64.0(3)
				Cp-C_6F_5 (C21-C26)	53.7(5)	58.5(5)	57.5(3)
				Cp-C_6F_5 (C31-C36)	53.3(5)	55.7(5)	58.8(3)
				Cp-C_6F_5 (C41-C46)	41.2(5)	45.9(5)	47.4(3)

centroid to C_6D_6-centroid distance of 3.558(4) Å which is slightly longer than the distance of 3.54(1) Å found between a intramolecular C_6H_5-C_6F_5 stacking interaction in a mixed ferrocene complex.[100] The stacking in **5** is tighter than that reported for a C_6F_5 group of a disilazane molecule and two C_6H_6 solvate molecules where the aryl centroid separation is 3.713 and 3.719 Å.[101] The cyclopentadiene-C_6F_5 dihedral angles for the inner rings (57.5º, 58.8º) are similar to those found in the previous X-ray crystal structure of **5**. However, one of the dihedral angles for the outer two rings (64.0º, 47.4º) is substantially larger than one would predict. No obvious interactions that might perturb this dihedral angle could be located within the crystal packing diagram.

Cp Anion Synthesis and Characterization

As depicted in Figure 2.5, the cyclopentadienes **3**, **4**, and **5** react with NaH to form their respective alkali metal Cp salts (**3Na**, **4Na**, and **5Na**). Longer reaction times than those reported

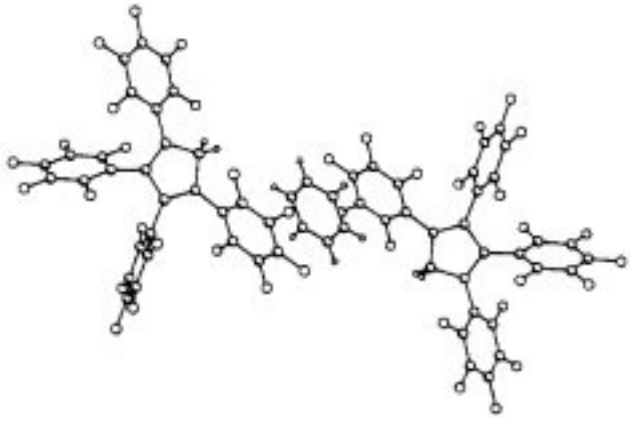

Figure 2.10. Stacking of C_6D_6 solvate in **5**.

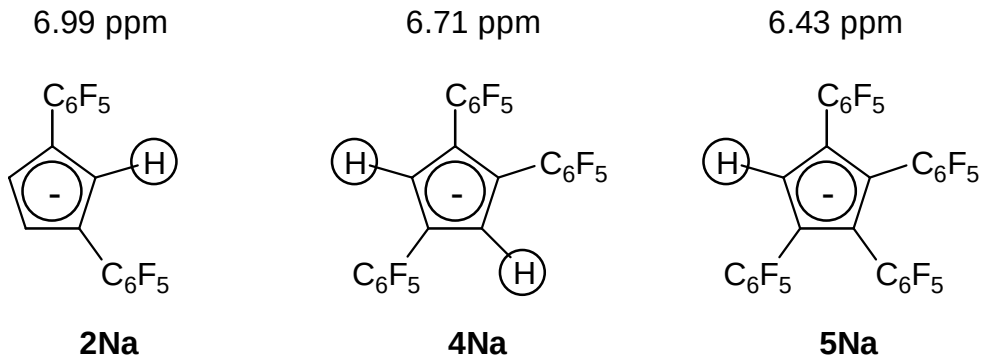

Figure 2.11. ^{1}H NMR resonances in Cp anions (THF-d_8 solution).

for the syntheses of **1Na** and **2Na** (2 – 3 hours) were employed. Use of shorter reaction times resulted in yields that were 10 – 20% lower. Compounds **3Na**, **4Na**, and **5Na** were isolated as tan solids and retained small amounts of THF. All three Cp salts are indefinitely stable when stored in a glovebox.

All three Cp anions have C_{2v} symmetry in solution. Anions **3Na** and **4Na** each display one CH signal in the ^{1}H NMR (6.16 and 6.71 ppm, respectively) and two sets of C_6F_5 signals in a 2:1 ratio in the ^{19}F NMR. Anion **5Na** exhibits one CH signal in the ^{1}H NMR (6.43 ppm) and two equally integrating sets of C_6F_5 signals in the ^{19}F NMR. A comparison of the ^{1}H NMR resonances for the CH group with two adjacent C_6F_5 groups reveals a large chemical shift variation despite subtle changes in the CH environment (Figure 2.11). Initially, one might expect **5Na** to have the furthest downfield shift because it has the most electron-withdrawing C_6F_5 groups. However, **5Na** has the furthest upfield shift while **2Na** has the furthest downfield shift. This trend might be a result of the aryl crowding in **4Na** and **5Na** which diminishes the electron-accepting ability of the C_6F_5 rings through resonance. Figure 2.12 illustrates three electron-accepting resonance structures which require a coplanar alignment between the Cp and C_6F_5 rings. Additional evidence that aryl crowding inhibits C_6F_5 electron-withdrawing ability is

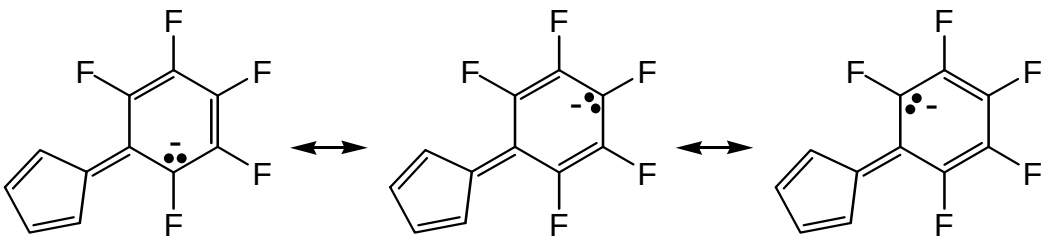

Figure 2.12. Cp-C_6F_5 anion resonance structures.

presented in subsequent chapters.

Conclusion

By varying the reaction conditions for C_6F_5-substitution of cyclopentadiene, two isomeric trisubstituted cyclopentadienes (**3**, **4**) and a tetrasubstituted cyclopentadiene (**5**) were synthesized. The stable Cp anions **3Na**, **4Na**, and **5Na** were synthesized upon the reaction of their respective cyclopentadienes with NaH. ^{1}H NMR spectra of **2Na**, **4Na**, and **5Na** suggest that aryl crowding can diminish the electron-withdrawing ability of the C_6F_5 ring. After this research was completed and published,[93,96] another synthesis of **3**, **4**, and **5** appeared in a European patent application.[102]

Experimental Section

General Procedures. Standard inert-atmosphere techniques were used for all reactions. C_6F_6 (99% purity) was received as a gift from Albemarle Corporation and used without further purification. NaH was purchased as a 60% mineral oil dispersion from Aldrich, washed with hexanes, dried under vacuum, and stored in a glovebox. NaCp was prepared from freshly distilled cyclopentadiene and excess NaH in THF. Melting points were obtained using a Mel-Temp apparatus and are uncorrected. All NMR experiments used a Varian Unity (400) instrument. THF-d_8 was vacuum-transferred from Na/K alloy. ^{19}F NMR spectra were referenced to external C_6F_6 in $CDCl_3$ at –163.00 ppm. $\{^{19}F\}^{13}C$ NMR spectra were useful for resolving signals in the aromatic C-F regions, particularly when extensive ^{19}F couplings in the ^{1}H-decoupled spectra prevented us from distinguishing closely spaced signals. C-F coupling constants were approximated from apparent splittings. Elemental analyses were performed by Desert Analytics (Tucson, AZ).

Crystallographic Studies. Crystallography was performed by Carla Slebodnick (Virginia Tech) for **3** and **5** or Frank Fronczek (Louisiana State University) for **5**$\cdot$ $^1/_2$**C$_6$D$_6$**. Crystals of **3** were obtained by slow evaporation of a concentrated hexanes solution at 25 ºC. Crystals of **5** were obtained by allowing a solution of **5** in ethyl acetate/hexane to evaporate completely. Crystals of **5** were also obtained serendipitously during NMR-scale experiments in which **5** was reacted with $(C_6F_5C_5H_4)CpZr(CH_3)_2$ and $B(C_6F_5)_3$ in benzene-d_6. The reaction afforded a red, viscous oil that we were unable to characterize and a few colorless crystals. X-ray diffraction analysis of the colorless crystals found **5**$\cdot$ $^1/_2$**C$_6$D$_6$**. These crystals were highly unstable toward solvent loss, so crystals were removed quickly from the mother liquor, mounted on a fiber under oil, and transferred to the cold stream of the diffractometer.

1,2,3-Tris(pentafluorophenyl)cyclopentadiene (3). A mixture of lithium cyclopentadienide (0.790 g, 11.0 mmol), hexafluorobenzene (9.74 g, 52.3 mmol), NaH (1.36 g, 56.7 mmol), and diglyme (50 mL) was stirred at 110 ºC for 14 h. The mixture was cooled and filtered through Celite, using 30 mL of THF to wash the filter. The filtrate was evaporated, and the residue was taken up in 50 mL of THF and added by canulla to a stirred 10% aqueous NH_4Cl solution (250 mL). The mixture was stirred for 20 min and then rotary-evaporated until the organic solvents were removed. The resulting aqueous mixture was extracted with 150 mL of benzene. The

organic layer was washed with water, dried over $MgSO_4$, filtered, and evaporated to afford a dark brown residue. The mixture was redissolved in about 1 L of hexanes, filtered through alumina to remove highly colored impurities, and evaporated. The resulting residue was taken up in about 25 mL of hexanes and filtered; the insoluble portion was pure **3**. The filtrate was loaded onto a 10 × 70 cm column of silica gel, which was eluted with hexanes. After a long forerun, an initial band afforded 1,4-bis(pentafluorophenyl)cyclopentadiene (**2a**/**b**) and a second band afforded **4**. A third band was eluted to afford 1.04 g (1.84 mmol, 17%) of **3** as an off-white crystalline solid. This yield includes the solid obtained in the filtration immediately prior to the chromatographic separation. Mp: 216-217 ºC. ^{1}H NMR ($CDCl_3$): δ 6.97 (t, J = 1.5 Hz, 1 H), 3.80 (d, J = 1.2 Hz, 2 H). ^{19}F NMR ($CDCl_3$): δ -141.61 (m, 4 F), -142.11 (d, ^3J = 23 Hz, 2 F), -153.24 (t, ^3J = 21 Hz, 1 F), -154.27 (t, ^3J = 20 Hz, 1 F), -154.66 (t, ^3J = 21 Hz, 1 F), -161.76 (m, 2 F), -162.22 (m, 2 F), -162.56 (m, 2 F). {^{19}F}^{13}C NMR ($CDCl_3$): δ 144.1 (s, CF), 143.9 (s, CF), 143.7 (s, CF), 141.2 (s, CF), 141.0 (s, CF), 140.9 (s, CF), 139.7 (d, J = 175 Hz, CH), 137.8 (s, CF), 137.6 (s, CF), 137.4 (s, CF), 134.4 (m, *C*-C_6F_5), 133.9 (m, *C*-C_6F_5), 132.3 (m, *C*-C_6F_5), 110.0 (s, C_{ipso}), 109.5 (d, J = 2 Hz, C_{ispo}), 108.9 (s, C_{ipso}), 45.6 (td, J = 134 Hz, J = 8 Hz, CH_2). {^{1}H}^{13}C NMR ($CDCl_3$): δ 143.8 (br d, 3 unresolved CF), 141.1 (br d, J = 284 Hz, 3 unresolved CF), 139.7 (s, CH), 137.6 (br d, 3 unresolved CF), 134.4 (s, *C*-C_6F_5), 133.9 (m, *C*-C_6F_5), 132.3 (s, *C*-C_6F_5), 45.5 (s, CH_2); the three C_{ipso} signals were not observed. Anal. Calcd for $C_{23}H_3F_{15}$: C, 48.96; H, 0.54. Found: C, 49.21; H, 0.48.

1,2,4-Tris(pentafluorophenyl)cyclopentadiene (4). From the chromatographic separation described above, the second band afforded 1.41 g (2.50 mmol, 23%) of **4** as an off-white solid. Mp: 106-108 ºC. ^{1}H NMR ($CDCl_3$): δ 7.32 (s, 1 H), 4.14 (s, 2 H). ^{19}F NMR ($CDCl_3$): δ -141.03 (d, ^3J = 21 Hz, 2 F), -141.40 (d, ^3J = 22 Hz, 2 F), -141.56 (d, ^3J = 22 Hz, 2 F), -154.21 (t, ^3J = 21 Hz, 1 F), -154.41 (t, ^3J = 21 Hz, 1 F), -156.49 (t, ^3J = 21 Hz, 1 F), -162.30 (m, 4 F), -163.46 (m, 2 F). {^{19}F}^{13}C NMR ($CDCl_3$): δ 144.6 (s, CF), 143.9 (s, CF), 143.8 (s, CF), 141.2 (s, CF), 141.0 (s, CF), 140.0 (s, CF), 138.0 (s, CF), 137.8 (s, CF), 137.8 (s, CF), 137.3 (d, J = 174 Hz, CH), 134.7 (t, J = 5 Hz, *C*-C_6F_5), 133.6 (m, 2 unresolved *C*-C_6F_5 signals), 110.3 (s, C_{ipso}), 110.1 (d, J = 2 Hz, C_{ipso}), 109.9 (s, C_{ipso}), 47.7 (td, J = 132 Hz, J = 8 Hz, CH_2). {^{1}H}^{13}C NMR ($CDCl_3$): δ 144.7 (d, J = 247 Hz, CF), 144.0 (d, J = 246 Hz, CF), 141.1 (d, J = 251 Hz, CF), 140.0 (d, J = 256 Hz, CF), 138.0 (d, J = 244, CF), 137.9 (d, J = 247 Hz, CF), 137.8 (d, J = 262, CF), 137.3 (t,

J = 8 Hz, CH), 134.7 (m, *C*-C_6F_5), 133.5 (s, 2 unresolved *C*-C_6F_5 signals), 110.2 (m, C_{ipso}), 110.1 (d, J = 4 Hz, C_{ispo}), 109.9 (m, C_{ipso}), 47.7 (s, CH_2). Anal. Calcd for $C_{23}H_3F_{15}$: C, 48.96; H, 0.54. Found: C, 49.02; H, 0.35.

1,2,3,4-Tetrakis(pentafluorophenyl)cyclopentadiene (5). A mixture of NaCp (2.00 g, 22.7 mmol), NaH (3.27 g, 136 mmol), and diglyme (250 mL) was stirred at reflux. Using a syringe, C_6F_6 (25.6 g, 138 mmol) was added cautiously to the refluxing reaction mixture over a period of 5 min. The mixture was stirred at reflux for 2 days. The diglyme was then removed by heating the dark mixture under vacuum. The black residue was taken up in 200 mL of THF and added, by a canulla, to an aqueous solution of NH_4Cl (10.0 g in 400 mL). The biphasic mixture was evaporated, and the resulting dark, oily residue was extracted with CH_2Cl_2, filtered through Celite, and evaporated to yield a brown, oily solid. The crude solid was triturated with warm hexane, collected on a filter, and dried under vacuum to afford 9.44 g (12.9 mmol, 57%) of a brown powder, which was found by ^{1}H and ^{19}F NMR analysis to be about 95% pure. An analytically pure sample was obtained by sublimation (125 ºC, 5 × 10^{-6} Torr): mp 196-197 ºC (open capillary). ^{1}H NMR ($CDCl_3$): δ 4.17 (s, 2 H). ^{19}F NMR ($CDCl_3$): δ -140.02 (dd, ^3J = 22 Hz, ^5J = 8 Hz, 4 F), -140.29 (dd, ^3J = 23 Hz, ^5J = 8 Hz, 4 F), -151.10 (t, ^3J = 21 Hz, 2 F), -152.00 (t, ^3J = 21 Hz, 2 F), -160.18 (m, 4 F), -160.62 (m, 4 F). {^{19}F}^{13}C NMR ($CDCl_3$): δ 144.1 (s, CF), 144.0 (s, CF), 141.8 (s, CF), 141.7 (s, CF), 138.1 (s, CF), 137.7 (s, CF), 136.1 (t, J = 6 Hz, *C*-C_6F_5), 134.5 (t, J = 4 Hz, *C*-C_6F_5), 109.3 (s, C_{ipso}), 108.3 (s, C_{ipso}), 48.1 (t, J = 132 Hz, CH_2). {^{1}H}^{13}C NMR ($CDCl_3$): δ 144.1 (d, $^1J_{CF}$ = 240 Hz, CF), 141.6 (d, $^1J_{CF}$ = 250 Hz, CF), 138.1 (d, $^1J_{CF}$ = 260 Hz, CF), 137.7 (d, $^1J_{CF}$ = 260 Hz, CF), 136.1 (s, *C*-C_6F_5), 134.5 (s, *C*-C_6F_5), 109.3 (m, C_{ispo}), 108.3 (m, C_{ipso}), 48.1 (s, CH_2). Anal. Calcd for $C_{29}H_2F_{20}$: C, 47.70; H, 0.28. Found C, 48.01; H, 0.29.

Sodium 1,2,3-Tris(pentafluorophenyl)cyclopentadienide (3Na). A mixture of 1,2,3-tris(pentafluorophenyl)cyclopentadiene (**3**, 1.73 g, 3.07 mmol), NaH (0.41 g, 17 mmol), and THF (50 mL) was stirred at 25 ºC for 1 day. The mixture was filtered to remove unreacted NaH, and the filtrate was evaporated. The residue was triturated with hexane, collected on a fritted filter, and dried under vacuum at 80 ºC to yield 1.53 g (2.62 mmol, 85%) of a tan solid. ^{1}H NMR (THF-d_8): δ 6.16 (s, 2 H). ^{19}F NMR (THF-d_8): δ -144.15 (d, ^3J = 20 Hz, 2 F), -144.45 (d, ^3J = 22 Hz, 4 F), -166.14 (tt, ^3J = 21 Hz, ^4J = 2 Hz, 1 F), -167.40 (m, 6 F), -168.12 (tt, ^3J = 21 Hz, ^4J = 3 Hz, 2 F). {^{19}F}^{13}C NMR (THF-d_8): δ 145.7 (s, CF), 145.4 (s, CF), 139.4 (s, CF), 139.2 (s, CF),

138.8 (CF), 138.1 (CF), 120.7 (s, C_{ipso}), 113.9 (d, J = 166 Hz, 2 CH), 107.2 (t, J = 7.6 Hz, *C*-C_6F_5), 105.2 (s, *C*-C_6F_5); no signal that we could assign to the second C_{ipso} was observed. $\{^1H\}^{13}C$ NMR (THF-d_8): δ 145.7 (d, J = 240 Hz, CF), 145.4 (d, J = 240 Hz, CF), 139.4 (m, 2 unresolved CF), 138.8 (d, J = 246 Hz, CF), 138.1 (d, J = 243 Hz, CF), 120.7 (t, J = 20 Hz, C_{ipso}), 113.9 (s, CH), 107.2 (s, *C*-C_6F_5), 105.2 (s, *C*-C_6F_5); no signal that we could assign to the second C_{ipso} was observed.

Sodium 1,2,4-Tris(pentafluorophenyl)cyclopentadienide (4Na). A mixture of 1,2,4-tris(pentafluorophenyl)cyclopentadiene (**4**, 3.04 g, 5.39 mmol), NaH (0.75 g, 31 mmol), and THF (50 mL) was stirred at 25 ºC for 1 day. The mixture was filtered to remove unreacted NaH, and the filtrate was evaporated. The residue was triturated with hexane, collected on a fritted filter, and dried under vacuum at 80 ºC to yield 2.99 g (5.10 mmol, 95%) of a tan solid. ^1H NMR (THF-d_8): δ 6.71 (2 H). ^{19}F NMR (THF-d_8): δ -146.64 (d, ^3J = 22 Hz, 4 F), -148.01 (d, ^3J = 18 Hz, 2 F), -169.36 (t, ^3J = 20 Hz, 4 F), -169.82 (tt, ^3J = 21 Hz, ^4J = 3 Hz, 2 F), -170.09 (m, 2 F), -175.29 (tt, ^3J = 21 Hz, ^4J = 5 Hz, 1 F). $\{^{19}F\}^{13}C$ NMR (THF-d_8): δ 143.5 (s, CF), 143.0 (s, CF), 137.9 (s, CF), 137.6 (s, CF), 136.3 (s, CF), 118.9 (s, CF), 117.6 (s, C_{ipso}), 115.2 (d, J = 165 Hz, CH), 107.0 (m, *C*-C_6F_5), 105.3 (m, *C*-C_6F_5). $\{^1H\}^{13}C$ NMR (THF-d_8): δ 143.0 (d, J = 240 Hz, CF), 143.0 (d, J = 243 Hz, CF), 138.0 (d, J = 242 Hz, CF), 137.6 (d, J = 220 Hz, CF), 136.4 (d, J = 240 Hz, CF), 133.9 (d, J = 234 Hz, CF), 118.9 (t, J = 18 Hz, C_{ipso}), 117.6 (t, J = 15 Hz, C_{ipso}), 115.2 (s, CH), 107.0 (s, *C*-C_6F_5), 105.3 (s, *C*-C_6F_5).

Sodium 1,2,3,4-Tetrakis(pentafluorophenyl)cyclopentadienide (5Na). A mixture of 1,2,3,4-tetrakis(pentafluorophenyl)cyclopentadiene (**5**, 2.05 g, 2.81 mmol), NaH (0.17 g, 7.08 mmol), and THF (50 mL) was stirred at 25 ºC for 1 day and then filtered to remove unreacted NaH. The filtrate was evaporated, and the residue was triturated with hexane, collected on a fritted filter, and dried under vacuum to afford 1.88 g (2.50 mmol, 89%) of a tan powder. The potassium salt can be prepared analogously by using KH in place of NaH. ^1H NMR (THF-d_8): δ 6.43 (p, ^5J = 1.6 Hz, 1 H). ^{19}F NMR (THF-d_8): δ -143.95 (dd, ^3J = 25 Hz, ^5J = 7 Hz, 4 F), -144.86 (d, ^3J = 25 Hz, ^5J = 6 Hz, 4 F), -165.00 (t, ^3J = 21 Hz, 2 F), -167.52 (m, 6 F, two unresolved signals), -167.83 (m, 4 F). $\{^{19}F\}^{13}C$ NMR (THF-d_8): δ 144.3 (s, CF), 143.8 (s, CF), 138.0 (s, CF), 137.8 (s, CF), 137.5 (s, CF), 137.1 (s, CF), 117.7 (s, C_{ispo}), 117.6 (s, C_{ispo}), 115.5 (d, J = 165 Hz, CH), 106.6 (d, J = 4.2 Hz, *C*-C_6F_5), 106.4 (d, J = 8.3 Hz, *C*-C_6F_5). $\{^1H\}^{13}C$ NMR (THF-d_8): δ 144.3 (d, J = 243 Hz, CF), 143.8 (d, J = 241 Hz, CF), 137.7 (d, J = 243 Hz, three unresolved CF),

137.1 (d, J = 233 Hz, CF), 117.6 (m, two unresolved C_{ispo}), 115.5 (s, CH), 106.6 (s, *C*-C_6F_5), 106.4 (*C*-C_6F_5).

Chapter 3: Acidities of Perfluoroarylated Cyclopentadienes and Indenes

Introduction

In organic compounds, carbon acidity depends on the functionalities and structure that surround the C-H bond. Cyclopentadiene (CpH) is one of the most commonly cited examples of a strong organic acid.[103-105] The acidity of CpH is attributed to the stabilization of the conjugate base through the formation of an aromatic Cp anion (Figure 3.1) as predicted by the Hückel 4n + 2 rule (n = 1). Substituents attached to Cp also influence both anion stability and the acidity of CpH. For example, electron withdrawing groups (NO_2[106], CN[49], COR[49]) increase CpH acidity by increasing Cp anion delocalization while electron-donating groups (Me[107]) have the opposite effect. The effect of the electron-withdrawing C_6F_5 group is described in this chapter.

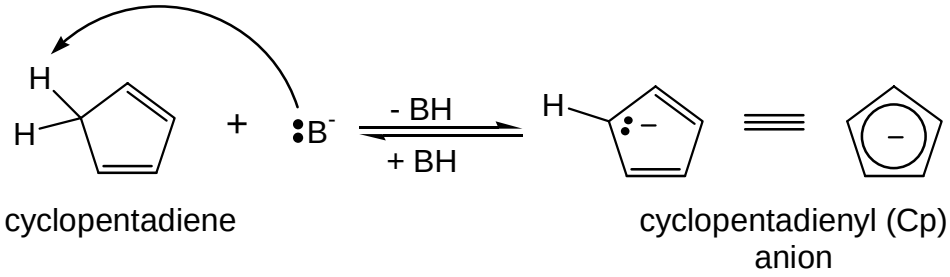

Figure 3.1. The acid/base chemistry of cyclopentadiene.

The Acidity of Cyclopentadiene

The pK_a of cyclopentadiene has been determined using a variety of techniques and solvent systems. One of the first reported values (15) came from combining several studies into the MSAD (McEwen-Streitwieser-Applequist-Dessy) pK_a scale (Table 3.1).[103] In this scale the kinetic acidity data of Streitwieser[108] and Dessy[109] (obtained from isotope exchange experiments) was combined with the thermodynamic acidity data of McEwen[110], Applequist[111], and Dessy[112] (obtained from ion-pair equilibrium measurements). The pK_a of CpH was approximated by Dessy who observed that cyclopentadiene in a CO_2 saturated methanol solution could be carbonated with sodium methoxide (methanol $pK_a \cong 15.5$) but not sodium phenoxide (phenol $pK_a \cong 10.0$).[109] The MSAD scale was the first to provide a broad range of pK_a values which readily illustrated the strong acidity of CpH relative to many other organic acids.

Breslow and Washburn used ^{1}H NMR spectroscopy to measure the pK_a of CpH.[113] Integrated spectra allowed the calculation of an equilibrium constant for the ion-pair equilibrium

Table 3.1. MSAD pK_a scale.

Compound	pK_a	Compound	pK_a
Cyclopentadiene (CpH)	15	Benzene	37
9-Phenylfluorene	18.5	Cumene (α-position)	37
Indene	18.5	Triptycene (α-position)	38
Phenylacetylene	18.5	Cyclopropane	39
Fluorene	22.9	Methane	40
Acetylene	25	Ethane	42
1,3,3-Triphenylpropene	26.5	Cyclobutane	43
Triphenylmethane	32.5	Neopentane	44
Toluene	35	Propane	44
Propene	35.5	Cyclopentane	44
Cycloheptatriene	36	Cyclohexane	45
Ethylene	36.5		

between Cp anion and *t*-butyl alcohol (pK_a = 19.0). From the equilibrium constant, the pK_a of CpH was determined to be 18.2(2). Schaeffer used the NMR chemical shift differences between several organic acids and their lithiated conjugate bases to establish a linear correlation with the MSAD scale pK_a values.[114] His calculations estimated a pK_a of 15.3 for CpH.

Streitweiser obtained a pK_a of CpH by using UV-Vis spectroscopy to measure Cp anion concentrations in ion-pair equilibria with acids of known pK_a (indicators).[115] In cyclohexylamine solution, a known amount of CpCs was mixed with known amounts of indicator and the calculated equilibrium constant gave an average CpH pK_a value of 16.65(5). Bordwell and coworkers used the same ion-pair acidity measurement in DMSO solution to calculate an average pK_a value of 18.0 for CpH.[116,117]

Breslow and coworkers used reduction potentials (RP) and bond dissociation energies (BDE) to measure acidity differences (ΔpK_a) between an organic acid of known pK_a (the indicator) and one with an unknown pK_a.[118] The three thermodynamic steps resulting in net acid dissociation are shown in Figure 3.2. The ionization potential (IP) of the hydrogen radical is the same for both acids. Therefore, ΔpK_a can be calculated by summing the two remaining energy differences ($\Delta BDE + \Delta RP$). Using this method, a pK_a range of 22.2 – 23.4 was calculated for CpH in a THF/HMPA solution.

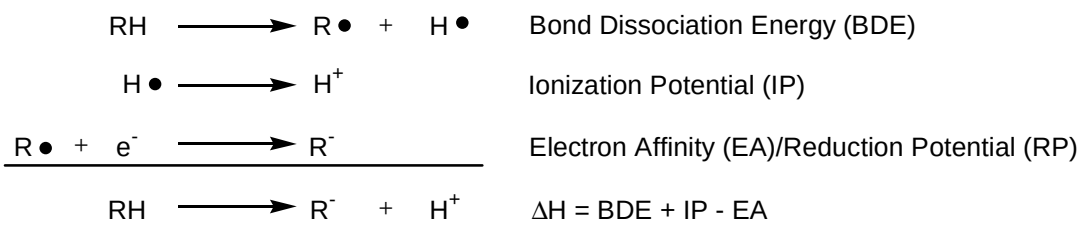

Figure 3.2. Thermodynamic cycle of acid dissociation.

Methods of Acidity Determination

The many different pK_a values presented above clearly illustrate the importance of the conditions and methods used for pK_a determination. For example, the studies described above use a variety of solvents. Often, standard aqueous methods cannot be employed due to the limited solubility of most organic acids and their conjugate bases. Therefore, pK_a values are typically measured in organic solvents such as cyclohexylamine (CHA), dimethylsulfoxide (DMSO), hexamethylphosphoramide (HMPA), N-methylpyrrolidin-2-one (NMP), tetrahydrofuran (THF), and various solvent mixtures. These different solvents afford pK_a values that will vary with the solvent's ability to stabilize the conjugate base of the carbon acid (and the metal counterion, if present).

The preferred method for determining the pK_a of strong organic acids like CpH involves monitoring an equilibrium spectrophotometrically between an acid/base pair of known pK_a (the indicator) and unknown pK_a.[103,105,117] The intense absorption of many carbanions in the UV-Vis spectral region provides a sensitive method for directly determining the indicator and unknown anion concentrations at equilibrium. Subsequently the equilibrium constant (K_{eq}) is calculated from the initial and equilibrium concentrations. The acidity difference between the indicator and unknown acid is then calculated from K_{eq} ($\Delta pK_a = \log K_{eq}$).

The use of NMR spectroscopy to determine equilibrium concentrations is not as well developed due to some practical limitations. ^{1}H NMR has a limited spectral range, resulting in overlapping signals. ^{13}C NMR has been successfully employed by Fraser and coworkers for the pK_a determination of various organic acids.[119-126] However, this technique is problematic because the pK_a values may be skewed by aggregation phenomena, which are more likely at the high concentrations required for ^{13}C NMR spectroscopy. NMR spectroscopy does, however, have a major advantage over traditional spectrophotometric techniques: the relative

concentrations of *all* equilibrium species can be determined from an integrated spectrum. Spectrophotometric techniques only allow the determination of equilibrium concentrations for the strongly absorbing anionic species. Acid concentrations must be determined from the difference of the initial concentrations (requiring mass and volume measurements) and the spectrophotometrically determined anion concentrations. The random error introduced by this technique can be avoided by using the relative concentrations obtained with NMR spectroscopy.

^{19}F NMR spectroscopy is seldom used for acidity measurements,[127,128] however, as an equilibrium measuring technique, it surpasses ^{1}H and ^{13}C NMR because of its broad spectral range, high natural abundance, and short relaxation times. The natural abundance of ^{19}F (100.0%) compared to ^{13}C (1.108%) allows the use of more dilute solutions thus minimizing the problem of ion aggregation.

Chapter Overview

The C_6F_5-substituted cyclopentadienes reported in the preceding chapter all contain ^{19}F as an NMR-active nucleus. Mono- and diarylated indenes are also available.[94] Additional unpublished results from our laboratories provide a series of alkyl-and-C_6F_5 substituted and tetrafluoropyridyl (C_5F_4N) substituted cyclopentadienes. The acidity of these cyclopentadienes and indenes can be conveniently determined by using ^{19}F NMR spectroscopy in conjunction with a ^{19}F-containing indicator acid. Fortunately, Streitwieser recently described a THF-based acidity scale that contained a substituted indene comprising the two double bond isomers **PTFI-a** and **PTFI-b** (Figure 3.3) whose equilibrium mixture has a reported pK_a of 9.66.[129] In this chapter an experimental method and an acidity scale obtained by ^{19}F NMR spectroscopy is presented for the ^{19}F-containing cyclopentadiene and indene acids shown in Figure 3.4.

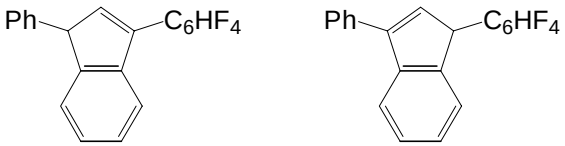

PTFI-a **PTFI-b**

Figure 3.3. Double bond isomers of Streitwieser's compound.

Results & Discussion

Method

Solvent, concentration, and metal counterion all play an important role in determining ion-pair acidity. Conditions that favor the formation of solvent separated ion pairs (SSIP) over contact ion pairs (CIP) are preferred. The presence of SSIPs ensures that the measured acidities are independent of the "spectator" cation's identity and truly reflect the stability of the "free" conjugate base.

Solvents with high dielectric constants such as DMSO (46.6) and water (80) promote SSIP formation. However, these solvents do not dissolve many of the highly fluorinated cyclopentadienes and indenes shown in Figure 3.4. Despite its low dielectric constant (7.6), THF is the only solvent we have found which effectively dissolves all of the relevant acid/base pairs. This low dielectric constant decreases SSIP formation, but this problem can be overcome to some extent by the proper choice of metal counterion.

Smaller cations like Li^+ tend to favor SSIP formation while larger cations such as Na^+,

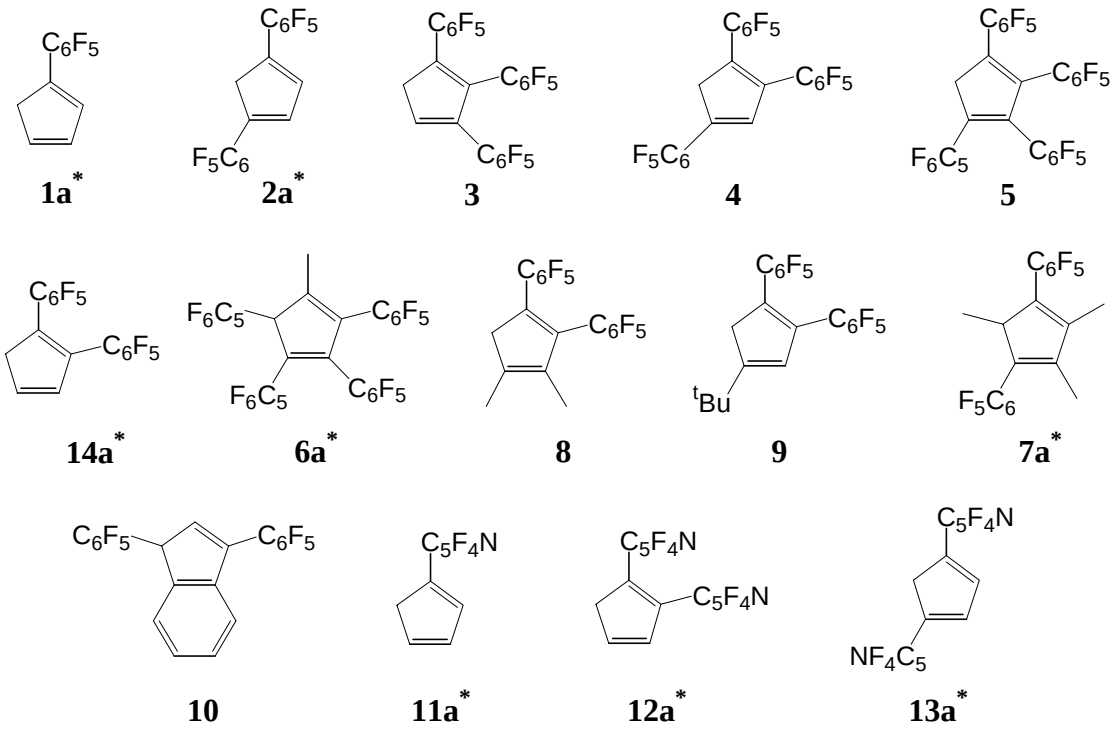

Figure 3.4. Fluorine-containing cyclopentadienes and indenes to be studied.

K^+, or Cs^+ tend to favor CIP formation.[130,131] To promote SSIP formation and minimize the presence of CIPs, the best metal counterion for these studies is Li^+. Fluorenyllithium is used to supply Li^+ to an equimolar mixture of unknown and indicator acids. Fluorene has a pK_a of 22.9 in THF,[129] while all of the acids in Figure 3.4 are expected to be substantially more acidic. This suggests that fluorenyllithium will react completely with any of the indene or cyclopentadiene acids. Therefore, when fluorenyllithium is introduced into an equimolar mixture of unknown and indicator acids, it will quickly exchange all of its Li^+ for H^+ from either of the acids. Subsequently, the unknown and indicator acid/base pairs will exchange Li^+ and H^+ until equilibrium is achieved. Despite their misleading names, fluorenyllithium and its conjugate acid (fluorene) do not contain any ^{19}F and will not clutter the equilibrium ^{19}F NMR spectrum.

Finally, the nature of the conjugate bases also has a direct effect on the formation of SSIPs. More delocalized anions such as cyclopentadienide, indenide, and fluorenide have shown a preference to form SSIPs in ethereal solvents such as diethyl ether, THF, and dimethoxyethane.[130,132] These studies suggest that the conjugate bases of the acids depicted in Figure 3.4 will preferentially exist as SSIPs. Furthermore, since all of the conjugate bases form similar delocalized carbanions and possess the same Li^+ counterion, the measured pK_a values will reflect the differences in acidity and not ion-pairing phenomena. However, since ion-pairing can not be completely ruled out, the acidities measured in this study are still called[133] "ion-pair acidities" and will be designated with the symbol "pK" rather than "pK_a" which generally refers to complete ion dissociation into SSIPs.

All acid/base equilibria in this study can be illustrated as the summation of the known (indicator) and unknown acid dissociation equations.

$$RH \Leftrightarrow R^- + H^+$$

$$\underline{Ind^- + H^+ \Leftrightarrow IndH}$$

$$RH + Ind^- + H^+ \Leftrightarrow IndH + R^- + H^+$$

The equilibrium constant for this reaction is shown below in eq 1.

$$K_{eq} = \frac{[IndH][R^-][H^+]}{[Ind^-][RH][H^+]} = \frac{[IndH][R^-]}{[Ind^-][RH]} \qquad (1)$$

Taking the logarithm of this equation and rearranging gives eq 2.

$$\log(K_{eq}) = -\log\frac{[Ind^-][H^+]}{[IndH]} + \log\frac{[R^-][H^+]}{[RH]}$$

$$\log(K_{eq}) = pK(IndH) - pK(RH) = \Delta pK \qquad (2)$$

The pK of the unknown acid is obtained upon subtracting the $\log(K_{eq})$ from the pK of the indicator. If ΔpK is positive, the unknown acid is more acidic than the indicator. A negative ΔpK indicates that the unknown acid is less acidic than the indicator.

The following example describes an equilibrium mixture which contains an indicator (IndH) its conjugate base (Ind^-), two cyclopentadiene double bond isomers (R^1H and R^2H), and their conjugate base (R^-). Since both double bond isomers are in equilibrium with one another, the following equation can be written.

$$R^1H + R^- + H^+ \Leftrightarrow R^2H + R^- + H^+$$

The difference in double bond isomer acidity is found by using the previously described derivation which, after simplifying, gives eq 3.

$$\Delta pK = pK(R^2H) - pK(R^1H) = \log\frac{[R^2H]}{[R^1H]} \qquad (3)$$

By comparing the equilibrium between a single isomer and the indicator, the actual pK values can be assigned for both double bond isomers.

Using the above formulas, ΔpK can be calculated for any two acid/base pairs that are in equilibrium and possess similar acidities. A reliable determination of ΔpK is limited by the spectral intensities of the equilibrium species. Therefore, ΔpK values are only measured for two acids within 3 pK units (max. ratio of RH/IndH integrals ≅ 32).

Analysis of NMR Equilibrium Data

A sample NMR equilibrium spectrum of acids **3** and **4** is shown in Figure 3.5. The spectrum of each individual species is adjacent to its respective structure. Comparison of the equilibrium spectrum with the four individual spectra clearly enables the assignment of each signal. Subsequently, each resolved signal is integrated, and the relative concentrations of all four species are determined (Table 3.2). The relative concentrations can be substituted into eq 1 to obtain K_{eq}. This value is then used in equation 3 to obtain a ΔpK of –0.61(5) which suggests that compound **4** is more acidic than **3**. The ΔpK value was determined from the average of

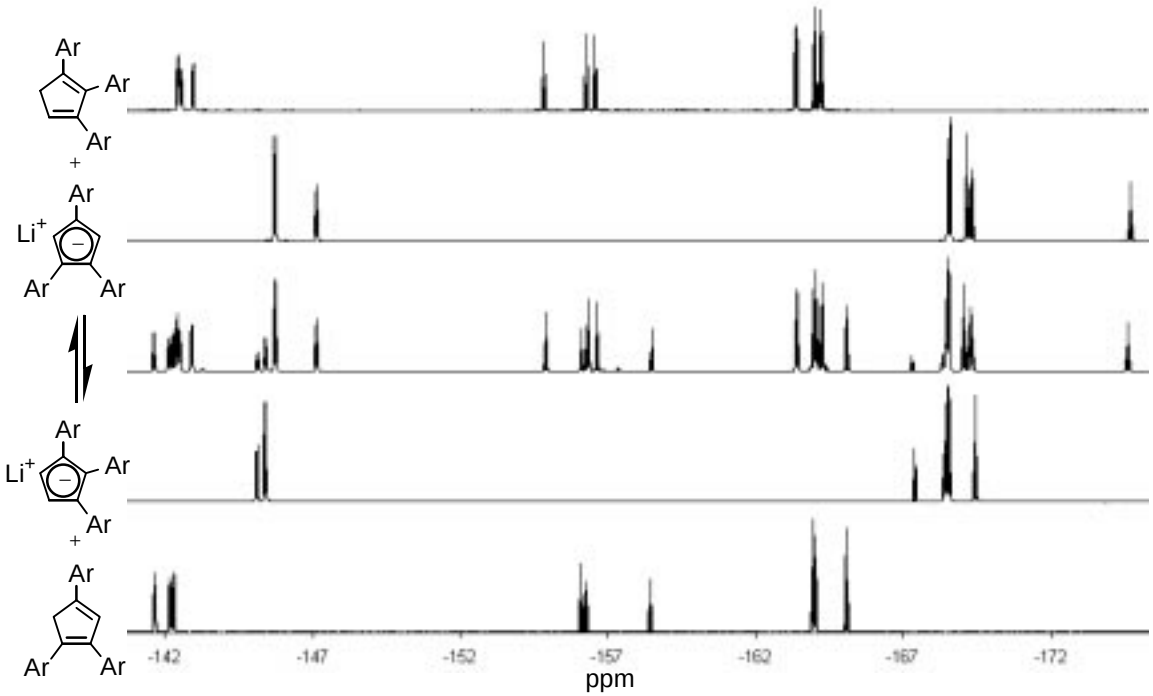

Figure 3.5. Individual and equilibrium spectra of **3**, **4**, and their conjugate bases.

three equilibrium spectra obtained over a three day period to ensure that equilibrium had been achieved. Doubling the concentrations produced no significant change in ΔpK suggesting that aggregation phenomena are insignificant. Integrated equilibria spectra were obtained for several other acid combinations and the results are presented in the experimental section (Tables 3.3 – 3.23). The ΔpK values for these acids are presented in Figure 3.6. Fortunately, we were able to cross check several ΔpK values with overlapping values. In the same manner, the ΔpK values for double bond isomer pairs were determined (eq 3) and are presented in Figure 3.7.

The equilibrium NMR spectra of **6a** and **6b** could not be assigned since each isomer produces similar signals in both the ^{19}F and ^{1}H NMR spectrum (four unique C_6F_5 groups, one methine signal, and one methyl signal). Fortunately, the eight equally integrating signals in the ^{19}F NMR para region indicate that the two isomers must have approximately equal concentrations. Therefore, the ΔpK for **6a/b** is approximately 0.

Using the ΔpK value for **PTFI-a/b**, the pK value for each individual isomer can be determined.

$$\Delta pK = pK(PTFI\text{-}b) - pK(PTFI\text{-}a) = \log K_{eq} = \log\left(\frac{[PTFI\text{-}b]}{[PTFI\text{-}a]}\right) = -0.35$$

$$[PTFI\text{-}b] = 0.45[PTFI\text{-}a] \quad \text{or} \quad [PTFI\text{-}a] = 2.24[PTFI\text{-}b] \tag{4}$$

Table 3.2. Integrations from the ^{19}F NMR equilibrium spectra.

spectra = X1F	3	+	4 (cb)	⇆	3 (cb)	+	4	K_{eq}	|Δ pK|
ortho (1)	5.99		10.82		2.21		3.74	0.25	0.60
ortho (2)	5.99		5.38		4.24		3.85		
ortho (3)	6.09						3.83		
para (1)	2.92		--		1.00		1.88		
para (2)	--		2.61		--		--		
para (3)	2.93						1.81		
meta (1)	5.96		--		--		--		
meta (2)	--		5.27		--		--		
meta (3)	--						3.64		
# of eq. rings (1)	1		2		1		1		
# of eq. rings (2)	1		1		2		1		
# of eq. rings (3)	1						1		
relative integral	2.99		2.68		1.06		1.88		
mole fraction	0.35		0.31		0.12		0.22		
spectra = X2F	**3**	**+**	**4 (cb)**	**⇆**	**3 (cb)**	**+**	**4**	**K_{eq}**	**|Δ pK|**
ortho (1)	6.40		11.09		2.18		3.97	0.24	0.61
ortho (2)	6.40		5.52		4.25		4.09		
ortho (3)	6.47						4.08		
para (1)	3.10		--		1.00		1.99		
para (2)	--		2.67		--		--		
para (3)	3.16						1.96		
meta (1)	6.24		--		--		--		
meta (2)	--		5.41		--		--		
meta (3)	--						3.96		
# of eq. rings (1)	1		2		1		1		
# of eq. rings (2)	1		1		2		1		
# of eq. rings (3)	1						1		
relative integral	3.18		2.74		1.06		2.01		
mole fraction	0.35		0.31		0.12		0.22		
spectra = X3F	**3**	**+**	**4 (cb)**	**⇆**	**3 (cb)**	**+**	**4**	**K_{eq}**	**|Δ pK|**
ortho (1)	6.67		10.86		2.12		4.24	0.25	0.61
ortho (2)	6.67		5.41		4.04		4.40		
ortho (3)	6.69						4.38		
para (1)	3.22		--		1.00		2.14		
para (2)	--		2.61		--		--		
para (3)	3.27						2.10		
meta (1)	6.55		--		--		--		
meta (2)	--		5.29		--		--		
meta (3)	--						4.22		
# of eq. rings (1)	1		2		1		1		
# of eq. rings (2)	1		1		2		1		
# of eq. rings (3)	1						1		
relative integral	3.31		2.69		1.02		2.15		
mole fraction	0.36		0.29		0.11		0.23		
Average:								0.25	0.61

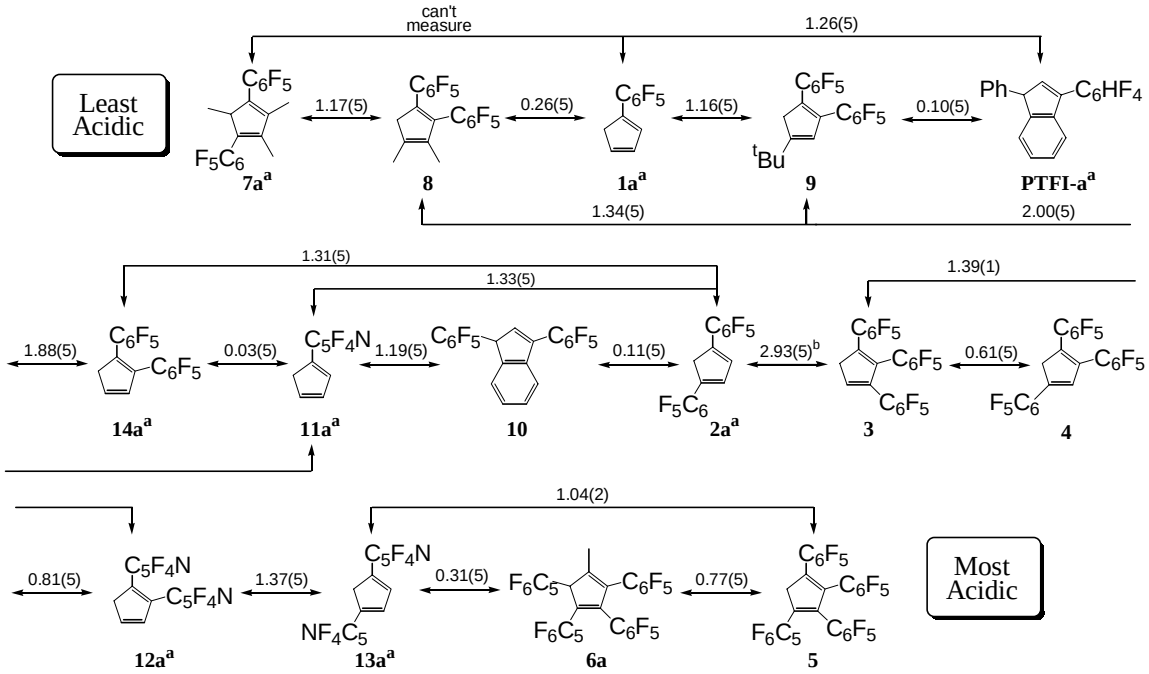

7a[a] **8** **1a**[a] **9** **PTFI-a**[a] **14a**[a] **11a**[a] **10** **2a**[a] **3** **4** **12a**[a] **13a**[a] **6a** **5**

a. only one of two double bond isomers shown; values are for an equilibrium mixture of both isomers; b. average for 2 individual measurements

Figure 3.6. ΔpK values.

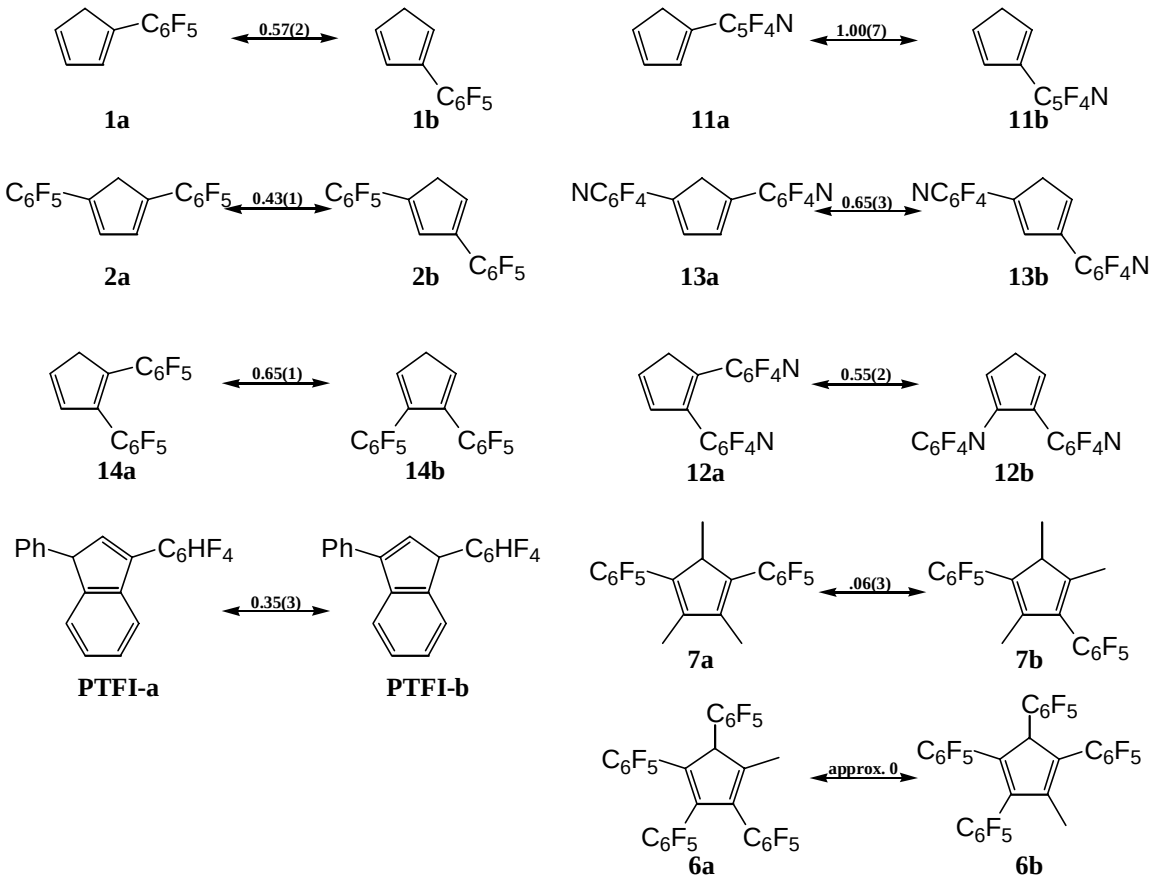

1a **1b** **11a** **11b** **2a** **2b** **13a** **13b** **14a** **14b** **12a** **12b** **PTFI-a** **PTFI-b** **7a** **7b** **6a** **6b**

Figure 3.7. ΔpK values for double bond isomers.

The acid dissociation of **PTFI-a/b** is defined by the following equation for which an equilibrium constant of 2.19×10^{-10} (pK = 9.66) was found by Streitwieser. [129]

$$K_{eq} = \frac{[H^+][PTFI(cb)]}{[PTFI\text{-}a/b]} = \frac{[H^+][PTFI(cb)]}{[PTFI\text{-}a]+[PTFI\text{-}b]} = 2.19\times10^{-10} \quad (5)$$

By combining the eqs 4 and 5, the pK of **PTFI-a** can be solved as follows.

$$K_{eq}(PTFI-a) = \frac{[H^+][PTFI(cb)]}{1.45[PTFI\text{-}a]} = 2.19\times10^{-10}$$

$$K_{eq}(PTFI-a) = \frac{[H^+][PTFI(cb)]}{[PTFI\text{-}a]} = 3.18\times10^{-10}$$

$$pK(PTFI-a) = -\log(K_{eq}(PTFI-a)) = 9.50$$

In the same manner, the pK of **PTFI-b** can be solved as follows.

$$K_{eq}(PTFI-b) = \frac{[H^+][PTFI(cb)]}{3.24[PTFI\text{-}b]} = 2.19\times10^{-10}$$

$$K_{eq}(PTFI-b) = \frac{[H^+][PTFI(cb)]}{[PTFI\text{-}b]} = 7.10\times10^{-10}$$

$$pK(PTFI-b) = -\log(K_{eq}(PTFI-b)) = 9.15$$

Using the pK values for **PTFI-a/b**, a pK scale for all 23 acids can be constructed (Figure 3.8). These results illustrate the dependence of pK on five key features which is discussed below in detail.

First, it is clear from Figure 3.8 that fluorinated aryl groups increase the acidity of cyclopentadiene and indene acids. The fluorines on the aryl group are electron-withdrawing and inductively stabilize the anionic conjugate base. This effect is clearly illustrated in Figure 3.9 which shows the pK values of four diarylated indenes. Each indene contains two aryl rings which are either phenyl, C_6HF_4, or C_6F_5. Streitwieser had previously reported a pK of 12.3 (in THF) for 1,3-diphenylindene.[129] If one Ph ring in 1,3-diphenylindene is replaced with a C_6HF_4 group, the acidity increases by 2.8-3.2 pK units. Replacing both Ph groups with C_6F_5 rings increases the acidity by 5.9 pK units. The position of the double bond also affects the acidity as illustrated by **PTFI-a** and **PTFI-b**. Since both isomers yield the same conjugate base upon deprotonation, ΔpK (0.36) reflects the relative stability of the two acids. Therefore, substitution

Acid	pK
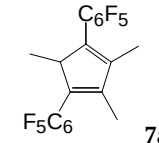 **7a**	12.08
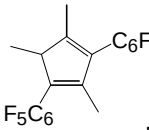 **7b**	12.02
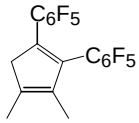 **8**	11.18
 **1a**	10.82
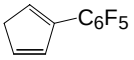 **1b**	10.25
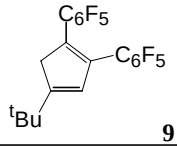 **9**	9.76
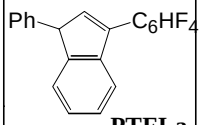 **PTFI-a**	9.50
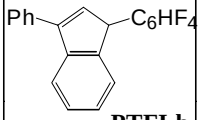 **PTFI-b**	9.14

Acid	pK
 **11a**	7.71
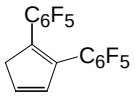 **14a**	7.68
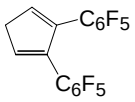 **14b**	7.03
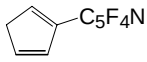 **11b**	6.73
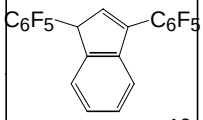 **10**	6.56
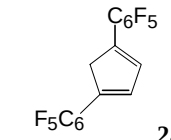 **2a**	6.31
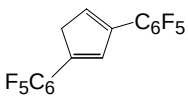 **2b**	5.88
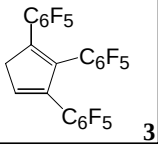 **3**	3.52

Acid	pK
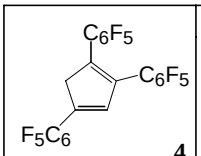 **4**	2.91
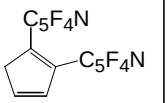 **12a**	1.99
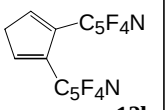 **12b**	1.44
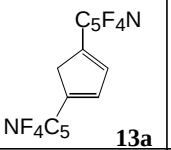 **13a**	0.64
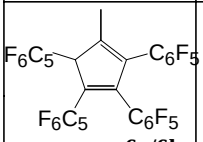 **6a/6b**	0.42[a]
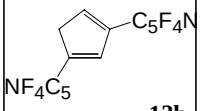 **13b**	-0.01
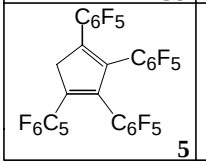 **5**	-0.35

a. for equal concentrations of two double bond isomers at equilibrium

Figure 3.8. Acidity scale for 23 different acids

of the double bond with Ph is less stabilizing relative to substitution with C_6HF_4. This is depicted with the energy diagram in Figure 3.10 which shows that **PTFI-a** has the more positive ΔG and, therefore, is less acidic. An isomer energy difference was calculated from ΔpK and showed **PTFI-a** to be more stable than **PTFI-b** by 0.5 kcal/mol. Density functional (DFT)

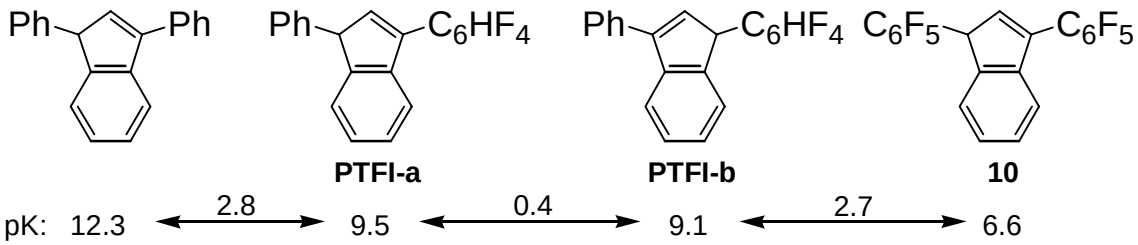

Figure 3.9. Comparison of aryl-substituted indenes.

calculations agree qualitatively with these findings and show **PTFI-a** to be 2.5 kcal/mol more stable than **PTFI-b**.

Secondly, the pK decreases substantially as the number of C_6F_5 or C_5F_4N substituents increases. Figure 3.11 illustrates the change in acidity with increasing aryl substitution. The slopes show that a sharper decline in pK accompanies C_5F_4N substitution (slope = –6.2) compared to C_6F_5 substitution (slope = –3.6). The enhanced ability of C_5F_4N to delocalize anionic charge can be attributed to a resonance contributor that delocalizes negative charge onto the nitrogen (Figure 3.12). A comparison of the mono- and diarylated cyclopentadienes gives pK shifts that are not complicated by the potential steric crowding in the tri- and tetraarylated cyclopentadienes. Figure 3.13 shows the effect of adding one substituent to the 4-position of several monoarylated cyclopentadienes. For the C_6F_5 group, the acidity increases by 4.4(1) pK

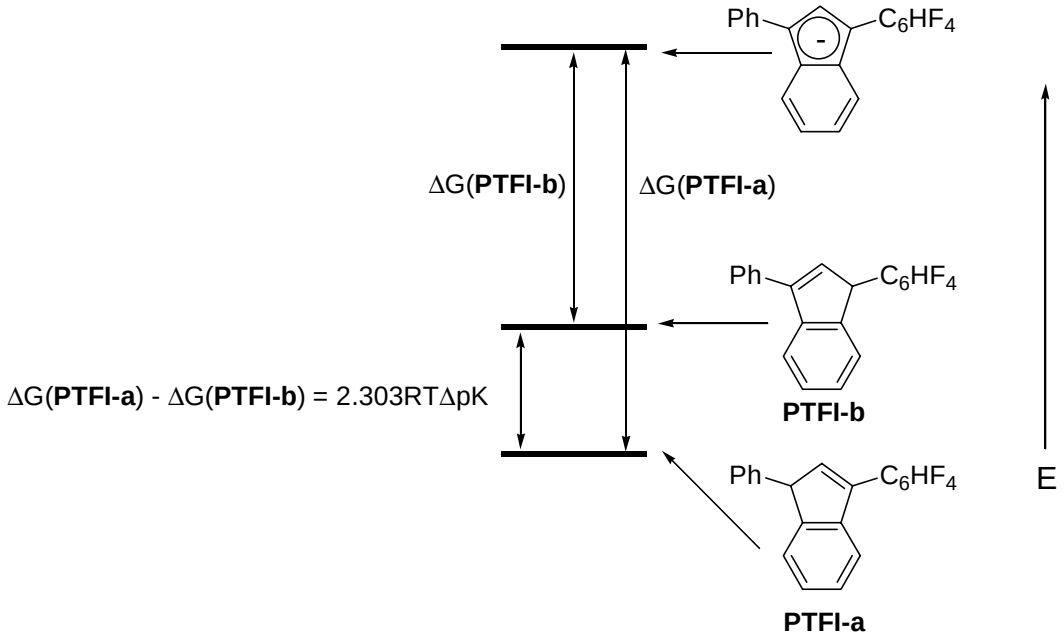

Figure 3.10. Energy diagram for **PTFI-a/b** and conjugate base.

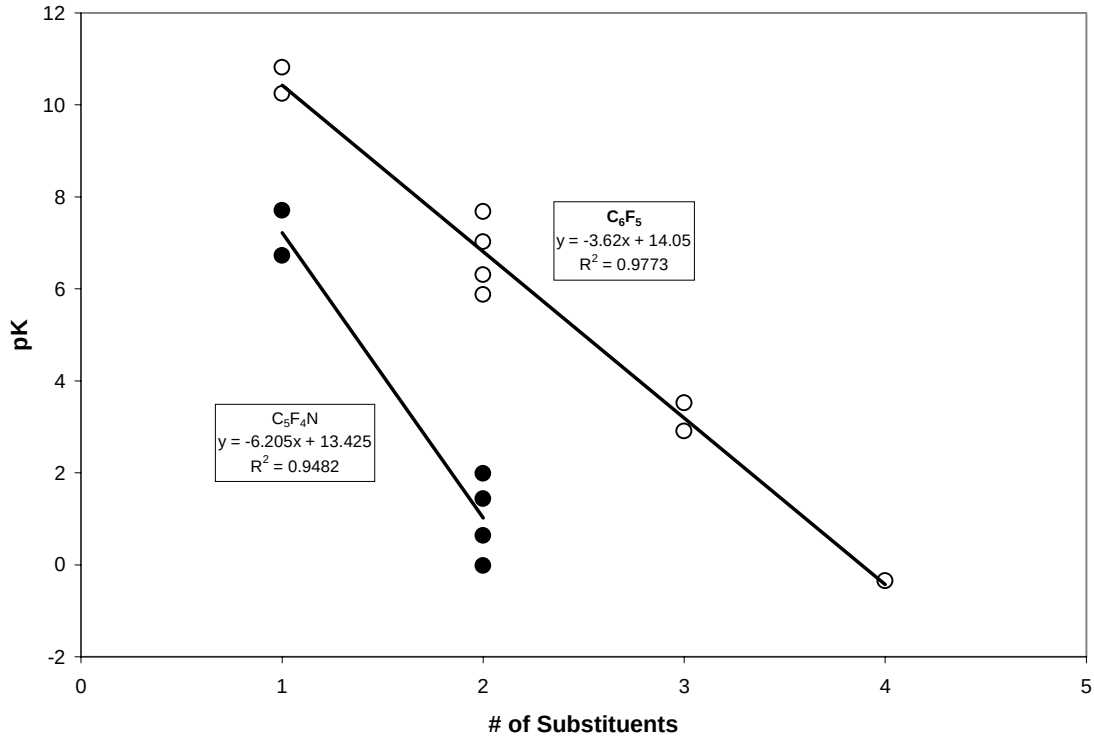

Figure 3.11. Plot of pK vs. the number of aryl substituents

units while the C_5F_4N group increases acidity by 6.9(2) pK units.

The extent of alkyl s ubstitution in the acids is the third feature influencing pK. The pK values in Figure 3.8 increase with increasing alkyl (methyl and *t*-butyl) substitution. The three highest pK values were obtained for acids containing two or three methyl groups in addition to two C_6F_5 groups. Comparison of compounds **7a** and **7b** with **2a** and **2b** reveals that the addition of three methyl substituents increases the pK by approximately 6 units (approx. 2 pK units per methyl group). Comparison of **8** and **14a** shows that two methyl substituents increase the pK by 3.5 pK units (approx. 2 pK units per methyl group). Comparison of **9** and **14a** reveals that a *t*-butyl substituent raises the pK by approximately 2 pK units. These decreases in acidity can be attributed to several factors. The alkyl substituents can destabilize the anionic conjugate base through an electron-donating effect. An increase in the alkene substitution has a stabilizing effect on the acid. Finally, steric congestion arising from alkyl substitution can limit the C_6F_5 stabilizing effect on the Cp anion (see below). All of these factors can increase the energy gap between the acid and conjugate base which results in the compounds decreased acidity.

The conjugation in each acid is the fourth factor affecting acidity. Analysis of the double bond isomer pairs **1a**/**b**, **2a**/**b**, **11a**/**b**, and **13a/b** reveals that the isomer of each pair that contains

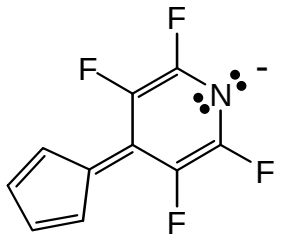

Figure 3.12. Cp-C_6F_4N anion resonance structure.

a cross-conjugated aryl group is more acidic. Therefore, fully-conjugated aryl substituents better stabilize the acids relative to cross-conjugated aryl substituents. As was previously described in Figure 3.10, if two isomers have the same conjugate base then the more stable isomer is the least acidic. DFT calculations agree qualitatively with these findings and show **1a** to be more stable than **1b** (calc. = 3.2 kcal/mol; exp. = 0.8 kcal/mol) and **2a** to be more stable than **2b** (calc. = 1.9 kcal/mol; exp. = 0.6 kcal/mol).

The extent of substituent crowding is the fifth and final factor affecting acidity. A comparison of **12a** and **13b** or **14a** and **2b** suggests that the crowding of adjacent aryl groups decreases acidity by approximately 2 pK units. Importantly, regioisomerism is not relevant in

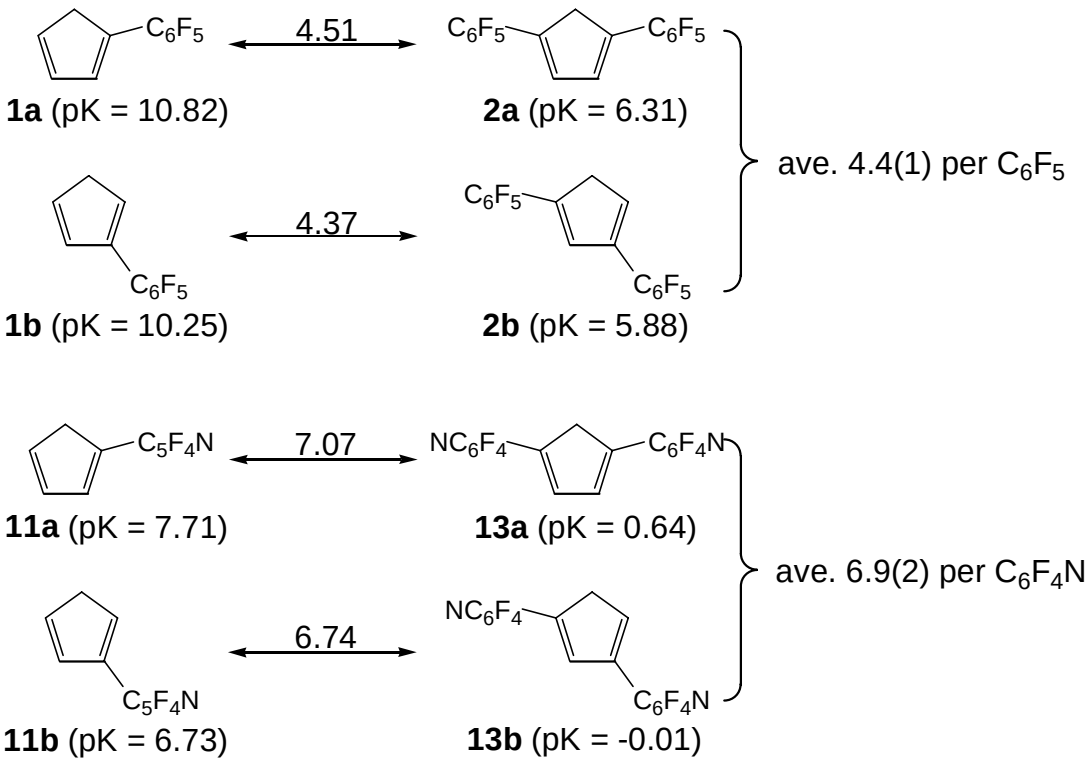

Figure 3.13. pK decrease per aryl substituent.

this example, as both acids possess one fully conjugated and one cross conjugated C_5F_4N group. The steric crowding associated with two vicinal substituents destabilizes both the acid and conjugate base. However, this destabilization is probably more exaggerated in the anionic base where electron-accepting resonance structures require coplanarity between the Cp and aryl planes (see Figures 2.12 and 3.12). The steric crowding inhibits these resonance contributors and destabilizes the conjugate base. As a result, **12a** and **14a** are less acidic than **13b** and **2b** because of vicinal crowding which increases the energy difference between the acid and conjugate base.

Conclusion

^{19}F NMR spectroscopy was shown to be an invaluable tool for determining concentrations in fluorine-containing equilibrium mixtures. Using this technique, the acidities for various cyclopentadiene and indene acids were obtained. The data show that fluorinated aryl groups (C_6F_5 and C_5F_4N) have a substantial acidifying effect in these acids. Additionally, the type and number of substituents, the nature of conjugation, and the intramolecular steric effects all influence acidity. Although the observed acidities are not entirely predictable, the trends improve our understanding of factors controlling acidities in carbon acids.

Experimental Section

General Procedures. Fluorene and *n*-butyllithium were used as received from Aldrich. Fluorenyllithium was prepared by reacting fluorene with an excess of *n*-butyllithium in hexane for one day. A yellow precipitate was collected on a filter, washed with additional hexane, and vacuum-dried to afford a quantitative yield of fluorenyllithium. Acids **3**, **4**, **5**, **6a/b** were prepared as described in the preceding chapter. Acids **1a/b**, **2a/b**, **10**, and **PTFI-a/b** were prepared as previously reported.[91,93,94,96,129] Syntheses for acids **11a/b**, **12a/b**, and **13a/b** have been communicated orally.[134] Acids **7a/b**, **8**, **9** and **14a/b** were prepared by coworkers and synthetic procedures have not yet been published. All acids were sublimed and transferred to a glovebox prior to use to ensure the removal of all water. All NMR experiments used a Varian Unity (400) instrument. THF-d_8 was vacuum-transferred from Na/K alloy. ^{19}F NMR spectra were referenced to external C_6F_6 in $CDCl_3$ at -163.00 ppm. Pulse delays of 10 sec were employed. Longer pulse delays produced no significant changes in the integrated spectra. Density functional calculations (pBP/DN*) were performed on a PC using Wavefunction's PC Spartan Pro (2000) software to calculate equilibrium geometries and energies.

Sample NMR Experiment. In a glovebox, 20 mg (0.035 mmol) each of **3** and **4** were placed in a resealable J-Young NMR tube which had been baked out in an oven for at least 24 h. Fluorenyllithium (5 mg, 0.03 mmol) was subsequently added to the tube. The NMR tube was sealed, transferred to a high vacuum line, and evacuated. Then, approximately 0.5 mL of THF-d_8 was vacuum-transferred into the tube. The tube was then backfilled with argon, warmed to room temperature, sealed, and shaken thoroughly. A minimum of three ^{19}F NMR spectra were taken over a 3-day period to ensure that equilibrium was reached. All reported ΔpK values represent an average of three equilibrium spectra.

Table 3.3. Integrations from the ^{19}F NMR equilibrium spectra.

spectra = AG1F	1a	+	1b	+	PTFI (cb)	⇆	1 (cb)	+	PTFI-b	+	PTFI-a	K_{eq}	|Δ pK|
ortho (1)	42.48		10.61		--		1.88		39.04		15.48	0.054	1.27
ortho (2)													
ortho (3)													
para (1)	20.94		5.51				1.00						
para (2)													
para (3)													
meta (1)	41.66		--		36.40		2.02		36.30		--		
meta (2)													
meta (3)													
# of eq. rings (1)	1		1		1		1		1		1		
# of eq. rings (2)													
# of eq. rings (3)													
relative integral	21.02		5.37		18.20		0.98		18.84		7.74		
mole fraction	0.29		0.07		0.25		0.01		0.26		0.11		
spectra = AG2F	**1a**	**+**	**1b**	**+**	**PTFI (cb)**	**⇆**	**1 (cb)**	**+**	**PTFI-b**	**+**	**PTFI-a**	**K_{eq}**	**|Δ pK|**
ortho (1)	46.79		11.25		--		2.13		43.72		19.86	0.054	1.26
ortho (2)													
ortho (3)													
para (1)	22.73		6.72				1.00						
para (2)													
para (3)													
meta (1)	46.00		--		43.32		2.12		47.04		--		
meta (2)													
meta (3)													
# of eq. rings (1)	1		1		1		1		1		1		
# of eq. rings (2)													
# of eq. rings (3)													
relative integral	23.10		5.99		21.66		1.05		22.69		9.93		
mole fraction	0.27		0.07		0.26		0.01		0.27		0.12		
spectra = AG3F	**1a**	**+**	**1b**	**+**	**PTFI (cb)**	**⇆**	**1 (cb)**	**+**	**PTFI-b**	**+**	**PTFI-a**	**K_{eq}**	**|Δ pK|**
ortho (1)	47.74		11.32		--		2.35		52.32		21.74	0.055	1.26
ortho (2)													
ortho (3)													
para (1)	23.41		7.27				1.00						
para (2)													
para (3)													
meta (1)	46.89		--		47.26		2.08		47.84		--		
meta (2)													
meta (3)													
# of eq. rings (1)	1		1		1		1		1		1		
# of eq. rings (2)													
# of eq. rings (3)													
relative integral	23.61		6.20		23.63		1.09		25.04		10.87		
mole fraction	0.26		0.07		0.26		0.01		0.28		0.12		
Average:												0.055	1.26

Table 3.4. Integrations from the ^{19}F NMR equilibrium spectra.

spectra = AH1F	12a	+	12b	+	3 (cb)	⇆	12 (cb)	+	3	K_{eq}	|Δ pK|
ortho (1)	4.91		--		2.54		34.58		21.47	25.29	1.40
ortho (2)	--				4.68				21.47		
ortho (3)									21.76		
para (1)					1				10.38		
para (2)					2.06				10.40		
para (3)									10.36		
meta (1)	5.25		3.02		2.11		36.38		20.51		
meta (2)	5.31				4.22				20.48		
meta (3)									--		
# of eq. rings (1)	1		2		1		2		1		
# of eq. rings (2)	1				2				1		
# of eq. rings (3)									1		
relative integral	2.58		0.76		1.11		8.87		10.52		
mole fraction	0.11		0.03		0.05		0.37		0.44		
spectra = AH2F	**12a**	**+**	**12b**	**+**	**3 (cb)**	**⇆**	**12 (cb)**	**+**	**12**	**K_{eq}**	**|Δ pK|**
ortho (1)	9.32		--		2.63		39.28		33.85	23.86	1.38
ortho (2)	--				4.56				33.85		
ortho (3)									34.57		
para (1)					1.16				16.24		
para (2)					2.00				16.36		
para (3)									16.45		
meta (1)	10.10		5.73		2.04		41.27		32.18		
meta (2)	10.24				4.09				32.27		
meta (3)									--		
# of eq. rings (1)	1		2		1		2		1		
# of eq. rings (2)	1				2				1		
# of eq. rings (3)									1		
relative integral	4.94		1.43		1.10		10.07		16.60		
mole fraction	0.14		0.04		0.03		0.29		0.49		
spectra = AH3F	**12a**	**+**	**12b**	**+**	**3 (cb)**	**⇆**	**12 (cb)**	**+**	**12**	**K_{eq}**	**|Δ pK|**
ortho (1)	10.83		--		--		41.28		38.58	24.86	1.40
ortho (2)	--				4.68				38.58		
ortho (3)									39.40		
para (1)					1.21				18.51		
para (2)					2				18.65		
para (3)									18.73		
meta (1)	11.94		6.71		2.06		43.72		36.96		
meta (2)	12.09				4.12				37.11		
meta (3)									--		
# of eq. rings (1)	1		2		1		2		1		
# of eq. rings (2)	1				2				1		
# of eq. rings (3)									1		
relative integral	5.81		1.68		1.08		10.63		18.96		
mole fraction	0.15		0.04		0.03		0.28		0.50		
Average:										24.67	1.39

Table 3.5. Integrations from the ^{19}F NMR equilibrium spectra.

spectra = Al1F	11a + 11b + 9 (cb) ⇆ 11 (cb) + 9					K_{eq}	|Δ pK|
ortho (1)	22.58	--	2.37	42.14	64.58	102.21	2.01
ortho (2)					64.14		
ortho (3)							
para (1)			1.00		31.28		
para (2)					31.13		
para (3)							
meta (1)	--	2.66	1.86	43.42	61.16		
meta (2)					63.10		
meta (3)							
# of eq. rings (1)	1	1	2	1	1		
# of eq. rings (2)					1		
# of eq. rings (3)							
relative integral	11.29	1.33	0.52	21.39	31.54		
mole fraction	0.17	0.02	0.01	0.32	0.48		
spectra = Al2F	**11a + 11b + 9 (cb) ⇆ 11 (cb) + 9**					**K_{eq}**	**|Δ pK|**
ortho (1)	19.45	--	2.59	38.92	63.32	103.38	2.01
ortho (2)					63.05		
ortho (3)							
para (1)			1.00		30.86		
para (2)					30.78		
para (3)							
meta (1)	--	2.09	1.95	40.40	60.28		
meta (2)					62.77		
meta (3)							
# of eq. rings (1)	1	1	2	1	1		
# of eq. rings (2)					1		
# of eq. rings (3)							
relative integral	9.73	1.05	0.55	19.83	31.11		
mole fraction	0.16	0.02	0.01	0.32	0.50		
spectra = Al3F	**11a + 11b + 9 (cb) ⇆ 11 (cb) + 9**					**K_{eq}**	**|Δ pK|**
ortho (1)	16.84	--	2.56	34.83	57.86	96.69	1.99
ortho (2)					57.57		
ortho (3)							
para (1)			1.00		28.62		
para (2)					28.48		
para (3)							
meta (1)	--	2.20	1.99	36.43	56.63		
meta (2)					57.59		
meta (3)							
# of eq. rings (1)	1	1	2	1	1		
# of eq. rings (2)					1		
# of eq. rings (3)							
relative integral	8.42	1.10	0.56	17.82	28.68		
mole fraction	0.15	0.02	0.01	0.31	0.51		
Average:						100.76	2.00

Table 3.6. Integrations from the ^{19}F NMR equilibrium spectra.

spectra = AJ4F	2a	+	2b	+	3 (cb)	⇆	2 (cb)	+	3	K_{eq}	|Δ pK|
ortho (1)	180.80		--		119.95		1.74		--	0.0012	2.94
ortho (2)			--		236.58				--		
ortho (3)									--		
para (1)	86.77		15.94		56.28		1.00		8.78		
para (2)			16.27		113.61				9.08		
para (3)									9.15		
meta (1)	--		33.38		115.60		--		17.70		
meta (2)			--		231.19				18.12		
meta (3)									--		
# of eq. rings (1)	2		1		1		2		1		
# of eq. rings (2)			1		2				1		
# of eq. rings (3)									1		
relative integral	44.60		16.40		58.21		0.46		8.98		
mole fraction	0.35		0.13		0.45		0.00		0.07		
spectra = AJ2F	**2a**	**+**	**2b**	**+**	**3 (cb)**	**⇆**	**2 (cb)**	**+**	**3**	**K_{eq}**	**|Δ pK|**
ortho (1)	149.19		--		101.37		1.90		--	0.0012	2.94
ortho (2)			--		201.91				--		
ortho (3)									--		
para (1)	72.60		13.33		48.32		1.00		5.94		
para (2)			13.25		96.58				6.14		
para (3)									6.14		
meta (1)	--		28.23		98.90		1.86		12.03		
meta (2)			--		197.79				12.41		
meta (3)									--		
# of eq. rings (1)	2		1		1		2		1		
# of eq. rings (2)			1		2				1		
# of eq. rings (3)									1		
relative integral	36.97		13.70		49.66		0.48		6.09		
mole fraction	0.35		0.13		0.46		0.00		0.06		
spectra = AJ3F	**2a**	**+**	**2b**	**+**	**3 (cb)**	**⇆**	**2 (cb)**	**+**	**3**	**K_{eq}**	**|Δ pK|**
ortho (1)	183.45		--		123.51		2.00		--	0.0011	2.97
ortho (2)			--		247.03				--		
ortho (3)									--		
para (1)	88.39		16.72		59.14		1.02		8.13		
para (2)			16.33		119.50				8.37		
para (3)									8.29		
meta (1)	--		34.63		120.72		--		15.86		
meta (2)			--		241.44				16.29		
meta (3)									--		
# of eq. rings (1)	2		1		1		2		1		
# of eq. rings (2)			1		2				1		
# of eq. rings (3)									1		
relative integral	45.31		16.92		60.76		0.50		8.13		
mole fraction	0.34		0.13		0.46		0.00		0.06		
Average:										0.0011	2.95

Table 3.7. Integrations from the ^{19}F NMR equilibrium spectra.

spectra = AE1F	1a	+	1b	+	8 (cb)	⇆	1 (cb)	+	8	K_{eq}	|Δ pK|
ortho (1)	48.75		--		24.85		--		102.30	1.88	0.27
ortho (2)					22.15				104.20		
ortho (3)											
para (1)	23.87		6.56		10.52		12.30		50.49		
para (2)					10.15				50.31		
para (3)											
meta (1)	48.20		--		23.13		27.37		99.63		
meta (2)					25.51				100.52		
meta (3)											
# of eq. rings (1)	1		1		1		1		1		
# of eq. rings (2)					1				1		
# of eq. rings (3)											
relative integral	24.16		6.56		11.63		13.22		50.75		
mole fraction	0.23		0.06		0.11		0.12		0.48		
spectra = AE2F	**1a**	**+**	**1b**	**+**	**8 (cb)**	**⇆**	**1 (cb)**	**+**	**8**	**K_{eq}**	**|Δ pK|**
ortho (1)	6.24		--		2.73		--		13.01	1.83	0.26
ortho (2)					2.21				13.09		
ortho (3)											
para (1)	2.99		0.82		1.02		1.21		6.18		
para (2)					1.00				6.31		
para (3)											
meta (1)	6.01		--		2.53		2.93		12.49		
meta (2)					2.90				12.64		
meta (3)											
# of eq. rings (1)	1		1		1		1		1		
# of eq. rings (2)					1				1		
# of eq. rings (3)											
relative integral	3.05		0.82		1.24		1.38		6.37		
mole fraction	0.24		0.06		0.10		0.11		0.50		
spectra = AE3F	**1a**	**+**	**1b**	**+**	**8 (cb)**	**⇆**	**1 (cb)**	**+**	**8**	**K_{eq}**	**|Δ pK|**
ortho (1)	45.79		--		16.47		--		95.22	1.79	0.25
ortho (2)					13.00				95.47		
ortho (3)											
para (1)	21.84		6.21		5.94		6.86		45.79		
para (2)					5.81				46.27		
para (3)											
meta (1)	43.88		--		16.04		18.13		90.99		
meta (2)					18.75				92.09		
meta (3)											
# of eq. rings (1)	1		1		1		1		1		
# of eq. rings (2)					1				1		
# of eq. rings (3)											
relative integral	22.30		6.21		7.60		8.33		46.58		
mole fraction	0.25		0.07		0.08		0.09		0.51		
Average:										1.83	0.26

Table 3.8. Integrations from the ^{19}F NMR equilibrium spectra.

spectra = AC3F	11a +	11b +	10 (cb) ⇆	11 (cb) +	10	K_{eq}	|Δ pK|
ortho (1)	49.04	--	--	6.89	--	0.063	1.20
ortho (2)					--		
ortho (3)							
para (1)			68.69		16.79		
para (2)					16.69		
para (3)							
meta (1)	--	4.86	141.71	7.46	33.31		
meta (2)					32.99		
meta (3)							
# of eq. rings (1)	1	1	2	1	1		
# of eq. rings (2)					1		
# of eq. rings (3)							
relative integral	24.52	2.43	35.07	3.59	16.63		
mole fraction	0.30	0.03	0.43	0.04	0.20		
spectra = AC4F	**11a +**	**11b +**	**10 (cb) ⇆**	**11 (cb) +**	**10**	**K_{eq}**	**|Δ pK|**
ortho (1)	59.46	--	--	8.29	--	0.064	1.20
ortho (2)					--		
ortho (3)							
para (1)			92.11		22.25		
para (2)					22.23		
para (3)							
meta (1)	--	4.86	190.41	9.12	44.39		
meta (2)					44.04		
meta (3)							
# of eq. rings (1)	1	1	2	1	1		
# of eq. rings (2)					1		
# of eq. rings (3)							
relative integral	29.73	2.43	47.09	4.35	22.15		
mole fraction	0.28	0.02	0.45	0.04	0.21		
spectra = AC5F	**11a +**	**11b +**	**10 (cb) ⇆**	**11 (cb) +**	**10**	**K_{eq}**	**|Δ pK|**
ortho (1)	55.44	--	--	8.22	--	0.066	1.18
ortho (2)					--		
ortho (3)							
para (1)			99.06		23.78		
para (2)					23.69		
para (3)							
meta (1)	--	4.86	205.28	8.98	47.31		
meta (2)					46.79		
meta (3)							
# of eq. rings (1)	1	1	2	1	1		
# of eq. rings (2)					1		
# of eq. rings (3)							
relative integral	27.72	2.43	50.72	4.30	23.60		
mole fraction	0.25	0.02	0.47	0.04	0.22		
Average:						0.064	1.19

Table 3.9. Integrations from the ^{19}F NMR equilibrium spectra.

spectra = Y2F	8	+	9 (cb)	⇆	8 (cb)	+	9	K_{eq}	|Δ pK|
ortho (1)	30.24		41.80		--		12.33	0.046	1.33
ortho (2)	--				2.04		--		
ortho (3)									
para (1)	14.59		20.38		--		6.13		
para (2)	14.75				1.00		6.08		
para (3)									
meta (1)	29.53		41.32		2.49		12.79		
meta (2)	--				2.51		--		
meta (3)									
# of eq. rings (1)	1		2		1		1		
# of eq. rings (2)	1				1		1		
# of eq. rings (3)									
relative integral	14.85		10.35		1.15		6.22		
mole fraction	0.46		0.32		0.04		0.19		
spectra = Y3F	**8**	**+**	**9 (cb)**	**⇆**	**8 (cb)**	**+**	**9**	**K_{eq}**	**|Δ pK|**
ortho (1)	31.64		43.45		--		13.99	0.044	1.36
ortho (2)	--				2.00		--		
ortho (3)									
para (1)	15.49		20.85		--		6.97		
para (2)	15.82				1.00		6.87		
para (3)									
meta (1)	31.30		42.23		--		14.37		
meta (2)	--				2.19		--		
meta (3)									
# of eq. rings (1)	1		2		1		1		
# of eq. rings (2)	1				1		1		
# of eq. rings (3)									
relative integral	15.71		10.65		1.04		7.03		
mole fraction	0.46		0.31		0.03		0.20		
spectra = Y4F	**8**	**+**	**9 (cb)**	**⇆**	**8 (cb)**	**+**	**9**	**K_{eq}**	**|Δ pK|**
ortho (1)	35.72		45.81		--		18.74	0.048	1.31
ortho (2)	--				2.06		--		
ortho (3)									
para (1)	17.47		22.29		1.00		9.23		
para (2)	--				0.90		9.08		
para (3)									
meta (1)	35.83		45.16		--		19.32		
meta (2)	--				2.28		--		
meta (3)									
# of eq. rings (1)	1		2		1		1		
# of eq. rings (2)	1				1		1		
# of eq. rings (3)									
relative integral	17.80		11.33		1.04		9.40		
mole fraction	0.45		0.29		0.03		0.24		
Average:								0.046	1.34

Table 3.10. Integrations from the ^{19}F NMR equilibrium spectra.

spectra = AM1F	2a	+	2b	+	10 (cb)	⇆	2 (cb)	+	10	K_{eq}	|Δ pK|
ortho (1)	11.28		2.07		14.57		17.62		8.06	1.28	0.11
ortho (2)			2.00						8.13		
ortho (3)											
para (1)	5.58		1.04		6.96		8.55		3.95		
para (2)			1.04						3.98		
para (3)											
meta (1)	--		2.05		14.17		17.33		8.09		
meta (2)			--						8.05		
meta (3)											
# of eq. rings (1)	2		1		2		2		1		
# of eq. rings (2)			1						1		
# of eq. rings (3)											
relative integral	2.81		1.03		3.57		4.35		4.03		
mole fraction	0.18		0.06		0.23		0.28		0.26		
spectra = AM2F	**2a**	**+**	**2b**	**+**	**10 (cb)**	**⇆**	**2 (cb)**	**+**	**10**	**K_{eq}**	**|Δ pK|**
ortho (1)	11.30		2.09		14.91		17.93		8.28	1.31	0.12
ortho (2)			2.00						8.49		
ortho (3)											
para (1)	5.64		1.04		6.83		8.59		4.07		
para (2)			1.04						4.06		
para (3)											
meta (1)	--		2.08		14.39		17.41		8.34		
meta (2)			--						8.23		
meta (3)											
# of eq. rings (1)	2		1		2		2		1		
# of eq. rings (2)			1						1		
# of eq. rings (3)											
relative integral	2.82		1.03		3.61		4.39		4.15		
mole fraction	0.18		0.06		0.23		0.27		0.26		
spectra = AM3F	**2a**		**2b**		**10 (cb)**	**⇆**	**2 (cb)**		**10**	**K_{eq}**	**|Δ pK|**
ortho (1)	10.69		2.02		14.34		16.89		7.89	1.28	0.11
ortho (2)			1.90						7.96		
ortho (3)											
para (1)	5.34		1.00		6.63		8.07		3.88		
para (2)			1.00						3.87		
para (3)											
meta (1)	--		1.98		13.82		16.34		7.92		
meta (2)			--						7.81		
meta (3)											
# of eq. rings (1)	2		1		2		2		1		
# of eq. rings (2)			1						1		
# of eq. rings (3)											
relative integral	2.67		0.99		3.48		4.13		3.93		
mole fraction	0.18		0.06		0.23		0.27		0.26		
Average:										1.29	0.11

Table 3.11. Integrations from the ^{19}F NMR equilibrium spectra.

spectra = W1F	2a	+	2b	+	3 (cb)	⇆	2 (cb)	+	3	K_{eq}	|Δ pK|
ortho (1)	144.45		--		88.75		9.48		--	0.0012	2.93
ortho (2)			--		175.19				--		
ortho (3)									--		
para (1)	66.75		12.25		39.22		4.31		1.00		
para (2)			12.07		78.47				1.06		
para (3)									1.08		
meta (1)	--		25.14		80.23		8.55		1.98		
meta (2)			--		160.46				2.07		
meta (3)									2.13		
# of eq. rings (1)	2		1		1		2		1		
# of eq. rings (2)			1		2				1		
# of eq. rings (3)									1		
relative integral	35.20		12.37		41.49		2.23		1.04		
mole fraction	0.38		0.13		0.45		0.02		0.01		
spectra = W2F	**2a**	**+**	**2b**	**+**	**3 (cb)**	**⇆**	**2 (cb)**	**+**	**3**	**K_{eq}**	**|Δ pK|**
ortho (1)	86.62		--		50.06		3.74		--	0.0012	2.91
ortho (2)			--		101.37				--		
ortho (3)									--		
para (1)	42.44		7.76		24.60		1.81		0.92		
para (2)			7.88		49.70				1.01		
para (3)									1.00		
meta (1)	--		16.00		50.81		3.99		1.89		
meta (2)			--		101.63				1.89		
meta (3)									1.99		
# of eq. rings (1)	2		1		1		2		1		
# of eq. rings (2)			1		2				1		
# of eq. rings (3)									1		
relative integral	21.51		7.91		25.21		0.95		0.97		
mole fraction	0.38		0.14		0.45		0.02		0.02		
spectra = W3F	**2a**	**+**	**2b**	**+**	**3 (cb)**	**⇆**	**2 (cb)**	**+**	**3**	**K_{eq}**	**|Δ pK|**
ortho (1)	70.19		--		41.46		2.30		--	0.0012	2.92
ortho (2)			--		81.97				--		
ortho (3)									--		
para (1)	34.21		6.31		19.60		1.20		0.94		
para (2)			6.26		39.45				1.00		
para (3)									1.00		
meta (1)	--		13.20		40.43		2.39		1.90		
meta (2)			--		80.87				2.00		
meta (3)									2.07		
# of eq. rings (1)	2		1		1		2		1		
# of eq. rings (2)			1		2				1		
# of eq. rings (3)									1		
relative integral	17.40		6.44		20.25		0.59		0.99		
mole fraction	0.38		0.14		0.44		0.01		0.02		
Average:										0.0012	2.92

Table 3.12. Integrations from the ^{19}F NMR equilibrium spectra.

spectra = V1F	PTFI-b	+	PTFI-a	+	9 (cb)	⇆	PTFI (cb)	+	9	K_{eq}	|Δ pK|
ortho (1)	2.14		1.00		6.38		--		3.50	1.26	0.10
ortho (2)									3.50		
ortho (3)											
para (1)					2.86				1.63		
para (2)									1.63		
para (3)											
meta (1)	--		--		5.81		3.56		3.33		
meta (2)									3.16		
meta (3)											
# of eq. rings (1)	1		1		2		1		1		
# of eq. rings (2)									1		
# of eq. rings (3)											
relative integral	1.07		0.50		1.51		1.78		1.68		
mole fraction	0.16		0.08		0.23		0.27		0.26		
spectra = V2F	**PTFI-b**	**+**	**PTFI-a**	**+**	**9 (cb)**	**⇆**	**PTFI (cb)**	**+**	**9**	**K_{eq}**	**|Δ pK|**
ortho (1)	2.12		1.00		6.35		--		3.45	1.27	0.10
ortho (2)									3.46		
ortho (3)											
para (1)					2.79				1.63		
para (2)									1.62		
para (3)											
meta (1)	--		--		5.67		3.53		3.14		
meta (2)									3.32		
meta (3)											
# of eq. rings (1)	1		1		2		1		1		
# of eq. rings (2)									1		
# of eq. rings (3)											
relative integral	1.06		0.50		1.48		1.77		1.66		
mole fraction	0.16		0.08		0.23		0.27		0.26		
spectra = V3F	**PTFI-b**	**+**	**PTFI-a**	**+**	**9 (cb)**	**⇆**	**PTFI (cb)**	**+**	**9**	**K_{eq}**	**|Δ pK|**
ortho (1)	2.04		1.00		6.13		--		3.34	1.22	0.09
ortho (2)									3.29		
ortho (3)											
para (1)					2.97				1.65		
para (2)									1.64		
para (3)											
meta (1)	--		--		6.01		3.38		3.30		
meta (2)									3.42		
meta (3)											
# of eq. rings (1)	1		1		2		1		1		
# of eq. rings (2)									1		
# of eq. rings (3)											
relative integral	1.02		0.50		1.51		1.69		1.66		
mole fraction	0.16		0.08		0.24		0.26		0.26		
Average:										1.25	0.10

Table 3.13. Integrations from the ^{19}F NMR equilibrium spectra.

spectra = U1F	12a	+	12b	+	13 (cb)	⇆	12 (cb)	+	13a	+	13b	K_{eq}	|Δ pK|
ortho (1)	38.03		--		113.26		39.34		--		--	0.043	1.37
ortho (2)	--										--		
ortho (3)													
para (1)													
para (2)													
para (3)													
meta (1)	35.95		20.39		106.17		35.97		9.63		0.98		
meta (2)	35.64										--		
meta (3)													
# of eq. rings (1)	1		2		2		2		2		1		
# of eq. rings (2)	1										1		
# of eq. rings (3)													
relative integral	18.27		5.10		27.43		9.41		2.41		0.49		
mole fraction	0.29		0.08		0.43		0.15		0.04		0.01		
spectra = U2F	**12a**	**+**	**12b**	**+**	**13 (cb)**	**⇆**	**12 (cb)**	**+**	**13a**	**+**	**13b**	**K_{eq}**	**|Δ pK|**
ortho (1)	30.06		--		85.89		23.99		--		--	0.043	1.37
ortho (2)	--										--		
ortho (3)													
para (1)													
para (2)													
para (3)													
meta (1)	28.85		16.26		80.05		21.87		9.49		0.99		
meta (2)	28.54										--		
meta (3)													
# of eq. rings (1)	1		2		2		2		2		1		
# of eq. rings (2)	1										1		
# of eq. rings (3)													
relative integral	14.58		4.07		20.74		5.73		2.37		0.50		
mole fraction	0.30		0.08		0.43		0.12		0.05		0.01		
spectra = U3F	**12a**	**+**	**12b**	**+**	**13 (cb)**	**⇆**	**12 (cb)**	**+**	**13a**	**+**	**13b**	**K_{eq}**	**|Δ pK|**
ortho (1)	19.41		--		49.29		10.32		--		--	0.043	1.37
ortho (2)	--										--		
ortho (3)													
para (1)													
para (2)													
para (3)													
meta (1)	19.86		11.13		49.59		9.73		8.70		1.00		
meta (2)	19.58										--		
meta (3)													
# of eq. rings (1)	1		2		2		2		2		1		
# of eq. rings (2)	1										1		
# of eq. rings (3)													
relative integral	9.81		2.78		12.36		2.51		2.18		0.50		
mole fraction	0.33		0.09		0.41		0.08		0.07		0.02		
Average:												0.043	1.37

Table 3.14. Integrations from the ^{19}F NMR equilibrium spectra.

spectra = S2F	1a	+	1b	+	9 (cb)	⇆	1 (cb)	+	9	K_{eq}	|Δ pK|
ortho (1)	--		3.35		--		--		23.54	0.068	1.16
ortho (2)									--		
ortho (3)											
para (1)	5.89		--		20.15		--		11.11		
para (2)									11.07		
para (3)											
meta (1)	13.41		--		41.61		1.00		22.38		
meta (2)									23.24		
meta (3)											
# of eq. rings (1)	1		1		2		1		1		
# of eq. rings (2)									1		
# of eq. rings (3)											
relative integral	6.43		1.68		10.29		0.50		11.42		
mole fraction	0.21		0.06		0.34		0.02		0.38		
spectra = S3F	**1a**	**+**	**1b**	**+**	**9 (cb)**	**⇆**	**1 (cb)**	**+**	**9**	**K_{eq}**	**|Δ pK|**
ortho (1)	--		2.75		--		--		17.07	0.069	1.16
ortho (2)									--		
ortho (3)											
para (1)	4.77		--		17.77		--		7.73		
para (2)									7.68		
para (3)											
meta (1)	10.34		--		37.21		1.02		15.32		
meta (2)									15.60		
meta (3)											
# of eq. rings (1)	1		1		2		1		1		
# of eq. rings (2)									1		
# of eq. rings (3)											
relative integral	5.04		1.38		9.16		0.51		7.93		
mole fraction	0.21		0.06		0.38		0.02		0.33		
spectra = S4F	**1a**	**+**	**1b**	**+**	**9 (cb)**	**⇆**	**1 (cb)**	**+**	**9**	**K_{eq}**	**|Δ pK|**
ortho (1)	--		2.29		--		--		12.14	0.069	1.16
ortho (2)									--		
ortho (3)											
para (1)	3.96		--		14.89		--		5.55		
para (2)									5.48		
para (3)											
meta (1)	8.47		--		31.32		1.00		10.74		
meta (2)									10.96		
meta (3)											
# of eq. rings (1)	1		1		2		1		1		
# of eq. rings (2)									1		
# of eq. rings (3)											
relative integral	4.14		1.15		7.70		0.50		5.61		
mole fraction	0.22		0.06		0.40		0.03		0.29		
Average:										0.069	1.16

Table 3.15. Integrations from the ^{19}F NMR equilibrium spectra.

spectra = Q1F	13a	+	13b	+	5 (cb)	⇆	13 (cb)	+	5	K_{eq}	|Δ pK|
ortho (1)	--		0.49		--		1.00		1.69	0.094	1.03
ortho (2)			--		3.35				1.74		
ortho (3)											
para (1)					1.51				0.74		
para (2)					1.54				0.73		
para (3)											
meta (1)	4.32		--		3.09		0.91		1.69		
meta (2)			0.53		3.15				1.74		
meta (3)											
# of eq. rings (1)	2		1		2		2		2		
# of eq. rings (2)			1		2				2		
# of eq. rings (3)											
relative integral	1.08		0.26		0.79		0.24		0.42		
mole fraction	0.39		0.09		0.28		0.09		0.15		
spectra = Q2F	**13a**	**+**	**13b**	**+**	**5 (cb)**	**⇆**	**13 (cb)**	**+**	**5**	**K_{eq}**	**|Δ pK|**
ortho (1)	--		0.55		--		1.09		1.89	0.090	1.05
ortho (2)			--		3.69				1.94		
ortho (3)											
para (1)					1.71				0.84		
para (2)					1.72				0.82		
para (3)											
meta (1)	4.77		--		3.43		1.00		1.70		
meta (2)			0.58		3.52				1.74		
meta (3)											
# of eq. rings (1)	2		1		2		2		2		
# of eq. rings (2)			1		2				2		
# of eq. rings (3)											
relative integral	1.19		0.28		0.88		0.26		0.45		
mole fraction	0.39		0.09		0.29		0.09		0.15		
spectra = Q3F	**13a**	**+**	**13b**	**+**	**5 (cb)**	**⇆**	**13 (cb)**	**+**	**5**	**K_{eq}**	**|Δ pK|**
ortho (1)	--		1.00		--		2.09		3.77	0.090	1.04
ortho (2)			--		7.22				3.89		
ortho (3)											
para (1)					3.33				1.65		
para (2)					3.36				1.63		
para (3)											
meta (1)	9.41		--		6.71		1.92		3.42		
meta (2)			1.14		6.85				3.50		
meta (3)											
# of eq. rings (1)	2		1		2		2		2		
# of eq. rings (2)			1		2				2		
# of eq. rings (3)											
relative integral	2.35		0.54		1.72		0.50		0.89		
mole fraction	0.39		0.09		0.29		0.08		0.15		
Average:										0.092	1.04

Table 3.16. Integrations from the ^{19}F NMR equilibrium spectra.

spectra = P4F	2a	+	2b	+	11 (cb)	⇆	2 (cb)	+	11a	+	11b	K_{eq}	|Δ pK|
ortho (1)	--		--		1.00		44.08		19.68		--	21.5	1.33
ortho (2)			5.29										
ortho (3)													
para (1)	14.16		2.67				19.27						
para (2)			2.60										
para (3)													
meta (1)	--		--		1.00		39.65		17.48		1.69		
meta (2)			--										
meta (3)													
# of eq. rings (1)	2		1		1		2		1		1		
# of eq. rings (2)			1										
# of eq. rings (3)													
relative integral	7.08		2.64		0.50		10.30		9.29		0.85		
mole fraction	0.23		0.09		0.02		0.34		0.30		0.03		
spectra = P5F	**2a**	**+**	**2b**	**+**	**11 (cb)**	**⇆**	**2 (cb)**	**+**	**11a**	**+**	**11b**	**K_{eq}**	**|Δ pK|**
ortho (1)	--		--		1.00		46.17		19.38		--	21.4	1.33
ortho (2)			5.44										
ortho (3)													
para (1)	14.85		2.75				20.05						
para (2)			2.76										
para (3)													
meta (1)	--		--		0.99		41.22		17.50		1.71		
meta (2)			--										
meta (3)													
# of eq. rings (1)	2		1		1		2		1		1		
# of eq. rings (2)			1										
# of eq. rings (3)													
relative integral	7.43		2.74		0.50		10.74		9.22		0.86		
mole fraction	0.24		0.09		0.02		0.34		0.29		0.03		
spectra = P6F	**2a**	**+**	**2b**	**+**	**11 (cb)**	**⇆**	**2 (cb)**	**+**	**11a**	**+**	**11b**	**K_{eq}**	**|Δ pK|**
ortho (1)	--		--		1.00		50.49		19.78		--	21.4	1.33
ortho (2)			6.23										
ortho (3)													
para (1)	16.88		3.20				23.03						
para (2)			3.18										
para (3)													
meta (1)	--		--		1.13		46.87		19.86		2.15		
meta (2)			--										
meta (3)													
# of eq. rings (1)	2		1		1		2		1		1		
# of eq. rings (2)			1										
# of eq. rings (3)													
relative integral	8.44		3.15		0.53		12.04		9.91		1.08		
mole fraction	0.24		0.09		0.02		0.34		0.28		0.03		
Average:												21.4	1.33

Table 3.17. Integrations from the ^{19}F NMR equilibrium spectra.

spectra = O1F	12a	+	12b	+	4 (cb)	⇆	12 (cb)	+	4	K_{eq}	|Δ pK|
ortho (1)	4.42		--		4.65		15.60		10.81	6.62	0.82
ortho (2)	--				2.29				11.03		
ortho (3)									10.94		
para (1)					2.14				5.31		
para (2)					1.00				5.37		
para (3)									5.20		
meta (1)	4.19		2.37		4.29		14.47		10.29		
meta (2)	4.18				2.16				10.29		
meta (3)									10.12		
# of eq. rings (1)	1		2		1		2		1		
# of eq. rings (2)	1				2				1		
# of eq. rings (3)									1		
relative integral	2.13		0.59		1.10		3.76		5.29		
mole fraction	0.17		0.05		0.09		0.29		0.41		
spectra = O2F	**12a**	**+**	**12b**	**+**	**4 (cb)**	**⇆**	**12 (cb)**	**+**	**4**	**K_{eq}**	**|Δ pK|**
ortho (1)	8.09		--		4.76		16.48		18.69	6.46	0.81
ortho (2)	--				2.35				18.78		
ortho (3)									18.67		
para (1)					1.00				8.93		
para (2)					2.18				9.03		
para (3)									8.81		
meta (1)	7.46		4.18		4.42		15.21		17.34		
meta (2)	7.46				2.23				17.34		
meta (3)									17.12		
# of eq. rings (1)	1		2		1		2		1		
# of eq. rings (2)	1				2				1		
# of eq. rings (3)									1		
relative integral	3.84		1.05		1.13		3.96		8.98		
mole fraction	0.20		0.06		0.06		0.21		0.47		
spectra = O3F	**12a**	**+**	**12b**	**+**	**4 (cb)**	**⇆**	**12 (cb)**	**+**	**4**	**K_{eq}**	**|Δ pK|**
ortho (1)	19.22		--		5.11		18.68		43.48	6.51	0.81
ortho (2)	--				2.59				43.21		
ortho (3)									42.98		
para (1)					1.00				20.80		
para (2)					2.32				20.89		
para (3)									20.22		
meta (1)	17.89		10.11		4.82		17.09		39.99		
meta (2)	18.19				2.34				39.99		
meta (3)									39.47		
# of eq. rings (1)	1		2		1		2		1		
# of eq. rings (2)	1				2				1		
# of eq. rings (3)									1		
relative integral	9.22		2.53		1.21		4.47		20.73		
mole fraction	0.24		0.07		0.03		0.12		0.54		
Average:										6.53	0.81

Table 3.18. Integrations from the ^{19}F NMR equilibrium spectra.

spectra = AA3F	7a	+	7b	+	8 (cb)	⇆	7 (cb)	+	8	K_{eq}	|Δ pK|
ortho (1)	--		--		--		--		--	0.07	1.17
ortho (2)			--		4.21				--		
ortho (3)											
para (1)	8.75		3.89		4.42		--		4.65		
para (2)			3.70		4.13				--		
para (3)											
meta (1)	--		--		2.01		1.00		9.39		
meta (2)			--		2.13				--		
meta (3)											
# of eq. rings (1)	2		1		1		2		1		
# of eq. rings (2)			1		1				1		
# of eq. rings (3)											
relative integral	4.38		3.80		2.11		0.25		4.68		
mole fraction	0.29		0.25		0.14		0.02		0.31		
spectra = AA4F	**7a**	**+**	**7b**	**+**	**8 (cb)**	**⇆**	**7 (cb)**	**+**	**8**	**K_{eq}**	**|Δ pK|**
ortho (1)	--		--		--		--		--	0.07	1.16
ortho (2)			--		4.09				--		
ortho (3)											
para (1)	10.54		4.31		1.98		--		5.41		
para (2)			4.29		2.00				--		
para (3)											
meta (1)	--		--		4.35		1.00		10.87		
meta (2)			--		4.01				--		
meta (3)											
# of eq. rings (1)	2		1		1		2		1		
# of eq. rings (2)			1		1				1		
# of eq. rings (3)											
relative integral	5.27		4.30		2.05		0.25		5.43		
mole fraction	0.30		0.25		0.12		0.01		0.31		
spectra = AA5F	**7a**	**+**	**7b**	**+**	**8 (cb)**	**⇆**	**7 (cb)**	**+**	**8**	**K_{eq}**	**|Δ pK|**
ortho (1)	--		--		--		--		--	0.07	1.17
ortho (2)			--		4.28				--		
ortho (3)											
para (1)	12.13		5.10		2.10		--		6.40		
para (2)			4.99		2.00				--		
para (3)											
meta (1)	--		--		4.59		1.00		12.72		
meta (2)			--		4.14				--		
meta (3)											
# of eq. rings (1)	2		1		1		2		1		
# of eq. rings (2)			1		1				1		
# of eq. rings (3)											
relative integral	6.07		5.05		2.14		0.25		6.37		
mole fraction	0.31		0.25		0.11		0.01		0.32		
Average:										0.07	1.17

Table 3.19. Integrations from the ^{19}F NMR equilibrium spectra.

spectra = AQ1F	PTFI-a	+	PTFI-b	+ 14 (cb)	⇆	PTFI (cb)	+	14a	+	14b	K_{eq}	Δ pK
ortho (1)	25.37		10.54	59.42		--		4.74		2.08	0.014	-1.87
ortho (2)								4.66				
ortho (3)												
para (1)				27.44				2.39		1.00		
para (2)								2.31				
para (3)												
meta (1)	24.61		--	56.11		2.40		4.64		2.13		
meta (2)								4.64				
meta (3)												
# of eq. rings (1)	1		1	2		1		1		2		
# of eq. rings (2)								1				
# of eq. rings (3)												
relative integral	12.50		5.27	14.30		1.20		2.34		0.52		
mole fraction	0.35		0.15	0.40		0.03		0.06		0.01		
spectra = AQ2F	**PTFI-a**	**+**	**PTFI-b**	**+ 14 (cb)**	**⇆**	**PTFI (cb)**	**+**	**14a**	**+**	**14b**	**K_{eq}**	**Δ pK**
ortho (1)	30.12		12.29	70.63		--		--		2.07	0.013	-1.88
ortho (2)								4.60				
ortho (3)												
para (1)				34.92				2.37		1.00		
para (2)								2.31				
para (3)												
meta (1)	28.73		--	70.57		3.38		4.70		2.12		
meta (2)								4.70				
meta (3)												
# of eq. rings (1)	1		1	2		1		1		2		
# of eq. rings (2)								1				
# of eq. rings (3)												
relative integral	14.71		6.15	17.61		1.69		2.34		0.52		
mole fraction	0.34		0.14	0.41		0.04		0.05		0.01		
Average:											0.013	-1.88

Table 3.20. Integrations from the ^{19}F NMR equilibrium spectra.

spectra = AP1F	11a	+	11b	+ 14 (cb)	⇆	11(cb)	+	14a	+	14b	K_{eq}	Δ pK
ortho (1)	9.17		--	27.04		9.62		12.45		5.47	1.083	0.03
ortho (2)								12.43				
ortho (3)												
para (1)				12.43				6.13		2.63		
para (2)								6.06				
para (3)												
meta (1)	9.97		0.89	25.40		10.06		12.05		5.42		
meta (2)								12.05				
meta (3)												
# of eq. rings (1)	1		1	2		1		1		2		
# of eq. rings (2)								1				
# of eq. rings (3)												
relative integral	4.79		0.45	6.49		4.92		6.12		1.35		
mole fraction	0.20		0.02	0.27		0.20		0.25		0.06		
spectra = AP2F	**11a**	**+**	**11b**	**+ 14 (cb)**	**⇆**	**11(cb)**	**+**	**14a**	**+**	**14b**	**K_{eq}**	**Δ pK**
ortho (1)	8.05		--	41.13		10.57		14.77		6.66	1.075	0.03
ortho (2)								15.11				
ortho (3)												
para (1)				19.31				7.68		3.36		
para (2)								7.23				
para (3)												
meta (1)	9.49		1.12	39.37		12.28		15.46		7.15		
meta (2)								15.46				
meta (3)												
# of eq. rings (1)	1		1	2		1		1		2		
# of eq. rings (2)								1				
# of eq. rings (3)												
relative integral	4.39		0.56	9.98		5.71		7.57		1.72		
mole fraction	0.15		0.02	0.33		0.19		0.25		0.06		
spectra = AP3F	**11a**	**+**	**11b**	**+ 14 (cb)**	**⇆**	**11(cb)**	**+**	**14a**	**+**	**14b**	**K_{eq}**	**Δ pK**
ortho (1)	7.42		--	48.77		10.48		--		6.59	1.045	0.02
ortho (2)								15.64				
ortho (3)												
para (1)				22.78				--		3.05		
para (2)								7.33				
para (3)												
meta (1)	8.03		1.14	46.67		12.05		16.40		7.87		
meta (2)								16.40				
meta (3)												
# of eq. rings (1)	1		1	2		1		1		2		
# of eq. rings (2)								1				
# of eq. rings (3)												
relative integral	3.86		0.57	11.82		5.63		7.97		1.75		
mole fraction	0.12		0.02	0.37		0.18		0.25		0.06		
Average:											1.067	0.03

Table 3.21. Integrations from the ^{19}F NMR equilibrium spectra.

spectra = AO1F	2a + 2b	+ 14 (cb) ⇆	2 (cb) + 14a + 14b			K_{eq}	Δ pK
ortho (1)	10.85 --	4.17	32.59 --		7.57	21.471	1.33
ortho (2)	2.00		17.47				
ortho (3)							
para (1)	5.22 0.99	1.96	14.84 8.46		3.66		
para (2)	0.99		8.47				
para (3)							
meta (1)	-- 2.11	4.16	30.81 16.93		7.74		
meta (2)	--		16.93				
meta (3)							
# of eq. rings (1)	2 1	2	2 1		2		
# of eq. rings (2)	1		1				
# of eq. rings (3)							
relative integral	2.68 1.02	1.03	7.82 8.53		1.90		
mole fraction	0.12 0.04	0.04	0.34 0.37		0.08		
spectra = AO2F	**2a + 2b**	**+ 14 (cb) ⇆**	**2 (cb) + 14a + 14b**			**K_{eq}**	**Δ pK**
ortho (1)	11.20 --	4.00	30.59 --		7.50	20.768	1.32
ortho (2)	2.08		17.24				
ortho (3)							
para (1)	5.42 1.00	1.71	13.81 8.36		3.57		
para (2)	1.03		8.38				
para (3)							
meta (1)	-- 2.27	3.81	28.92 16.85		7.70		
meta (2)	--		16.85				
meta (3)							
# of eq. rings (1)	2 1	2	2 1		2		
# of eq. rings (2)	1		1				
# of eq. rings (3)							
relative integral	2.77 1.06	0.95	7.33 8.46		1.88		
mole fraction	0.12 0.05	0.04	0.33 0.38		0.08		
spectra = AO3F	**2a + 2b**	**+ 14 (cb) ⇆**	**2 (cb) + 14a + 14b**			**K_{eq}**	**Δ pK**
ortho (1)	10.50 --	3.53	26.71 --		6.79	19.562	1.29
ortho (2)	1.98		15.57				
ortho (3)							
para (1)	5.20 1.00	1.55	12.89 7.73		3.29		
para (2)	0.98		7.73				
para (3)							
meta (1)	-- 2.27	3.72	26.24 15.84		7.11		
meta (2)	--		15.84				
meta (3)							
# of eq. rings (1)	2 1	2	2 1		2		
# of eq. rings (2)	1		1				
# of eq. rings (3)							
relative integral	2.62 1.04	0.88	6.58 7.84		1.72		
mole fraction	0.13 0.05	0.04	0.32 0.38		0.08		
Average:						20.601	1.31

Table 3.22. Integrations from the ^{19}F NMR equilibrium spectra.

spectra = AL1F	6a/b	+	6a/b	+	5 (cb)	⇆	6 (cb)	+	5	K_{eq}	|Δ pK|
ortho (1)	--		--		--		--		--	0.17	0.77
ortho (2)	--		--		--		--		--		
ortho (3)	--		--								
ortho (4)	--		--								
para (1)	1.06		0.97		2.24		0.62		2.60		
para (2)	1.08		1.02		--		0.62		2.50		
para (3)	1.00		1.02								
para (4)	1.13		1.03								
meta (1)	--		--		--		--		--		
meta (2)	--		--		--		--		--		
meta (3)	--		--								
meta (4)	--		--								
# of eq. rings (1)	1		1		2		2		2		
# of eq. rings (2)	1		1		2		2		2		
# of eq. rings (3)	1		1								
# of eq. Rings (4)	1		1								
relative integral	1.07		1.01		1.12		0.31		1.28		
mole fraction	0.22		0.21		0.23		0.06		0.27		
spectra = AL2F	**6a/b**	**+**	**6a/b**	**+**	**5 (cb)**	**⇆**	**6 (cb)**	**+**	**5**	**K_{eq}**	**|Δ pK|**
ortho (1)	--		--		--		--		--	0.17	0.77
ortho (2)	--		--		--		--		--		
ortho (3)	--		--								
ortho (4)	--		--								
para (1)	0.96		0.87		2.02		0.56		2.30		
para (2)	0.95		0.92		--		0.56		2.25		
para (3)	0.89		0.92								
para (4)	1.00		0.93								
meta (1)	--		--		--		--		--		
meta (2)	--		--		--		--		--		
meta (3)	--		--								
meta (4)	--		--								
# of eq. rings (1)	1		1		2		2		2		
# of eq. rings (2)	1		1		2		2		2		
# of eq. rings (3)	1		1								
# of eq. Rings (4)	1		1								
relative integral	0.95		0.91		1.01		0.28		1.14		
mole fraction	0.22		0.21		0.23		0.06		0.27		
spectra = AL3F	**6a/b**	**+**	**6a/b**	**+**	**5 (cb)**	**⇆**	**6 (cb)**	**+**	**5**	**K_{eq}**	**|Δ pK|**
ortho (1)	--		--		--		--		--	0.17	0.77
ortho (2)	--		--		--		--		--		
ortho (3)	--		--								
ortho (4)	--		--								
para (1)	1.72		1.55		3.62		1.01		4.18		
para (2)	1.72		1.67		--		1.00		4.07		
para (3)	1.62		1.67								
para (4)	1.82		1.67								
meta (1)	--		--		--		--		--		
meta (2)	--		--		--		--		--		
meta (3)	--		--								
meta (4)	--		--								
# of eq. rings (1)	1		1		2		2		2		
# of eq. rings (2)	1		1		2		2		2		
# of eq. rings (3)	1		1								
# of eq. Rings (4)	1		1								
relative integral	1.72		1.64		1.81		0.50		2.06		
mole fraction	0.22		0.21		0.23		0.06		0.27		
Average										0.17	0.77

Table 3.23. Integrations from the ^{19}F NMR equilibrium spectra.

spectra = AK1F	6a/b	+	6a/b	+	13 (cb)	⇆	6 (cb)	+	13a	+	13b	K_{eq}	|Δ pK|
ortho (1)	--		--		6.31		--		9.02		1.00	2.04	0.31
ortho (2)	--		--				--				--		
ortho (3)	--		--										
ortho (4)	--		--										
para (1)	0.85		0.83				4.14						
para (2)	0.92		0.88				4.11						
para (3)	0.84		0.88										
para (4)	0.92		0.85										
meta (1)	--		--		6.68		8.40		--		--		
meta (2)	--		--				8.45				--		
meta (3)	--		--										
meta (4)	--		--										
# of eq. rings (1)	1		1		2		2		2		1		
# of eq. rings (2)	1		1				2				1		
# of eq. rings (3)	1		1										
# of eq. Rings (4)	1		1										
relative integral	0.88		0.86		1.62		2.09		2.26		0.50		
mole fraction	0.11		0.11		0.21		0.27		0.29		0.06		
spectra = AK2F	**6a/b**	**+**	**6a/b**	**+**	**13 (cb)**	**⇆**	**6 (cb)**	**+**	**13a**	**+**	**13b**	**K_{eq}**	**|Δ pK|**
ortho (1)	--		--		7.47		--		10.60		1.21	2.04	0.31
ortho (2)	--		--				--				--		
ortho (3)	--		--										
ortho (4)	--		--										
para (1)	0.98		0.96				4.80						
para (2)	1.08		1.03				4.89						
para (3)	1.00		1.03										
para (4)	1.09		1.00										
meta (1)	--		--		7.93		9.73		--		--		
meta (2)	--		--				10.15				--		
meta (3)	--		--										
meta (4)	--		--										
# of eq. rings (1)	1		1		2		2		2		1		
# of eq. rings (2)	1		1				2				1		
# of eq. rings (3)	1		1										
# of eq. Rings (4)	1		1										
relative integral	1.04		1.01		1.93		2.46		2.65		0.61		
mole fraction	0.11		0.11		0.21		0.27		0.29		0.06		
spectra = AK3F	**6a/b**	**+**	**6a/b**	**+**	**13 (cb)**	**⇆**	**6 (cb)**	**+**	**13a**	**+**	**13b**	**K_{eq}**	**|Δ pK|**
ortho (1)	--		--		6.87		--		9.78		1.09	2.03	0.31
ortho (2)	--		--				--				--		
ortho (3)	--		--										
ortho (4)	--		--										
para (1)	0.93		0.90				4.46						
para (2)	1.00		0.95				4.45						
para (3)	0.92		0.95										
para (4)	1.00		0.91										
meta (1)	--		--		7.20		9.02		--		--		
meta (2)	--		--				9.13				--		
meta (3)	--		--										
meta (4)	--		--										
# of eq. rings (1)	1		1		2		2		2		1		
# of eq. rings (2)	1		1				2				1		
# of eq. rings (3)	1		1										
# of eq. Rings (4)	1		1										
relative integral	0.96		0.93		1.76		2.26		2.45		0.55		
mole fraction	0.11		0.11		0.21		0.27		0.29		0.06		
Average												2.036	0.31

Chapter 4: Quantitative Analysis of Electronic Effects Using Infrared Spectroscopy

Introduction

Carbon monoxide (CO) is a popular ligand in transition metal coordination chemistry. The metal-CO bonding can be described by the three resonance structures depicted in Figure 4.1. The strength of metal-carbon and carbon-oxygen bonding is sensitive to the metal, the metal's oxidation state, and the ligands bound to the metal. Changes in the carbon-oxygen bond strength are conveniently detected by infrared (IR) spectroscopy, which measures the vibrational frequency of the carbon-oxygen bond.

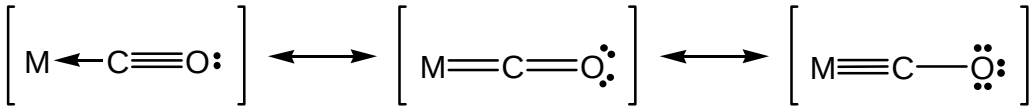

Figure 4.1. Resonance structures describing metal-CO bonding.

The electron lone pairs on the oxygen terminae of the CO ligand are Lewis basic and can interact with Lewis acids. IR spectroscopy is a convenient tool for analyzing these interactions by measuring the shift in the CO stretching frequency upon Lewis base addition. For example, the addition of $AlCl_3$ to a solution of $CpMn(CO)_3$ yields three new CO stretching frequencies which reflect the formation of an acid-base adduct possessing C_s symmetry (Figure 4.2).[135] Compared to the $CpMn(CO)_3$ precursor, the CO stretching frequency for the adduct is shifted to a lower energy (1747 cm^{-1}) while the two remaining CO ligands exhibit stretching frequencies with slightly higher energies (2056, 2001 cm^{-1}).

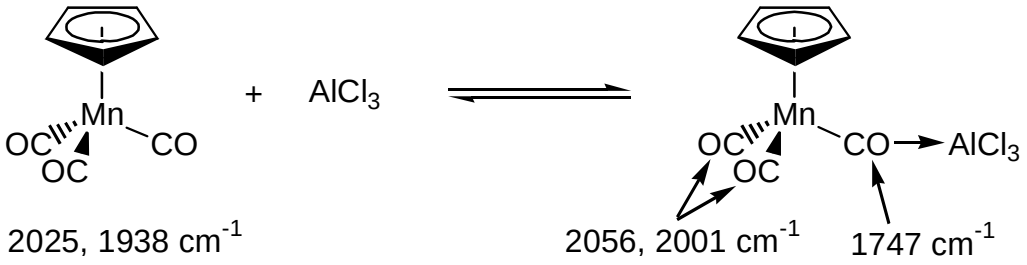

Figure 4.2. Lewis acid/base interaction between $AlCl_3$ and $CpMn(CO)_3$.

IR spectroscopy also provides a fingerprint of the environment around the metal to which the ligand is coordinated. When a Cp ligand is coordinated to the metal, any attached Cp substituents can influence the extent of metal-CO bonding. Electron-donating substituents increase metal electron density and favor resonance structures with increased metal-CO pi bonding. This increased pi bonding also lowers the bond order of the carbon-oxygen bond. Electron-withdrawing substituents diminish metal-CO pi bonding and increases the bond order of the carbon-oxygen bond. This feature is the basis of electronic effect studies that correlate Cp substituents to IR stretching frequencies.

Electronic Effect Studies

Piano stool complexes of the formula $CpM(CO)_3$ have been the subject of several IR-based electronic effect studies. In 1987, Lyatifov and coworkers showed how methyl substitution affects CO stretching frequencies for several substituted $CpRe(CO)_3$ complexes.[136] Table 4.1 summarizes the changes in the symmetric (A) and unsymmetric (E) CO stretches for complexes containing one, two, three, four, and five methyl substituents. As methyl substitution increases, the IR frequencies decrease and reflect a decline in carbon-oxygen pi bonding. Coville and coworkers obtained similar findings for $Cp'Fe(CO)(PPh_3)I$ complexes where the Cp substituents vary.[137,138] Table 4.2 lists the symmetric stretching frequencies for several electron-donating and -withdrawing substituents. As expected, electron-donating alkyl and trimethylsilyl

Table 4.1. IR CO stretching frequencies for methyl-substituted $CpRe(CO)_3$ complexes.

$Cp'Re(CO)_3$	ν(CO) (cm^{-1})[a]	
Cp' Ligand	A	E
Cp	2033	1941
C_5H_4Me	2029	1937
$C_5H_3(1,3\text{-}Me_2)$	2027	1936
$C_5H_2(1,2,4\text{-}Me_3)$	2023	1931
C_5HMe_4	2021	1929
C_5Me_5	2018	1927

a. recorded in chloroform

Table 4.2. IR CO stretching frequencies for substituted $CpFe(CO)(PPh_3)I$ complexes.

$Cp'Fe(CO)(PPh_3)I$	sym. CO stretch (cm^{-1})
Cp' Ligand	$\nu(cm^{-1})$
$C_5Me_4{}^tBu$	1921[a]
C_5HMe_4	1932[a]
$C_5H_4(SiMe_3)$	1951[b]
C_5H_4Me	1951[b]
$C_5H_4{}^tBu$	1951[b]
Cp	1958[b]
C_5H_4I	1964[b]
$C_5H_4(COOMe)$	1971[b]

a. recorded in dichloromethane
b. recorded in chloroform

groups lower the stretching frequencies while electron-withdrawing iodo and methoxycarbonyl substituents raise the frequencies.

Many studies have correlated CO stretching frequencies to other variables that are dependent on the electronic nature of the Cp substituent. For example, NMR chemical shifts are sensitive to fluctuations in metal electron density which can be controlled by fine tuning the substituents of an attached Cp ligand.[24,136,139] Rausch and coworkers related the IR CO stretching frequencies of monosubstituted $CpRh(CO)_2$ complexes with their ^{103}Rh NMR chemical shifts.[13] Their data are presented in Table 4.3 and show that increasing electron-withdrawing group functionalization increases both IR stretching frequencies and ^{103}Rh NMR chemical shifts. However, functionalization with weak electron-donating groups (methyl, trimethylsilyl) does not produce the expected decrease in chemical shift.

The rates of reactions in Cp containing carbonyl complexes are also dependent on electronic effects of attached substituents. Many studies have successfully correlated reaction rates with CO stretching frequencies.[31,32,44] Basolo and coworkers studied the kinetics of associative substitution reactions between $Cp'Rh(CO)_2$ and PPh_3 to yield the complex $Cp'Rh(CO)(PPh_3)$.[30] Table 4.4 shows the IR stretching frequencies for the $Cp'Rh(CO)_2$ complexes and the respective reaction rates with PPh_3. Electron-withdrawing substituents

Table 4.3. IR CO stretching frequencies and ^{103}Rh NMR chemical shifts for substituted $CpRh(CO)_2$ complexes.

$Cp'Rh(CO)_2$	ν(CO) (cm^{-1})[a]		
Cp' Ligand	A	B	^{103}Rh NMR (ppm)[b]
C_5H_4Me	2044	1981	-1310
$C_5H_4(CH_2Ph)$	2044	1982	-1278
$C_5H_4(SiMe_3)$	2045	1983	-1322
C_5H_5	2048	1985	-1322
$C_5H_4(COMe)$	2057	1998	-1208
$C_5H_4(CO_2Me)$	2057	1997	-1205
$C_5H_4(CHO)$	2061	2002	-1191
$C_5H_4(NO_2)$	2068	2010	-1117

a. recorded in hexane
b. recorded in C_6D_6

increase the reaction rates by stabilizing the allylic, ring slipped intermediate. The electron-donating Cp^* ligand destabilizes this electron-rich, allylic intermediate and exhibits the slowest reactions rates. The indenyl ligand is electron-donating relative to Cp but exhibits the largest reaction rate. This rate enhancement is attributed to the complete aromatization of the indenyl's benzene ring in the ring slipped intermediate.

Chapter Overview

This chapter describes the synthesis and characterization of several $Cp'M(CO)_3$ complexes (M = Mn, Re) containing one to four C_6F_5 substituents. The CO stretching frequencies of these complexes suggest an additive electron-withdrawing effect for the C_6F_5 substituent. The electron-withdrawing ability of the C_6F_5 substituent is also compared to other known electron-withdrawing substituents. Crystal structures of several piano stool complexes reveal structural motifs such as Lewis basic CO donor interactions and arene stacking. Finally, the impact of adjacent C_6F_5 substituents on the rate of C_6F_5-rotation is examined by variable temperature NMR measurements.

Table 4.4. IR CO stretching frequencies and rate constants for $CpRh(CO)_2$ complexes.

$Cp'Rh(CO)_2$	$\nu(CO)$ $(cm^{-1})^a$		
Cp' Ligand	A	B	k_{rel} [d]
$C_5H_4(NO_2)$	2067	2011	1.2×10^4
$C_5H_4(\overset{+}{P}Ph_3)$	2062[b]	2002[b]	1.1×10^2
C_5H_5	2051[c]	1985[c]	1
indenyl	2048	1993	3.8×10^8
C_5Me_5	2020	1967	2.2×10^{-2}

a. recorded in decalin unless otherwise specified; b. recorded in nitromethane; c. recorded in cyclohexane; d. recorded in toluene

Results & Discussion

Complex Synthesis

C_6F_5-substituted piano stool complexes are easily made by reacting the appropriate Cp anion with either $Mn(CO)_5Br$ or $Re(CO)_5Br$ (Figure 4.3). The syntheses for complexes **15Re** and **16Re** were previously reported.[91] All syntheses were carried out in refluxing THF except for complexes **17Re**, **19Mn**, **19Re**, which required refluxing toluene and a small amount of NaH (moisture scavenger) for significant product formation. The yields for all complexes are low to moderate (25 – 78%) with yields decreasing as C_6F_5-substitution increases. The diminished product yields are not surprising since increased arylation should decrease the Cp anion's nucleophilic character and increase its overall steric bulk.

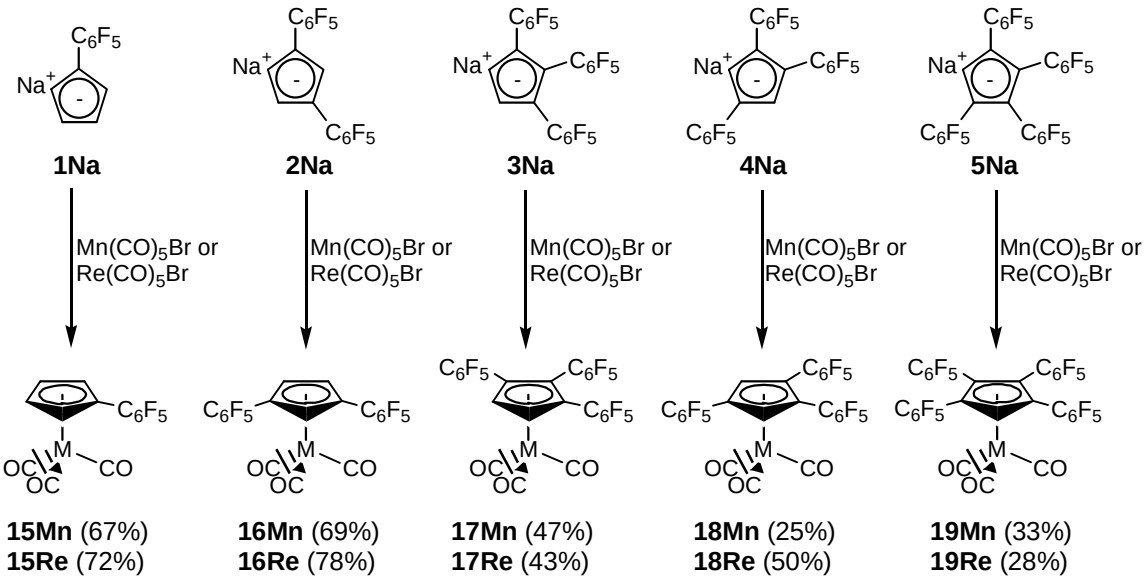

Figure 4.3. Synthetic scheme for $CpM(CO)_3$ complexes (M = Mn, Re).

Infrared Spectroscopic Analysis

The IR spectra of all piano stool complexes were recorded in hexane or octane solution. The A and E symmetry-based CO stretching frequencies are listed in Table 4.5. For several complexes, the unsymmetric stretching mode (E) has split into two separate peaks. This feature is attributed to the loss of C_{3v} symmetry which accompanies Cp functionalization. The frequencies for the A and E stretching modes increase with increasing C_6F_5-substitution. Figure

Table 4.5. IR CO stretching frequencies for C_6F_5-substituted $CpM(CO)_3$ complexes.

	ν(CO) (cm^{-1})[a]			ν(CO) (cm^{-1})[b]	
$Cp'M(CO)_3$	A	E	$Cp'M(CO)_3$	A	E
$CpMn(CO)_3$	2028	1944	$CpRe(CO)_3$	2031	1939
15Mn	2032	1954	**15Re**	2034	1947
16Mn	2035	1966, 1960	**16Re**	2038	1953
17Mn	2041	1975, 1963	**17Re**	2043	1965, 1954
18Mn	2040	1973, 1965	**18Re**	2042	1963, 1957
19Mn	2044	1980, 1970	**19Re**	2047	1970, 1959

a. recorded in octane; b. recorded in hexane

4.4 illustrates this trend graphically for the symmetric stretching modes (A). Complexes of Mn and Re both exhibit an additive substituent effect with an approximate 4 cm^{-1} rise in CO stretching frequency accompanying each additional C_6F_5 group as indicated by the slopes.

While it is clear that the C_6F_5 group is electron-withdrawing, it is difficult to compare it to other electron-withdrawing substituents. The piano stool complex $Cp'Mn(CO)_3$ is the most popular Cp transition metal complex implemented in IR-based electronic effect studies.

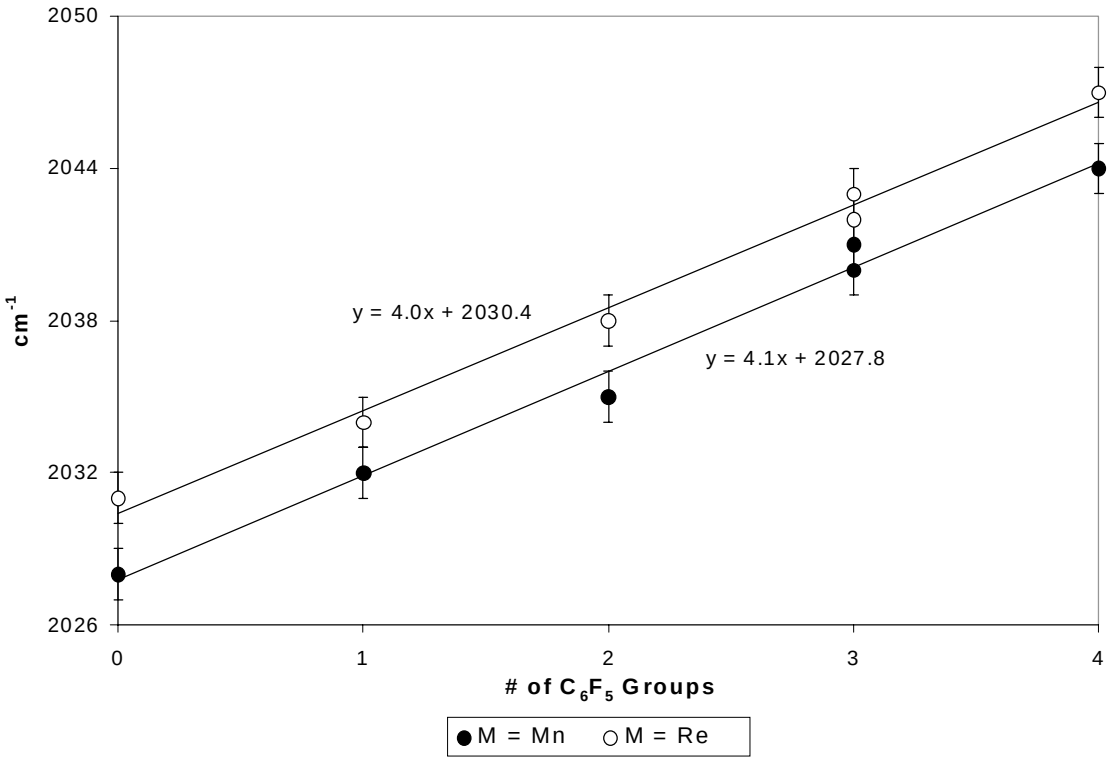

Figure 4.4. Plot of CO stretching frequency vs. the number of C_6F_5 substituents.

Table 4.6. IR CO stretching frequencies in substituted $CpMn(CO)_3$ complexes.

$Cp'Mn(CO)_3$	sym. CO stretch (cm^{-1})	$Cp'Mn(CO)_3$	sym. CO stretch (cm^{-1})
Cp' Ligand	$\Delta\nu(cm^{-1})$	Cp' Ligand	$\Delta\nu(cm^{-1})$
C_5Et_5	-20[a]	C_5H_4Br	4[d]
			6[c]
C_5Me_5	-19[b]	C_5H_4I	4[d]
$C_5H_4NH_2$	-10[c]		4[c]
C_5H_4Me	-9[d]	$C_5H_3(1,3\text{-}C_6F_5)_2$, **16Mn**	7[e]
C_5Ph_4Cl	-6[d]	$C_5H_4(COOH)$	9[c]
$C_5H_4(CH_2Ph)$	-3[a]	$C_5H_2(1,2,4\text{-}C_6F_5)_3$, **18Mn**	12[e]
Cp	0	$C_5H_2(1,2,3\text{-}C_6F_5)_3$, **17Mn**	13[e]
$C_5H_4(C_6F_5)$, **15Mn**	4[e]	$C_5H(C_6F_5)_4$, **19Mn**	16[e]
C_5H_4F	4[c]	C_5Cl_5	17[b]
C_5H_4Cl	4[d]		18[d]
	4[c]		

a. dichloromethane; b. methylcyclohexane; c. chloroform; d. cyclohexane; e. hexane

However, spectra are often recorded in different media (chloroform, hexane, Nujol, KBr) making numerical comparisons difficult. It is possible to express the effect of a particular functional group as a frequency shift ($\Delta\nu$) relative to the unsubstituted complex, $CpMn(CO)_3$. Table 4.6 presents the IR shifts ($\Delta\nu$) from the previously described C_6F_5-substituted complexes and includes the IR shifts from four other studies.[51,70,135,140] All data were obtained from studies using a resolution of 1 cm^{-1} or better. The similar $\Delta\nu$ values for C_5H_4X (X = Cl, Br, I) in chloroform and cyclohexane suggest a minimal solvent effect on $\Delta\nu$. The electron-withdrawing capacity of one C_6F_5 group is similar to one halogen substituent but considerably lower than a carboxylic acid. Four C_6F_5 groups (**19Mn**) have a similar electron-withdrawing effect (16 cm^{-1}) as five chloro substituents (17 or 18 cm^{-1}).

Crystal structures of Piano Stool Complexes

The crystal structures for complexes **18Mn**, **18Re**, **19Mn**, and **19Re** are shown in Figures 4.5, 4.6, 4.7, and 4.8 while relevant crystallographic data are shown in Table 4.7. Important bond distances and angles are presented in Table 4.8 and reveal no significant structural distortions. The C_6F_5-Cp dihedral angles vary between 36.4º and 66.3º. The isolated (iso) C_6F_5 groups in **18Mn** and **18Re** are free of intramolecular steric crowding and adopt the smallest dihedral angles (36.4º and 41.5º). These angles are similar to those adopted by **16Re** (23.0º and

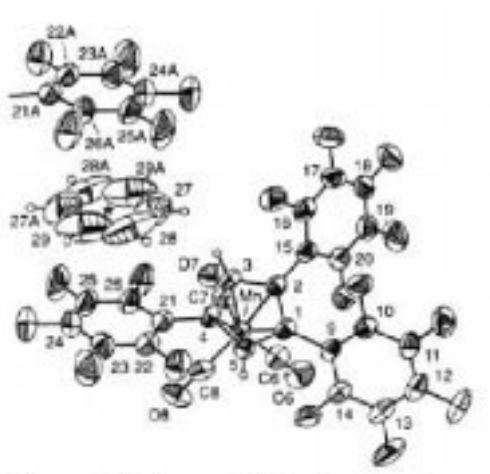

Figure 4.5. Thermal ellipsoid plot of **18Mn(1/2C_6D_6)** (50% probability) showing arene stacking between C_6F_5 substituents and C_6D_6 solvate.

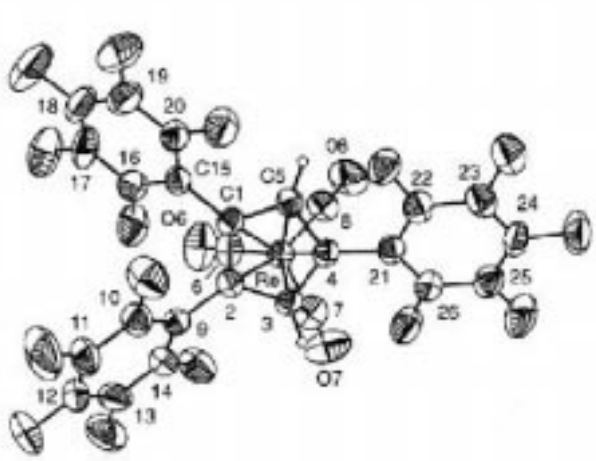

Figure 4.6. Thermal ellipsoid plot of **18Re** (50% probability).

Figure 4.7. Thermal ellipsoid plot of **19Mn** (50% probability).

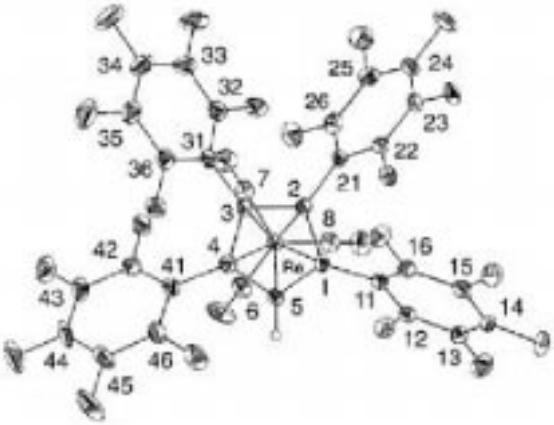

Figure 4.8. Thermal ellipsoid plot of **19Re** (50% probability).

39.3°).[93] Table 4.9 compares the average M-C(ring) bond distances in these complexes with other piano stool complexes containing different substituents.[78,93,141-148] The C_6F_5-substituted complexes exhibit larger average distances than other bulky Cp ligands (C_5Me_5, C_5H_2[1,2,3-$(SiMe_3)_3$]). This elongation is attributed to the C_6F_5 substituent's steric interaction with the $M(CO)_3$ tripod. As expected, the tetra-substituted complexes **19Mn** and **19Re** exhibit the largest M-C(ring) bond distances which are elongated by approximately 0.05 Å relative to the unsubstituted complexes.

The data in Table 4.9 also suggest that steric effects may contribute to the increase in CO stretching frequency that accompanies increasing C_6F_5 substitution. As the M-C(ring) bond distance increases in these complexes, the overlap between the Cp pi cloud and metal orbitals is

Table 4.7 Crystallographic data for piano stool complexes.

compound	**18Mn· ½C_6D_6**	**18Re**	**19Mn**	**19Re**
empirical formula	$C_{26}H_2F_{15}MnO_3$· ½ C_6D_6	$C_{26}H_2F_{15}O_3Re$	$C_{32}HF_{20}MnO_3$	$C_{32}HF_{20}O_3Re$
fw	744.29	833.48	868.27	999.54
diffractometer	Siemens P4[b]	Siemens P4[b]	Siemens P4[b]	Nonius Kappa CCD
cryst dimens (mm)	0.48 × 0.49 × 0.32	0.17 × 0.19 × 0.48	0.13 × 0.29 × 0.48	0.08 × 0.20 × 0.20
cryst system	triclinic	monoclinic	triclinic	triclinic
a (Å)	7.5933(8)	7.6570(7)	10.515(2)	8.1450(2)
b (Å)	14.2469(15)	10.8461(10)	11.345(3)	13.1900(4)
c (Å)	38.263(4)	29.606(2)	13.910(3)	14.4900(3)
α (deg)	90	90	93.097(16)	75.9910(18)
β (deg)	91.728(8)	92.696(7)	97.264(18)	81.0610(16)
γ (deg)	90	90	117.174(17)	79.9430(18)
V $(Å)^3$	4137.5(7)	2452.8(4)	1452.6(6)	1476.73(7)
space group	$P2_1/c$ (No. 14)	$P2_1/c$ (No. 14)	P-1 (No. 2)	P-1 (No. 2)
Z	4	4	2	2
D_{calc} (Mg m ^{3})	1.903	2.257	1.985	2.248
abs coeff (mm ^{1})	0.588	5.100	0.622	4.3
F_{000}	2308	1568	844	944
λ (Mo K_α) (Å)	0.71073	0.71073	0.71073	0.71073
temp (K)	293	293	293	120
range for collection	1.06-21.50	2.00-26.00	2.0-27.5	2.5-32.6
no. of reflns colld	6508	6677	7744	15805
no. of indep reflns	4752	4828	6649	10352
abs corr method	integration	integration	*ψ* scans	multiscan
data/restrs/params	4750/0/694	4826/0/406	6649/0/509	10352/0/506
R [$I > 2\sigma(I)$]	0.0467	0.0348	0.041	0.031
R_w [$I > 2\sigma(I)$]	0.1054	0.0986	0.077	0.063
GoF on F^2	0.915	0.896	0.81	1.00
peak, hole (e $Å^{-3}$)	0.266, -0.319	1.052, -1.358	0.26, -0.22	1.28, -1.71

Table 4.8. Distances and angles in C_6F_5-substituted piano stool complexes.

	18Mn	**18Re**	**19Mn**	**19Re**
M-C(ring) (**Å**)	2.174(3)	2.309(6)	2.193(3)	2.343(2)
	2.164(3)	2.331(6)	2.196(3)	2.345(2)
	2.130(3)	2.299(5)	2.191(3)	2.332(3)
	2.149(3)	2.302(6)	2.159(3)	2.309(3)
	2.139(3)	2.298(6)	2.158(3)	2.317(3)
ave. M-C(ring)	2.15(2)	2.31(1)	2.18(2)	2.33(2)
M-Cp (**Å**)[a]	1.780(4)	1.968(6)	1.812(3)	1.983(3)
M-CO (**Å**)	1.795(4)	1.904(7)	1.770(3)	1.893(3)
	1.790(4)	1.915(9)	1.787(3)	1.919(3)
	1.790(4)	1.902(6)	1.797(3)	1.921(3)
C-O (**Å**)	1.155(5)	1.141(9)	1.158(4)	1.151(3)
	1.147(4)	1.141(11)	1.150(4)	1.147(4)
	1.152(5)	1.138(9)	1.150(4)	1.148(5)
Cp-C_6F_5 dihedral angles (deg)[b]	43.5 (vic)	66.3 (vic)	50.0 (ext)	61.0 (ext)
	47.7 (vic)	51.0 (vic)	56.9 (int)	56.8 (int)
	36.4 (iso)	41.5 (iso)	46.9 (int)	49.3 (int)
			47.8 (ext)	45.8 (ext)

a. Cp is the C1-C5 centroid; b. vic = vicinal C_6F_5 group; iso = isolated C_6F_5; ext = external C_6F_5 group; int = internal C_6F_5 group

Table 4.9. Average C_{ring}-M distances in piano stool complexes.

Cp'Mn(CO)$_3$		**Cp'Re(CO)$_3$**	
Cp'	**ave. Mn-C(ring) (Å)[a]**	**Cp'**	**ave. Re-C(ring) (Å)[a]**
C_5H_5	2.124(5)	C_5H_4(COMe)	2.28(4)
	2.138(4)	C_5H_5	2.284(4)
C_5I_5	2.14(2)	C_5Me_5	2.299(12)
C_5Bz_5	2.14(1)		2.308(8)
C_5H_2[1,2,3-($SiMe_3$)$_3$]	2.150	C_5H_3[1,3-(C_6F_5)$_2$], **16Re**	2.303(21)
C_5H_2[1,2,4-(C_6F_5)$_3$], **18Mn**	2.15(2)	C_5H_2[1,2,4-(C_6F_5)$_3$], **18Re**	2.31(1)
C_5H[1,2,3,4-(C_6F_5)$_4$], **19Mn**	2.179(19)	C_5H[1,2,3,4-(C_6F_5)$_4$], **19Re**	2.33(2)

a. values from literature cited in text except for **18Mn**, **19Mn**, **18Re**, and **19Re**

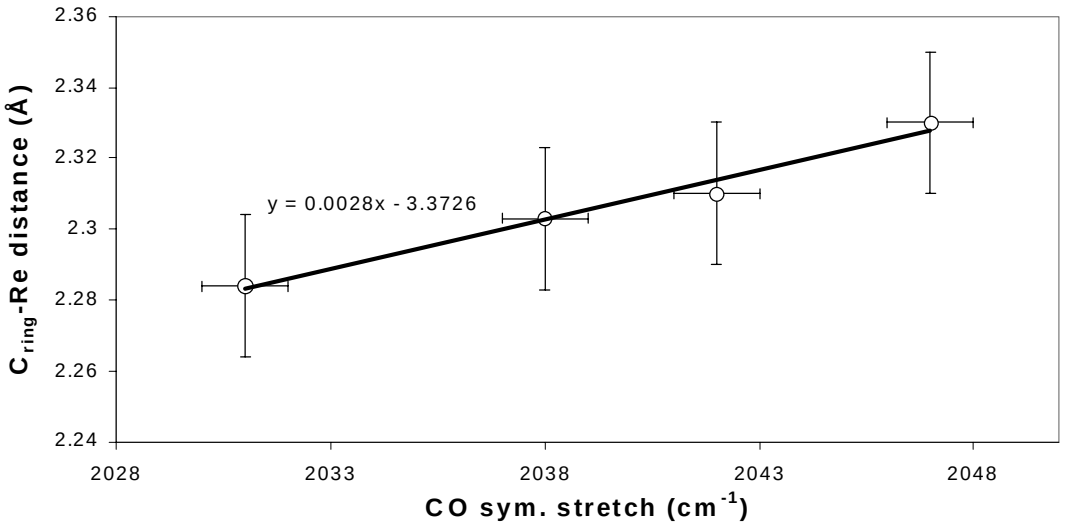

Figure 4.9. Plot of C_{ring}-Re distances vs. CO stretching frequency.

diminished. Poor orbital overlap should increase the metal's electrophilicity while decreasing the extent of Re-CO pi backbonding which lowers CO stretching frequencies. Figure 4.9 illustrates this effect in a series of C_6F_5-substituted $CpRe(CO)_3$ complexes.

The packing diagrams of **18Mn**, **18Re**, and **19Mn** all reveal donor-acceptor interactions between the Lewis-basic oxygen terminae of the CO ligands and the Lewis-acidic centers of the C_6F_5 rings. Metric parameters are defined in Figure 4.10 and summarized in Table 4.10. The oxygen-centroid distances (OX) range from 3.12 to 3.65 Å and are offset from the C_6F_5 centroid (D) by 0.33 to 1.88 Å. As shown in Table 4.8, these interactions do not significantly perturb the M-C-O bond angles from 180º.

The crystal structure of **18Mn** exhibits an additional stacking interaction between two isolated C_6F_5 rings and one molecule of C_6D_6 solvate. An inversion center exists at the centroid

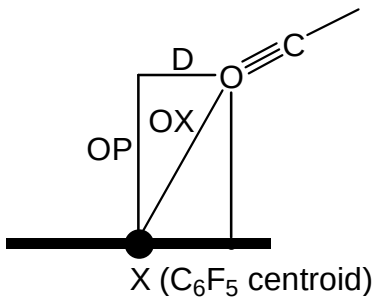

Figure 4.10. Definition of parameters used to characterize the intermolecular interactions of C_6F_5 groups with CO ligands.

Table 4.10. Metric parameters for intermolecular C_6F_5/CO interactions.

	Donor-Acceptor Distances (Å)		
complex	**OX**	**OP**	**D**
18Mn	3.12	3.10	0.33
	3.15	3.11	0.51
18Re	3.65	3.13	1.88
	3.36	2.86	1.76
	3.18	3.06	0.85
19Mn	3.29	3.23	0.65

of the C_6D_6 molecule making the two Mn complexes crystallographically identical. The centroids of the stacking C_6F_5 and C_6D_6 rings are separated by 3.57 Å while the aryl planes are deviated 5º from parallel. Similar stacking arrangements between a C_6F_5 group of a disilazane molecule and two C_6H_6 solvate molecules was reported by Sowerby and coworkers. The aryl centroid separation is slightly longer with distances of 3.713 and 3.719 Å and interplanar angles of 3.4º and 5.3º, respectively.[101]

NMR Spectroscopic Analysis

The ^{19}F NMR spectra of the mono (**15Mn**, **15Re**) and disubstituted (**16Mn**, **16Re**) piano stool complexes possess one signal in the *ortho*, *para*, and *meta* fluorine regions in a 2:1:2 ratio f

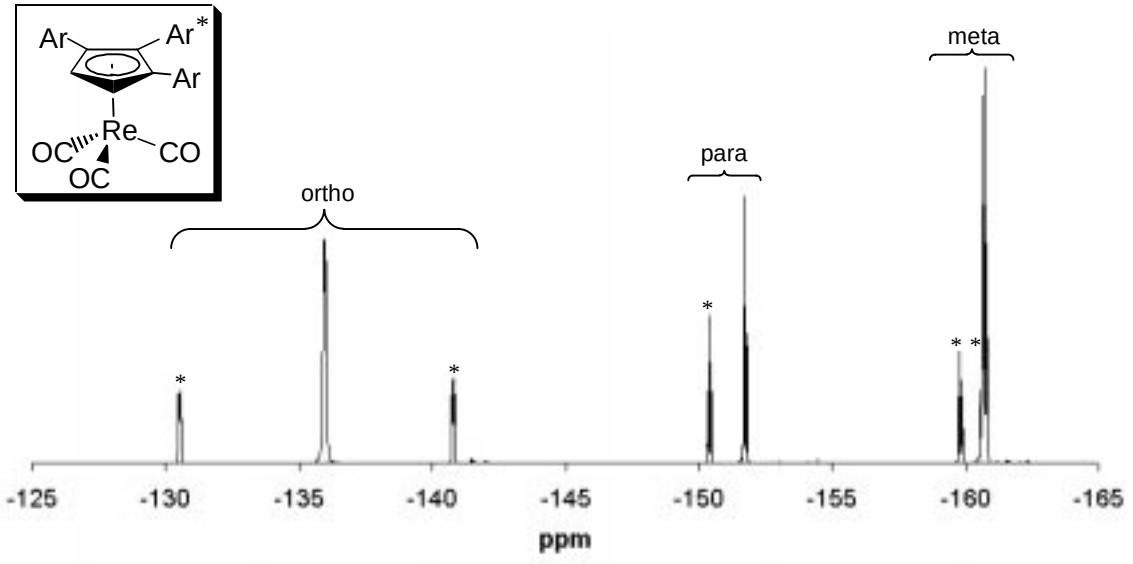

Figure 4.11. Room temperature ^{19}F NMR spectrum of **17Re**.

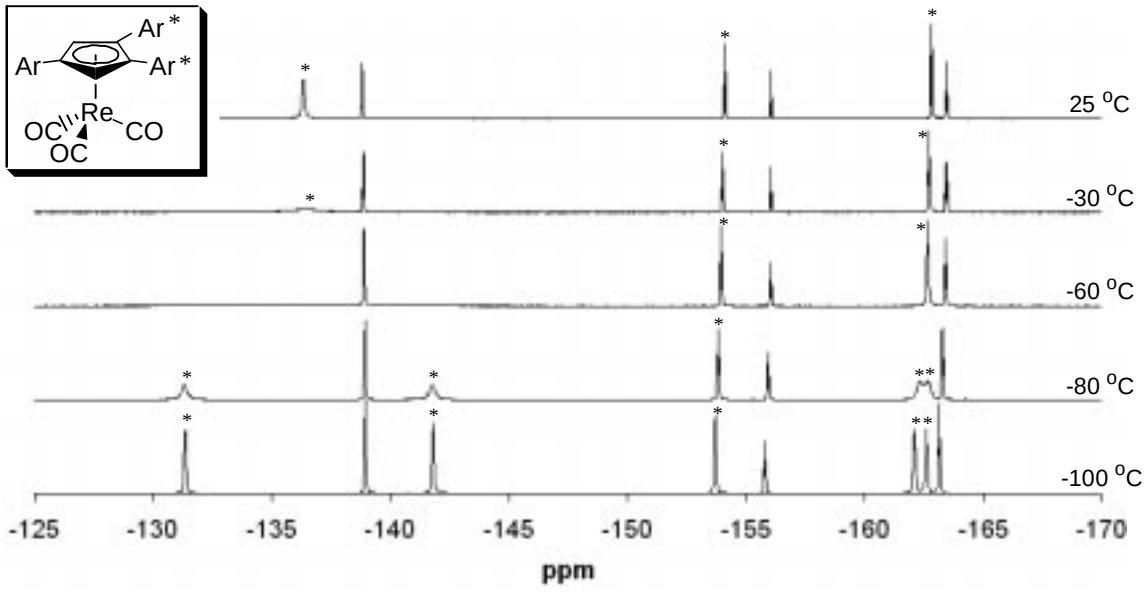

Figure 4.12. Stacked ^{19}F NMR spectra of **18Re** at several temperatures.

or each distinct C_6F_5 group. This is consistent with fast exchange between the *endo* and *exo* p ositions for the *ortho* and *meta* fluorines. The ^{19}F NMR spectra for **17Mn** and **17Re** display three signals in both the *ortho* and *meta* regions (both are 1:2:1) as well as 2 signals in the *para* region (1:2). The room temperature ^{19}F NMR spectrum for **17Re** is shown in Figure 4.11 and the signals arising from the internal C_6F_5 group are labeled with an asterisk. These five signals integrate equally indicating that aryl rotation is impeded by the two adjacent C_6F_5 rings. When the sample was heated to 100 ºC, no significant broadening occurred suggesting that the barrier to rotation is large.

The room temperature ^{19}F NMR spectrum for **18Re** is shown at the top of Figure 4.12. The spectra for –30, –60, –80, and –100 ˚C are stacked below the room temperature spectrum. A signal in each of the three spectral regions (*ortho*, *para*, and *meta*) arises from the two vicinal C_6F_5 groups and they are marked with an asterisk. The two aryl rings are related by a mirror plane that contains the Cp-C_6F_5 bond of the isolated aryl group. As the temperature is lowered, the *ortho* and *meta* signals of the adjacent C_6F_5 groups decoalesce into two signals of equal intensity. Line shape analysis of these spectra allows the construction of an Arrhenius plot from which an activation energy (E_a) of 9(1) kcal/mol was determined for vicinal C_6F_5 rotation. An Erying treatment yields and an enthalpy of activation ($\Delta H^{\ddagger}$) of 8(1) kcal/mol and an entropy of activation ($\Delta S^{\ddagger}$) of –2(5) cal/(mol×K). The low entropy value is in agreement with an intramolecular rotational process.

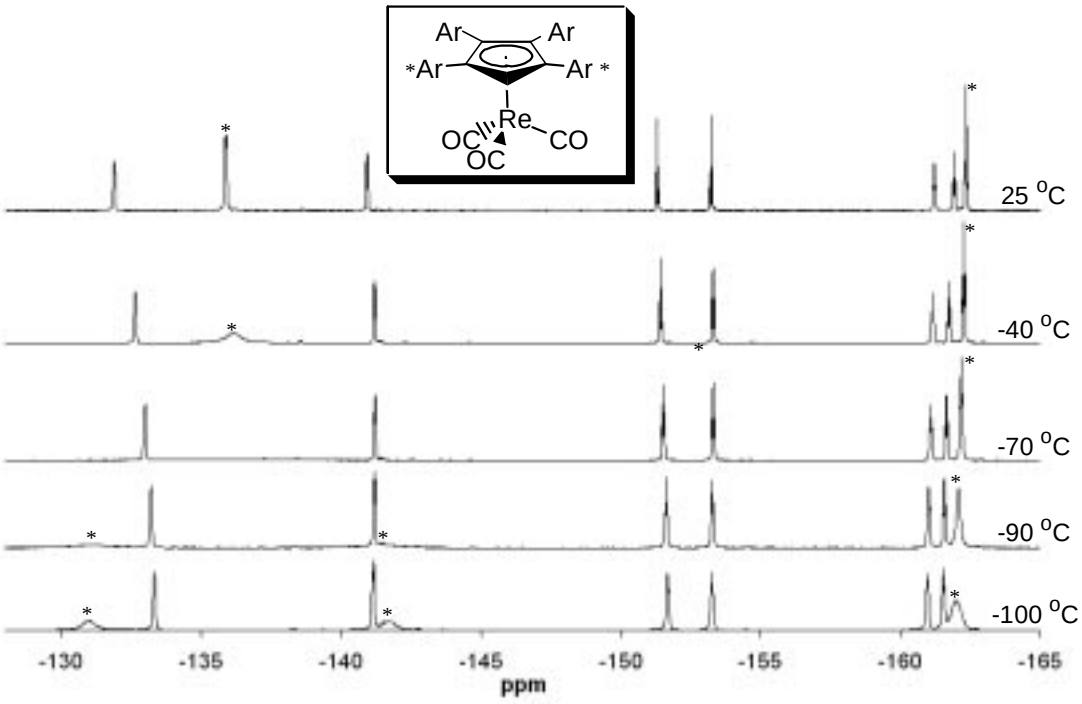

Figure 4.13. Stacked ^{19}F NMR spectra of **19Re** at several temperatures.

The room temperature ^{19}F NMR spectrum for **19Re** is displayed at the top of Figure 4.13. The internal and external C_6F_5 groups are related by a mirror plane that is orthogonal to the Cp plane and parallel to the C-H bond of the methine carbon. As previously seen in **18Re**, the large barrier to internal C_6F_5 rotation produces five ^{19}F NMR signals (*exo ortho*, *endo ortho*, *para*, *exo meta*, *endo meta*). Three signals (*ortho*, *para*, *meta*) represent the two external C_6F_5 rings because their *exo* and *endo* fluorines are in fast exchange at room temperature. The spectra for –40, –70, –90, and –100 ˚C are stacked below the room temperature spectrum and show decoalescence of the *ortho* signal at approximately –75 ˚C. The temperature could not be lowered enough to observe *meta* signal decoalescence. An Arrhenius and Erying treatment of the *ortho* signal at all temperatures gave the following activation parameters: E_a = 7(1) kcal/mol, $\Delta H^{\ddagger}$ = 7(1) kcal/mol, $\Delta S^{\ddagger}$ = –5(5) cal/(mol×K). Complex **19Mn** gave similar low temperature results and the activation parameters were determined to be E_a = 6(1) kcal/mol, $\Delta H^{\ddagger}$ = 6(1) kcal/mol, $\Delta S^{\ddagger}$ = –6(5) cal/(mol×K). The low entropy values are consistent with an intramolecular rotational process.

Conclusion

The electron-withdrawing effect of the C_6F_5 substituent in several piano stool complexes was characterized with IR spectroscopy. Each C_6F_5 substituent increases the CO symmetric stretching frequency by approximately 4 cm^{-1}. X-ray crystal structures of these complexes display aryl stacking and CO-C_6F_5 interactions. The long M-C(ring) distances in **19Mn** and **19Re** illustrate the steric bulk of the tetraarylated Cp ligand. NMR spectroscopy allowed the determination of C_6F_5-Cp rotational barriers for C_6F_5 groups possessing one vicinal neighbor (E_a = 6 – 9 kcal/mol). Substituents with two C_6F_5 neighbors had rotational barriers that were too large to measure by variable temperature NMR spectroscopy.

Experimental Section

General Procedures. Standard inert-atmosphere techniques were used for all reactions. $Mn(CO)_5Br$ and $Re(CO)_5Br$ were used as received from Aldrich. NaH was purchased as a 60% mineral oil dispersion from Aldrich, washed with hexanes, dried under vacuum, and stored in a glovebox. Melting points were obtained using a Mel-Temp apparatus and are uncorrected. Infrared spectra were recorded on a Midac M-series instrument operating at 1 cm^{-1} resolution, using dilute hexane or octane solutions and KBr-windowed cells. NMR experiments used JEOL ECP500 or Varian U400 instruments. THF-d_8 (Isotec) was vacuum-transferred from NaK_2 alloy. ^{19}F NMR spectra were referenced to external C_6F_6 in $CDCl_3$ (-163.00 ppm) at 25 °C. Crystallography was performed by Carla Slebodnick (Virginia Tech) for **18Mn**, **18R**e, and **19Mn** or Frank Fronczek (Louisiana State University) for **18Re**. Elemental analyses were performed by Desert Analytics (Tucson, AZ).

Tricarbonyl[η^5-pentafluorophenylcyclopentadienyl]manganese(I) (**15Mn**). A mixture of $Mn(CO)_5Br$ (0.42 g, 1.5 mmol), **1Na** (0.42 g, 1.6 mmol), and THF (50 mL) was refluxed for 1 day. The THF was evaporated, and the resulting crude solid was dissolved in hexane and filtered. The filtrate was cooled to –20 °C for 1 day, and 0.38 g (1.0 mmol, 67%) of a yellow solid was collected. IR (hexane): ν_{CO} (cm^{-1}) = 2032 (A_1), 1954 (E). ^1H NMR (C_6D_6): δ 4.67 (pentet, J = 2.0 Hz, 2 H), 3.87 (t, J = 2.2 Hz, 2 H). ^{19}F NMR (C_6D_6): δ -139.56 (dd, ^3J = 22.0 Hz, ^5J = 5.5 Hz, 2 F), -155.50 (t, ^3J = 22.2 Hz, 1 F), -162.33 (m, 2 F). Anal. Calcd for $C_{14}H_4F_5MnO_3$: C, 45.43; H, 1.09. Found: C, 45.64; H, 0.95.

Tricarbonyl[η^5-1,3-bis(pentafluorophenyl)cyclopentadienyl]manganese(I) (**16Mn**). A mixture of $Mn(CO)_5Br$ (0.23 g, 0.84 mmol), **2Na** (0.36 g, 0.86 mmol), and THF (50 mL) was stirred under reflux for 2 days. The THF was then evaporated, and the resulting crude solid was dissolved in hexane and filtered. Cooling the filtrate to –78 °C for about 5 h precipitated the product, which was collected on a filter and dried under vacuum to afford 0.31 g (0.58 mmol, 69%) of a yellow solid. IR (hexane): ν_{CO} (cm^{-1}) 2035 (A_1), 1966, 1960. ^1H NMR (C_6D_6): δ 5.65 (pentet, J = 1.3 Hz, 1 H), 4.76 (s, 2 H). ^{19}F NMR (C_6D_6): δ -139.34 (d, ^3J = 18.0 Hz, 4 F), -154.24 (tt, ^3J = 21.8 Hz, 2 F), -161.66 (m, 4 F). Anal. Calcd for $C_{20}H_3F_{10}MnO_3$: C, 44.80; H, 0.56. Found: C, 45.03; H, 0.37.

Tricarbonyl[η^5-1,2,3-tris(pentafluorophenyl)cyclopentadienyl]manganese(I) (**17Mn**). A mixture of $Mn(CO)_5Br$ (0.104 g, 0.378 mmol), **3Na** (0.227 g, 0.387 mmol), and THF (20 mL)

was stirred under reflux for 1 day. The THF was evaporated, and the resulting crude solid was recrystallized from toluene at –78 °C to afford 0.124 g (0.176 mmol, 47%) of an orange solid. IR (hexane): ν_{CO} (cm^{-1}) 2041 (A_1), 1975, 1963. ^{1}H NMR (C_6D_6): δ 4.47 (s, 1 H). ^{19}F NMR (C_6D_6): δ -131.13 (d, ^3J = 22 Hz, 1 F), -137.13 (d, ^3J = 18 Hz, 4 F), -141.14 (d, ^3J = 23 Hz, 1 F), -150.34 (t, ^3J = 22 Hz, 1 F), -151.83 (t, ^3J = 22 Hz, 2 F), -160.61 (td, ^3J = 22 Hz, ^5J = 7 Hz, 1 F), -161.51 (td, ^3J = 23 Hz, ^5J = 8 Hz, 4 F), -161.76 (td, ^3J = 22 Hz, ^5J = 8 Hz, 1 F). Anal. Calcd for $C_{26}H_2F_{15}MnO_3$: C, 44.47; H, 0.29. Found: C, 44.07; H, 0.17.

Tricarbonyl[η^5-1,2,3-tris(pentafluorophenyl)cyclopentadienyl]rhenium(I) (**17Re**). A mixture of $Re(CO)_5Br$ (57.5 mg, 0.142 mmol), **3Na** (81.0 mg, 0.138 mmol), sodium hydride (35 mg, 1.4 mmol), and toluene (25 mL) was stirred at 105 °C for 24 h, and then the hot mixture was filtered. The filtrate was evaporated, and the residue was triturated with hexanes and collected on a filter to afford 50 mg (0.060 mmol, 43%) of a tan solid. IR (octane): ν_{CO} (cm^{-1}) 2043 (A_1), 1965, 1954. ^{1}H NMR ($CDCl_3$): δ 5.87 (s, 2 H). ^{19}F NMR ($CDCl_3$): δ -130.53 (m, 1 F), -135.96 (d, ^3J = 22 Hz, 4 F), -140.79 (d, $^3J_{FF}$ = 24 Hz, 1 F), -150.40 (t, $^3J_{FF}$ = 21 Hz, 1 F), -151.75 (t, J = 24 Hz, 2 F), -159.80 (m, 1 F), -160.72 (m, 5 F). Anal. Calcd for $C_{26}H_2F_{15}O_3Re$: C, 37.47; H, 0.24. Found: C, 37.27; H, 0.20.

Tricarbonyl[η^5-1,2,4-tris(pentafluorophenyl)cyclopentadienyl]manganese(I) (**18Mn**). A mixture of $Mn(CO)_5Br$ (0.102 g, 0.371 mmol), **4Na** (7, 0.224 g, 0.382 mmol), and THF (20 mL) was refluxed for 1 day. The THF was evaporated, and the resulting crude solid was recrystallized from hexanes to afford 0.065 g (0.093 mmol, 25%) of an orange crystalline solid. IR (hexane): ν_{CO} (cm^{-1}) 2040 (A_1), 1973, 1965. ^{1}H NMR (C_6D_6): δ 5.51 (s, 2 H). ^{19}F NMR (C_6D_6): δ -137.37 (d, ^3J = 18 Hz, 4 F), -140.24 (d, ^3J = 18 Hz, 2 F), -152.17 (d, ^3J = 22 Hz, 2 F), -154.20 (t, ^3J = 22 Hz, 1 F), -161.66 (td, ^3J = 23 Hz, ^5J = 7 Hz, 4 F), -162.10 (m, 2 F). Anal. Calcd for $C_{26}H_2F_{15}MnO_3$: C, 44.47; H, 0.29. Found: C, 44.32; H, 0.12.

Tricarbonyl[η^5-1,2,4-tris(pentafluorophenyl)cyclopentadienyl]rhenium(I) (**18Re**). A mixture of $Re(CO)_5Br$ (0.149 g, 0.367 mmol), **4Na** (0.225 g, 0.384 mmol), and THF (20 mL) was stirred under reflux for 1 day, and then the solvent was evaporated. The residue was dissolved in hexane and filtered through a pad of neutral alumina. The filtrate was evaporated, and the residue was recrystallized from methanol to yield 0.153 g (0.184 mmol, 50%) of a tan solid. IR (octane): ν_{CO} (cm^{-1}) 2042 (A_1), 1963, 1957. ^{1}H NMR ($CDCl_3$): δ 6.36 (s, 2 H). ^{19}F NMR ($CDCl_3$): δ -136.42

(s, 4 F), -139.22 (d, ^3J = 15 Hz, 2 F), -152.22 (t, ^3J = 21 Hz, 2 F), -153.95 (t, ^3J = 21 Hz, 1 F), -161.00 (m, 4 F), -161.46 (m, 2 F). Anal. Calcd for $C_{26}H_2F_{15}O_3Re$: C, 37.47; H, 0.24. Found: C, 37.65; H, 0.08.

Tricarbonyl[η^5-1,2,3,4-tetrakis(pentafluorophenyl)cyclopentadienyl]manganese(I) (**19Mn**). A mixture of $Mn(CO)_5Br$ (0.223 g, 0.811 mmol), **5Na** (2, 0.597 g, 0.794 mmol), NaH (20 mg), and toluene (50 mL) was stirred under reflux for 1 day. The mixture was then filtered while still warm, and the filtrate was evaporated. The resulting residue was triturated with hexane, collected on a filter, and dried under vacuum to afford 0.197 g (0.259 mmol, 33%) of a yellow solid. An analytically pure sample was obtained by recrystallization from toluene. mp (sealed, nitrogen-filled capillary): 190-192 °C. IR (octane) ν_{CO} = 2044, 1980, 1970 cm^{-1}. ^{1}H NMR (THF-d_8): δ 6.29 (s, 1 H). ^{19}F NMR (THF-d_8): δ -131.53 (m, 2 F), -135.82 (d, ^3J = 21 Hz, 4 F), -140.30 (d, ^3J = 21 Hz, 2 F), -151.57 (t, ^3J = 24 Hz, 2 F), -153.27 (t, ^3J = 22 Hz, 2 F), -161.51 (m, 2 F), -162.04 (m, 2 F), -162.47 (m, 4 F). Anal. Calcd for $C_{32}HF_{20}MnO_3$: C, 44.27; H, 0.12. Found: C, 44.09; H, 0.05.

Tricarbonyl[η^5-1,2,3,4-tetrakis(pentafluorophenyl)cyclopentadienyl]rhenium(I) (**19Re**). A mixture of $Re(CO)_5Br$ (0.325 g, 0.800 mmol), **5Na** (2, 0.603 g, 0.802 mmol), NaH (20 mg), and toluene (50 mL) was refluxed for 1 day and then filtered while still warm. The filtrate was evaporated, and the resulting residue was triturated with hexane, collected on a filter, and dried under vacuum to afford 0.196 g (0.220 mmol, 28%) of an off-white solid. An analytically pure sample was obtained by recrystallization from toluene. mp (sealed, nitrogen-filled capillary): 205-207 °C. IR (hexane) ν_{CO} = 2047, 1970, 1959 cm^{-1}. ^{1}H NMR (THF-d_8): δ 6.95 (s, 1 H). ^{19}F NMR (THF-d_8): δ-131.89 (d, ^3J = 24 Hz, 2 F), -135.88 (m, 4 F), -140.94 (d, ^3J = 22 Hz, 2 F), -151.30 (t, ^3J = 21 Hz, 2 F), -153.23 (t, ^3J = 22 Hz, 2 F), -161.21 (m, 2 F), -161.93 (m, 2 F), -162.34 (m, 4 F). Anal. Calcd for $C_{32}HF_{20}O_3Re$: C, 38.45; H, 0.10. Found: C, 38.60; H, 0.05.

Chapter 5: Analysis of Substituent Effects In C_6F_5-Substituted Metallocenes

Introduction

Since its discovery over a half century ago, ferrocene and its derivatives have become the most intensely studied class of cyclopentadienyl compounds in organometallic chemistry. The diversity and ease by which these compounds are synthesized and characterized is one of their most attractive features.[149,150] As shown in Figure 5.1, ferrocene is easily functionalized by many simple reactions with various bases and electrophiles.[2] These reaction products can be further modified to afford a wide variety of unsymmetrical ferrocene analogs. Alternatively, functionalization of the Cp ligand before Fe(II) coordination affords symmetric ferrocene derivatives (Figure 5.2).[45,149,151,152]

The diversity of ferrocene analogues and their inherent chemical/thermal stability allow for their characterization by numerous analytical techniques. Of these techniques, electrochemistry, X-ray crystallography, and NMR spectroscopy are particularly useful and

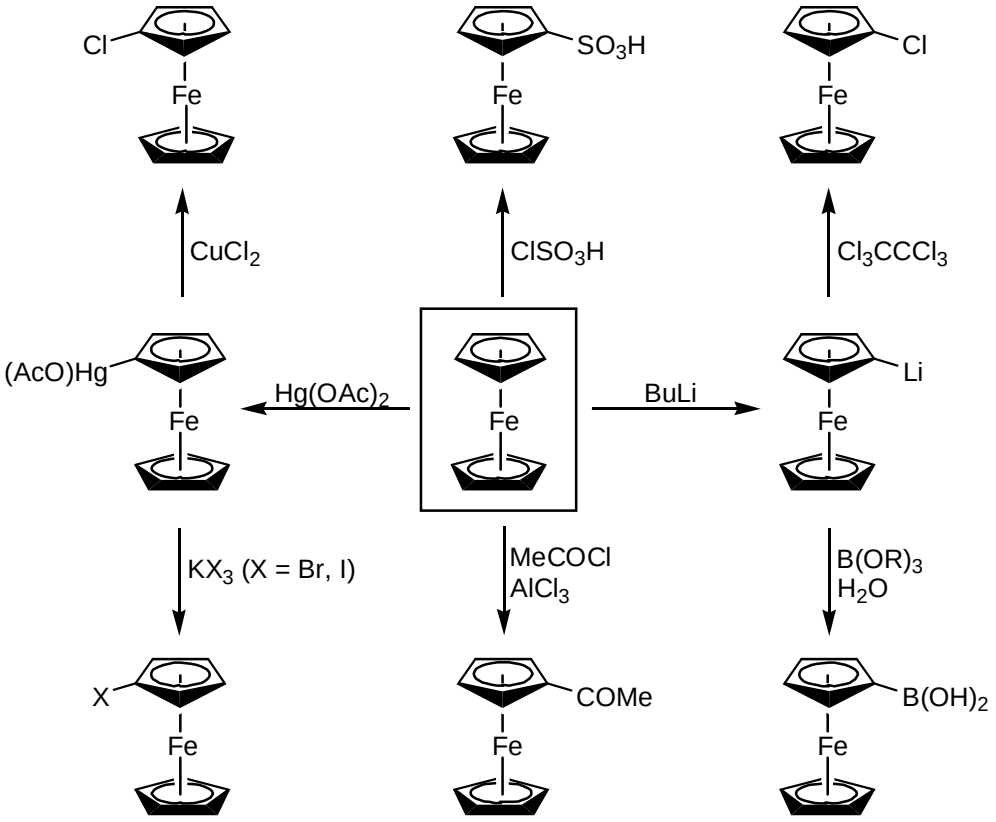

Figure 5.1. The functionalization of ferrocene.

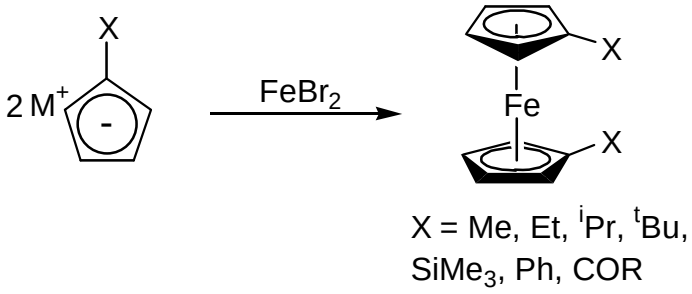

Figure 5.2. Synthesis of symmetrically substituted ferrocenes.

informative methods for analyzing the electronic and steric effects of ferrocene substituents. The characterization of ferrocene derivatives, especially those with C_6F_5 substituents, by the above techniques is the focus of this chapter.

Electrochemistry was initially applied to ferrocene and its derivatives as a method for predicting the reactivity of the complex toward electrophiles. More electronegative metals (Ru, Os) and electron-withdrawing substituents (acetyl) were known to diminish the electron-richness of the Cp ligand and slowed reactions with electrophilic substrates. It was suggested that this reactivity could be predicted by using electrochemistry (oxidation potentials) as a measure of ferrocene electron density.

Electronic Effect Studies

The effects of ferrocene substituents on metal electron density was first reported by Rosenblum in 1953. He observed that 1,1'-diacetylferrocene was not oxidized by $FeCl_3$ while ferrocene itself was readily oxidized under analogous conditions.[153] In the late 1950s, hydroxyferrocenes were shown to rapidly oxidized in air while ferrocene itself was stable.[154,155] It was not until 1960 that Mason used electrochemistry to quantify electronic effects on ferrocene electron density in a series of phenylferrocenes.[153] The *para*-position of the phenyl group was modified with various substituents and the oxidation potentials were measured. Electron-withdrawing groups (NO_2, COMe, Br) increased the oxidation potential by decreasing Fe(II) electron density while electron-releasing substituents (OMe) lowered the oxidation potential by increasing Fe(II) electron density. Mason also demonstrated how these oxidation potentials could be successfully correlated to Hammett substituent constants (σ_p) as shown in Figure 5.3.

In that same year, Kuwana and coworkers added to Mason's results with a similar study on mono- and disubstituted ferrocenes bearing substituents other than the phenyl group.[156] As

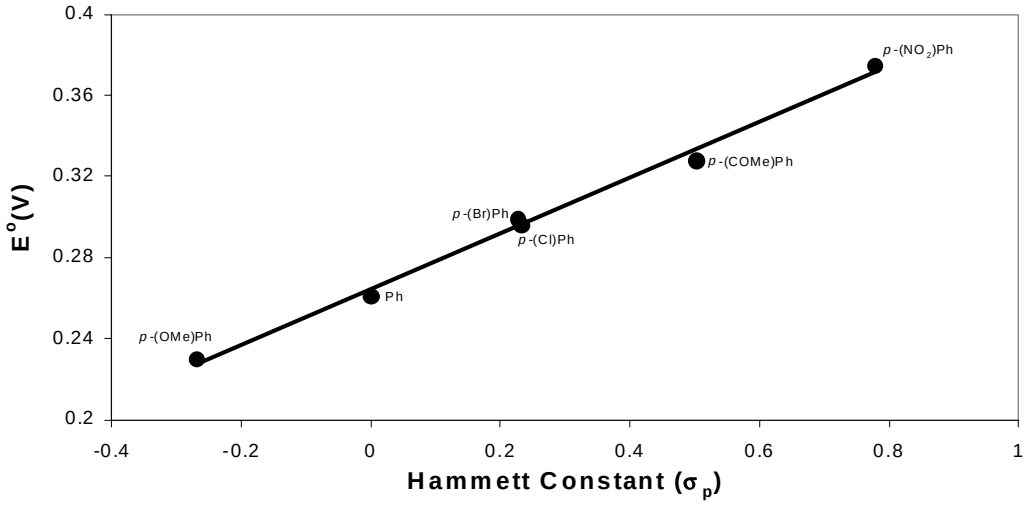

Figure 5.3. Plot of oxidation potential (E^o) vs. Hammett substituent constants.

shown in Table 5.1,[156] their study showed that electron-withdrawing substituents attached directly to the Cp ring (COMe, COOH) raised the potential required for oxidation while electron-releasing substituents (Et) lowered the Fe(II) oxidation potential. Additionally, ruthenocene exhibited a much higher oxidation potential relative to ferro0cene, suggesting that ferrocene is more electron-rich. Ferrocene is also more reactive than ruthenocene towards electrophilic substitution. The study also suggested that electronic effects on oxidation potentials were

Table 5.1. Oxidation potentials of substituted ferrocenes.

complex	$E_{1/4}(V)^a$
$[(COMe)Cp]_2Fe$	0.796(4)
Cp_2Ru	0.693(3)
[(COMe)Cp]CpFe	0.573(4)
[(COOH)Cp]CpFe	0.550(2)
$[(CH_2=CH)Cp]CpFe$	0.325(2)
Cp_2Fe	0.307(2)
[EtCp]CpFe	0.245(3)
$[EtCp]_2Fe$	0.194(1)

a. vs. SCE in 0.2 M $LiClO_4$-acetonitrile

additive. For example, Table 5.1 shows that each ethyl (Et) substituent lowers the oxidation potential by roughly 0.05 V. Since this study, several researchers have verified the additivity of electronic effects and estimated oxidation potentials from Hammett constants or vice versa.[157-160]

Steric Effect Studies

Since the pioneering work of Mason and of Kuwana, some researchers have suggested that the impact of steric effects on oxidation potentials is negligible.[161] To better understand the role of steric effects, oxidation potentials of heavily substituted ferrocene derivatives began to appear in several studies.[161-163] Figure 5.4 shows the oxidation potentials (relative to ferrocene) of four substituents (Me,[161] Et,[161] Ph,[161] $SiMe_3$[162]) in polysubstituted ferrocenes. An additive electronic effect is exhibited by the Me, Et, and Ph groups with the electron-releasing Me and Et substituents lowering the oxidation potential and the electron-withdrawing Ph substituent raising the oxidation potential. The $SiMe_3$-substituted ferrocenes initially exhibit an additive electron-withdrawing effect, however, the hexasubstituted derivative deviates from this linear trend by displaying an oxidation potential that is 0.137 V lower than the tetrasubstituted derivative. This is attributed to the release of steric strain that occurs upon oxidation. The oxidized Fe(III) complex possesses longer metal-carbon distances which are due to a Jahn-Teller distortion which

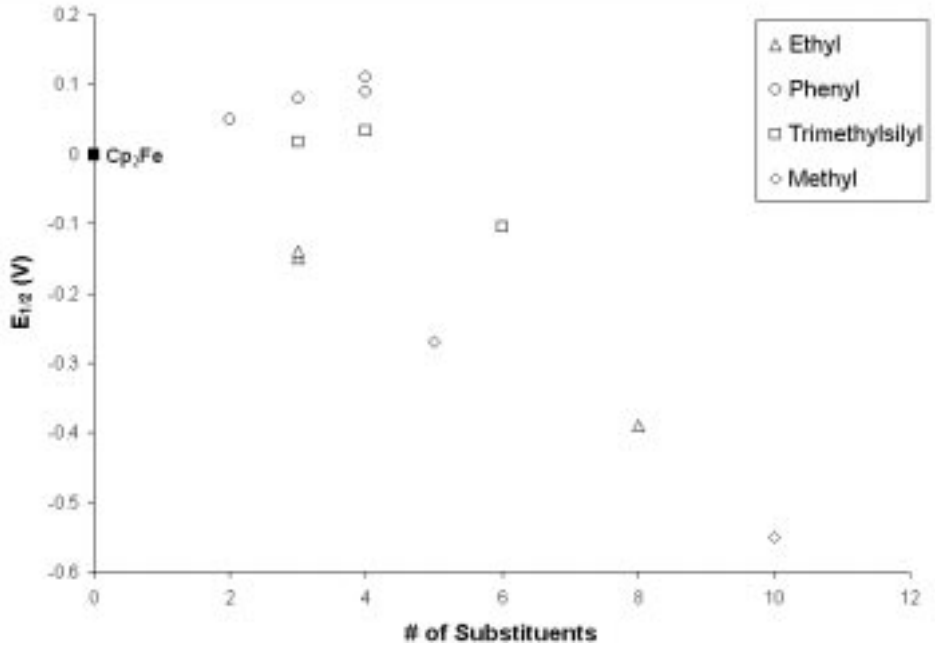

Figure 5.4. Plot of oxidation potentials vs. number of substituents.

is not possible in the low spin, d^6 Fe(II) precursor.[164,165]

Steric effects in ferrocene derivatives are more effectively examined by X-ray crystallography. Elongation of the Cp-Fe bond and deviation of substituents out of the Cp plane away from Fe(II) are both strong indicators of steric effects perturbing the ferrocene framework. The crystal structure of octaisopropylferrocene demonstrates how dramatic these steric effects can be.[45] A Fe-Cp(centroid) distance of 1.71 Å is substantially larger than that of ferrocene (1.654 Å). Additionally, the isopropyl-Cp bonds are displaced from the Cp plane by 13.9º with the isopropyl methine carbons displaced 0.34 Å from the Cp plane.

Recently, Hughes and coworkers examined the C_6F_5 group as a ferrocene substituent in an X-ray crystallographic study.[100] A crystal structure of the previously reported[91] 1,1'-bis(pentafluorophenyl)ferrocene (**20Fe**) exhibited a C_6F_5/C_6F_5 intramolecular stacking interaction. A distance of 3.58 Å defined the separation of the two aryl centroids which are nearly parallel and canted with respect to the Cp ring by an average torsion angle of 25º. The structure of 1,1'-bis(pentafluorophenyl)-2-(N,N-dimethylaminomethyl)ferrocene exhibits similar C_6F_5/C_6F_5 stacking.[95] A slightly longer aryl centroid separation distance (3.66 Å) can be attributed to the N,N-dimethylaminomethyl substituent. The steric effect of the dimethylaminomethyl group causes the adjacent C_6F_5 ring to adopt a larger interplanar torsion angle (40.7º) relative to the **20Fe** (25º). Despite this perturbation, the transannular C_6F_5 ring also increases its interplanar torsion angle (32.4º) and maintains the stacking interaction. It is still not clear whether or not similar intramolecular stacking interactions will exist in more crowded C_6F_5-substituted ferrocenes.

The rotational dynamics of Cp-Fe and Cp-substituent bonds are conveniently monitored with NMR spectroscopy. In 1981, Streitwieser and Luke described the measurement of the Cp rotational barrier in 1,1',3,3'-tetrakis(*t*-butyl)ferrocene.[166] At room temperature, the ^{1}H NMR shows one *t*-butyl resonance and two Cp ring resonances indicating time-averaged C_{2h} symmetry. Upon cooling to –60 ºC, two distinct *t*-butyl resonances are present while the Cp ring resonances have significantly broadened. A line-shape analysis of the *t*-butyl resonances yielded a $\Delta G^{\ddagger}$ value of 13.3 kcal/mol.[167] This rotational barrier is large relative to those measured for ferrocene (1.8 – 2.3 kcal/mol).[168-170] Figure 5.5 illustrates all ten possible rotamers, five staggered (s) and five eclipsed (e). Of the ten rotamers, there are four enantiomeric pairs (**b**/**b′**, **c**/**c′**, **d**/**d′**, **e**/**e′**) of C_2 symmetry. An arbitrary energy value of 1 is assigned for an eclipsing

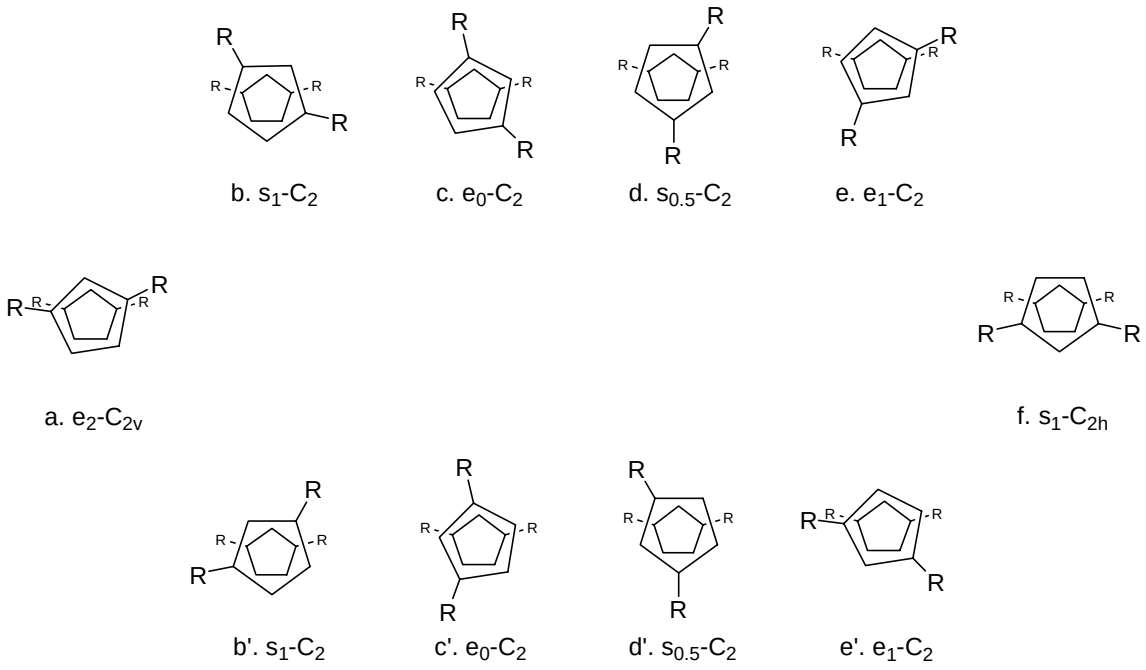

Figure 5.5. Rotamer diagram for a 1,1',3,3'-tetrasubstituted metallocene. Notation is described in the text.

transannular substituent interaction while staggered interactions are assigned a value of 0.5. The energy sum is displayed as a subscript and represents the destabilization due to transannular steric effects. The two *t*-butyl resonances in the low temperature ^{1}H NMR spectra eliminate **a** and **f** as rotamer ground state structures. Of the remaining enantiomeric pairs, **c**/**c′** possess the lowest enthalpic descriptors and are the most likely ground state structures. Additionally, the crystal structure of 1,1',3,3'-tetrakis(trimethylsilyl)ferrocene was shown to adopt a structure similar to rotomer **c′**.[171]

Variable temperature NMR spectroscopy has also been used to measure barriers to substituent rotation in crowded cyclopentadienyl ligands.[151,172] For example, Castellani and coworkers examined both Cp and aryl ring rotation in the octaphenylferrocene.[173] A variable temperature ^{1}H NMR analysis showed a decoalescence of the *meta* and *ortho* resonances into pairs of equally integrating signals. A free energy of activation ($\Delta G^{\ddagger}$ = 9 kcal/mol) was calculated at the coalescence temperature (–65 ºC) for the internal phenyl rings. No peak broadening attributable to slowed Cp-Fe rotation was detectable at temperatures as low as –95 ºC).

Chapter Overview

Electrochemistry, X-ray crystallography, and NMR spectroscopy are invaluable tools for understanding and evaluating substituent effects in ferrocene derivatives. This chapter describes the syntheses of several C_6F_5-substituted ferrocenes and cobaltocenes. The C_6F_5 substituent effect is evaluated by measuring the oxidation potentials of substituted ferrocenes while the C_6F_5 structural implications are characterized by X-ray crystallography and variable temperature NMR spectroscopy. These studies highlight the electron-withdrawing ability of the C_6F_5 substituent and its steric influence on metallocene structure.

Results & Discussion

Complex Synthesis

As shown in Figure 5.6, various C_6F_5-substituted Cp ligands react with 0.5 equivalents of $FeBr_2$ or $CoBr_2$ to afford the corresponding metallocenes. The synthetic details and characterization for complexes **20Fe**, **21Fe**, **20Co**, and **21Co** are described elsewhere.[91,93] The crystal structure of **20Fe** was also reported elsewhere.[100] The yields vary (34 – 88%) and decrease as C_6F_5-substitution increases. The diminished product yields are not surprising since increased arylation decreases the Cp anion's nucleophilic character and increases the crowding around the metal coordination sphere. The solubility of these metallocenes also decreases with increasing C_6F_5-substitution which makes isolation and purification difficult. The hexasubstituted metallocenes are virtually insoluble in hydrocarbon solvents at room temperature. However, they are soluble enough in CH_2Cl_2 and THF for ^1H and ^{19}F NMR characterization.

Attempts to synthesize metallocenes from **5Na** and various transition metal salts ($FeBr_2$, $CoBr_2$, $Fe(acac)_2$) were unsuccessful. Hedberg has reported similar problems with lithium

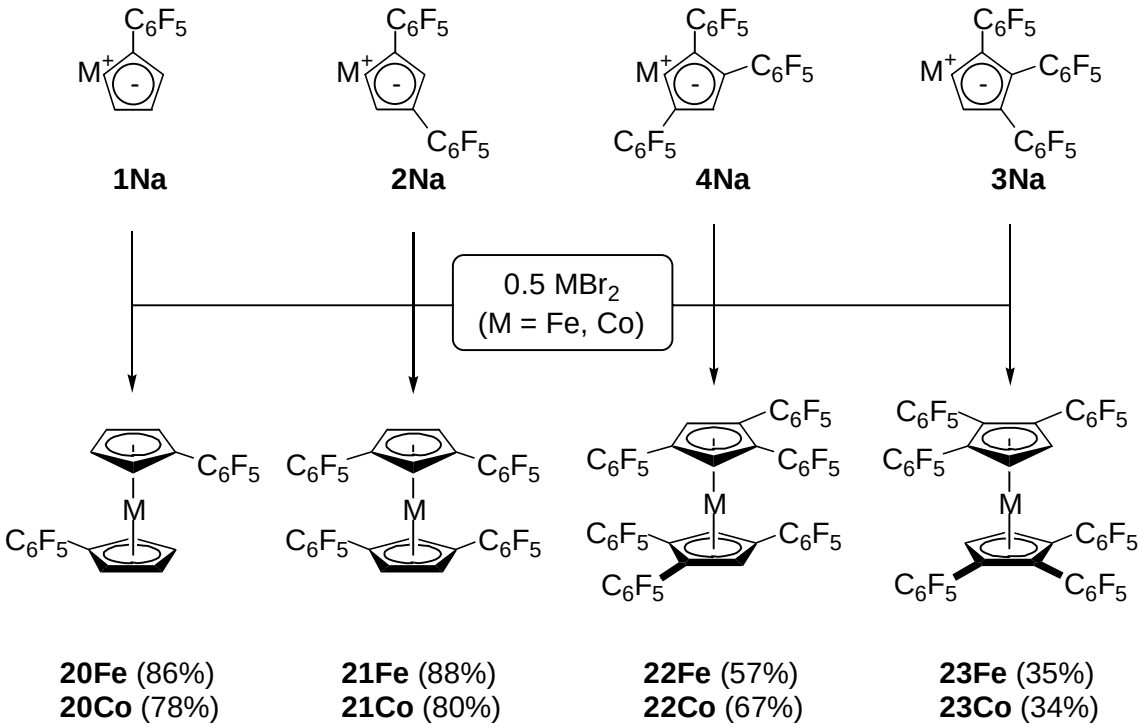

Figure 5.6. Synthetic scheme for C_6F_5-substituted metallocenes.

pentachlorocyclopentadienide.[64] The electron-withdrawing C_6F_5 and Cl substituents prevent metallocene synthesis by lowering the electron-donating ability of the Cp ligand. The bulky C_6F_5 groups in **5Na** could also impede substitution reactions with transition metal salts.

Electrochemical Analysis

Cyclic voltammograms of the C_6F_5-substituted ferrocenes indicate that all Fe(III)/Fe(II) couples are reversible. Square-wave voltammetry was used to obtain oxidation potentials relative to internal ferrocene (ΔE^o) and are listed as Table 5.2 along with the values for other studied substituents.[54,160,174] The electron-withdrawing nature of the C_6F_5 substituent increases the oxidation potential (ΔE^o) of ferrocene by as much as an entire volt (see **23Fe** and **22Fe**). Inspection of the net change in the potential per substituent (ΔE^o/group) reveals that the electron-withdrawing power of each C_6F_5 substituent is about 0.16 – 0.17 V. This narrow range for all four C_6F_5-substituted ferrocenes suggests an additive electronic effect on the oxidation potential. Compared to the other substituents in Table 5.2, the C_6F_5 group is moderately electron-withdrawing. The halo substituents are equally electron-withdrawing while the cyano,

Table 5.2. Comparison of oxidation potentials for substituted ferrocenes.

	E^o Data (V)			E^o Data (V)	
complex	ΔE^{oa}	ΔE^o/group[b]	complex	ΔE^{oa}	ΔE^o/group[b]
[1,2,3-$(C_6F_5)_3$]$_2$Fe (**23Fe**)	0.95[d]	0.16	[(HO_2C)Cp]CpFe	0.24	0.24
[1,2,4-$(C_6F_5)_3$]$_2$Fe (**22Fe**)	0.94[d]	0.16	[BrCp]CpFe	0.17	0.17
[1,3-$(C_6F_5)_2$]$_2$Fe (**21Fe**)	0.68[d]	0.17	[ClCp]CpFe	0.16	0.16
[(CF_3)Cp]$_2$Fe	0.64[d]	0.32	[ICp]CpFe	0.16	0.16
[(COMe)Cp]$_2$Fe	0.49	0.24	[PhCp]$_2$Fe	0.05[c]	0.02
[(NC)Cp]CpFe	0.37[c]	0.37	[$(SiMe_3)$Cp]$_2$Fe	0.005	0.002
[(C_6F_5)Cp]$_2$Fe (**20Fe**)	0.35[d]	0.17	Cp_2Fe	0.00	0.00
[BrCp]$_2$Fe	0.32	0.16	[MeCp]$_2$Fe	-0.10	-0.05
[(HCO)Cp]CpFe	0.28	0.28	Cp^*_2Fe	-0.54[d]	-0.05
[(MeCO)Cp]CpFe	0.25	0.25			

a. values are from literature cited in text except for **20Fe - 23Fe**; uncertainties are 10% or less; measured in CH_3CN unless specified otherwise; b. ΔE^o per substituent; c. average from two independently determined values; d. measured in CH_2Cl_2

trifluoromethyl, and carbonyl-based substituents are all significantly stronger. Accordingly, the order of substituent electron-withdrawing ability (from strongest to weakest) is as follows: CN > CF_3 > CHO > COMe, COOH > C_6F_5, Cl, Br, I > Ph > $SiMe_3$. As expected, the methyl group is electron-donating and lowers oxidation potentials by approximately 0.05 V per substituent.

As mentioned in the chapter introduction, oxidation potentials generally show a linear correlation with Hammett constants (σ_p). Figure 5.7 illustrates this trend with a plot of the ΔE^o values from Table 5.2 versus their substituent Hammett constants.[175,176] The plot exhibits the expected linear trend and the substituents that deviate have unique electronic (NH_2)[174] or steric ($SiMe_3$, ^iPr)[162,163] attributes. This plot indicates that the C_6F_5 electronic effect is additive and that the steric effect is minimal.

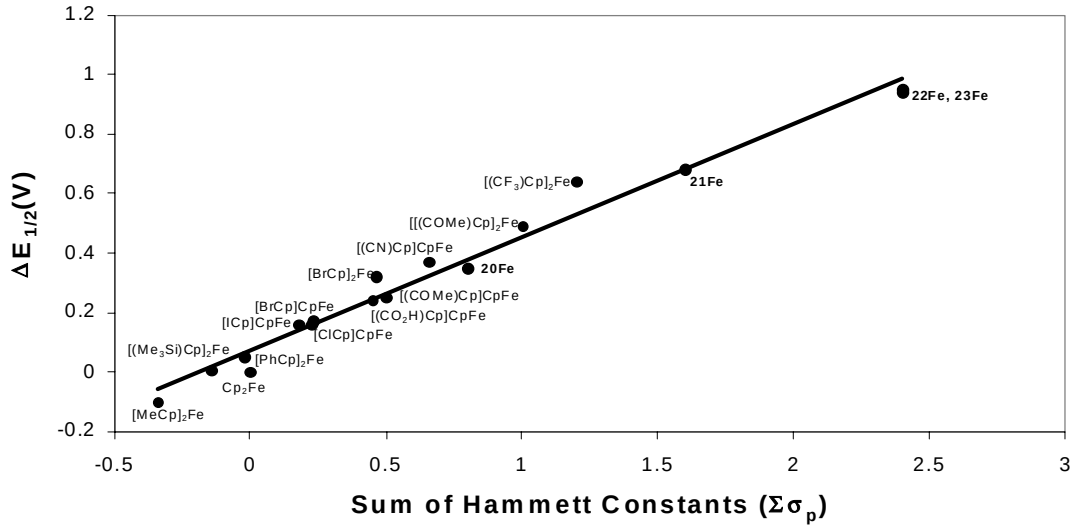

Figure 5.7. Plot of oxidation potential shifts vs. Hammett substituent constants.

Crystal Structures of Metallocenes

The X-ray crystal structure of **22Fe** is shown in Figure 5.8 and relevant crystallographic data are presented in Table 5.3. Some important bond distances are presented in Table 5.4 along with other ferrocene derivatives for comparison.[45,100,163,164,171,173,177-181] In **22Fe**, the Cp ligands are bonded in the typical pentahapto fashion with the M-C(ring) distances varying by 0.032 Å and 0.027 Å in either Cp ligand. Comparison of the average Fe-C(ring) and Fe-Cp(centroid) distances with other complexes indicates that these distances are not substantially elongated relative to other hexa- ($SiMe_3$[180]) and octasubstituted (Ph[173], ^iPr[45]) ferrocenes. However, the average M-C(ring) and M-Cp(centroid) distances are approximately 0.3 Å and 0.015 Å longer

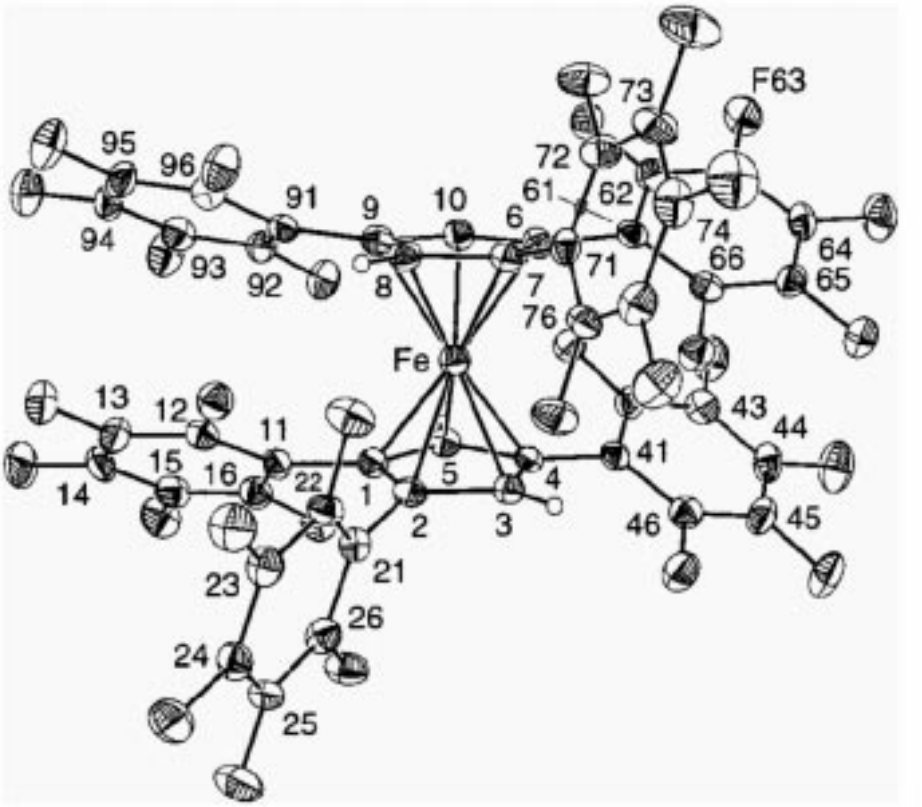

Figure 5.8. Thermal ellipsoid plot of **22Fe** shown at 50% probability. Benzene solvate molecules were omitted for clarity.

than those found in ferrocene.[178] The similar bond distances between **22Fe** and [1,2,4-$(C_6H_{11})_3Cp]_2Fe$ suggest that the C_6F_5 and C_6H_{11} (cyclohexyl) substituents exhibit similar steric effects.[181]

The Cp-C_6F_5 dihedral angles in **22Fe** are listed in Table 5.5 and are compared with other ferrocenes.[95,100,165,173] The angles range from 27.3º to 77.0º with the isolated (iso) C_6F_5 groups possessing the smallest angles and the C_6F_5 groups with vicinal (vic) C_6F_5 rings possessing the largest angles. These angles are much larger than those previously observed in **20Fe** (24.1º – 26.0º).[100] The presence of two intramolecular C_6F_5/C_6F_5 stacking interactions significantly lowers the dihedral angles of the involved C_6F_5 groups. Among the C_6F_5 substituents with a vicinal C_6F_5 group, the stacking C_6F_5 rings have smaller dihedral angles (by roughly 40º) relative to the nonstacking C_6F_5 rings. Clearly, the stacking interaction forces the aryl rings to become increasingly coplanar with the plane of the Cp ring. However, the presence of a vicinal C_6F_5 group prevents the stacking rings from attaining dihedral angles as small as those in **20Fe**.

Table 5.3. Crystallographic data for C_6F_5-substituted metallocenes.

compound	**22Fe**	**23Co**
empirical formula	$C_{46}H_4F_{30}Fe \cdot 4C_6H_6$	$C_{46}H_4CoF_{30}$
fw	1494.77	1185.42
diffractometer	Nonius Kappa	Siemens P4
cryst dimens (mm)	0.12 × 0.15 × 0.25	0.51 × 0.16 × 0.08
cryst system	triclinic	monoclinic
a (Å)	11.7507(4)	7.5933(8)
b (Å)	13.1551(4)	14.2469(15)
c (Å)	20.7085(6)	38.263(4)
α (deg)	84.443(2)	90
β (deg)	78.008(2)	91.728(8)
γ (deg)	70.1770(10)	90
V (Å)^3	2944.41(16)	4137.5(7)
space group	Pī (No. 2)	$P2_1/c$ (No. 14)
Z	2	4
D_{calc} (Mg m^{-3})	1.686	1.903
abs coeff (mm^{-1})	0.4	0.588
F_{000}	1488	2308
λ (Mo K_α) (Å)	0.71073	0.71073
temp (K)	100	293
range for collection	0.0-30.0	1.06-21.50
no. of reflns colld	16606	6508
no. of indep reflns	16603	4752
abs corr method	empirical	integration
data / restrs / params	16603/0/910	4750/0/694
R [$I > 2\sigma(I)$]	0.040	0.0467
R_W [$I > 2\sigma(I)$]	0.078	0.1054
GoF on F^2	0.762	0.915
peak, hole (e Å^{-3})	0.58, -0.42	0.266, -0.319

Table 5.4. Selected bond distances of substituted metallocenes.

	bond distances (Å)[a]		
complex	ave. M-C(ring)	M-Cp	Cp-M-Cp
Cp_2Fe	2.033	1.654	3.308
Cp^*_2Fe	2.050(2)	1.662	3.324
$[1,2,4\text{-}(^iPr)_3Cp]_2Fe$	2.055(9)	1.662(7)	3.324(10)
$[1,3\text{-}(Me_3Si)_2Cp]_2Fe$	2.059(4)	1.660	3.320
$[1,2,4\text{-}(C_6H_{11})_3Cp]_2Fe$	2.06(1)	1.66	3.32
$[1,2,4\text{-}(C_6F_5)_3Cp]_2Fe$ (**22Fe**)	2.062(4) 2.063(4)	1.669(2) 1.669(2)	3.338
$[(C_6F_5)Cp]_2Fe$	2.08(3) 2.11(3)		
$[1,2,4\text{-}(Me_3Si)_3Cp]_2Fe$	2.082(2)	1.686	3.372
$[1,2,3,4\text{-}Ph_4Cp]_2Fe$	2.086(6)	1.695(2)	3.390(3)
$[1,2,3,4\text{-}(^iPr)_4Cp]_2Fe$	2.095(8) 2.098(7)	1.707 1.708	3.415
Cp_2Co	2.096(8)		
Cp^*_2Co	2.105(2)		
$[1,2,4\text{-}(^iPr)_3Cp]_2Co$	2.122(7)	1.745(3)	3.49
$[1,2,3\text{-}(C_6F_5)_3Cp]_2Co$ (**23Co**)	2.133(15) 2.121(15)	1.760(7) 1.743(7)	3.503

a. values are from literature cited in the text except for **22Fe** and **23Co**

The crystal of **22Fe** was isolated as a benzene solvate (**22Fe** + $4C_6H_6$) and the partial packing diagram is shown in Figure 5.9. Interestingly, every C_6F_5 ring is involved in some form of intra- (C_6F_5) or intermolecular (C_6H_6) pi stacking. The intramolecular C_6F_5/C_6F_5 stacking interactions are defined by centroid-centroid distances of 3.78 Å and 3.72 Å while the intermolecular C_6F_5/C_6H_6 stacking distances are generally larger (3.79, 3.92, 4.02, 4.17 Å). Vicinal C_6F_5 rings presumably prohibit shorter stacking distances like those seen in **20Fe** (3.58 Å).[100]

The crystal structure of **23Co** is shown in Figure 5.10 and relevant crystallographic data are presented in Table 5.3. Some important bond distances are listed in Table 5.4 along with

Table 5.5. Dihedral angles for some aryl substituted metallocenes.

complex	dihedral angle (deg)[a]	complex	dihedral angle (deg)[a]
[1,2,4-$(C_6F_5)_3Cp]_2Fe$ (**22Fe**)	77.0 (vic) 75.2 (vic) 39.6 (vic, s) 36.7 (vic, s) 30.7 (iso, s) 27.3 (iso, s)	[1,2,3-$(C_6F_5)_3Cp]_2Co$ (**23Co**)	83.8 (int) 56.6 (int) 52.6 (ext) 49.4 (ext, s) 46.9 (ext) 45.4 (ext, s)
$[1,2,3,4\text{-}Ph_4Cp]_2Fe$	77.1 (int) 47.5 (int) 33.0 (ext) 15.3 (ext)	$[1,2,3,4\text{-}Ph_4Cp]_2Co$	71.1 (int) 46.0 (int) 32.6 (ext) 18.8 (ext)
$[(C_6F_5)Cp]_2Fe$[b]	24.1, 26.0 (s) 25.3, 24.5 (s)	[1-(C_6F_5)-2-(CH_2NMe_2)Cp] $[(C_6F_5)Cp]Fe$	40.7 (s) 32.4 (s)

a. values are from literature cited in the text except for **22Fe** and **23Co**; uncertainties are 2% or less; aryl group abbreviations (vic = vicinal; iso = isolated; int = internal; ext = external; s = intramolecular C_6F_5 stacking interaction); b. torsion angles

other cobaltocene derivatives for comparison.[163,177,179] The Cp ligands are bound in a slightly distorted pentahapto bonding mode with the M-C(ring) distances varying by 0.110 Å and 0.098 Å in either Cp ligand. As steric effects suggest, the longer M-C(ring) bond distances occur at the C_6F_5-substituted positions. The average Co-C(ring) distances (2.133, 2.121 Å) are slightly longer than those seen in cobaltocene (2.096 Å) and decamethylcobaltocene (2.105 Å). The bond distances for **23Co** are similar to those found in [1,2,4-$(^iPr)_3Cp]_2Co$.

The Cp-C_6F_5 dihedral angles in **23Co** are listed in Table 5.5 and are compared with other

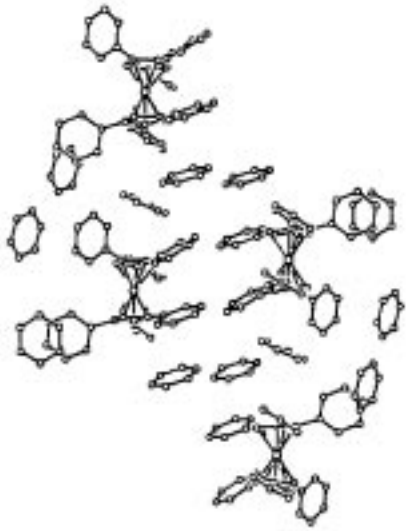

Figure 5.9. Partial packing diagram of **22Fe**, showing arene stacking motifs.

Figure 5.10. Thermal ellipsoid plot of **23Co** at 50% probability.

cobaltocenes.[95,100,165,173] The angles range from 45.4º to 83.8º with the external (ext) C_6F_5 groups possessing the smallest angles an d the internal (int) C_6F_5 groups possessing the largest angles. The internal C_6F_5 ring dihedral angles (83.8º, 56.6º) are larger than those measured for the internal phenyl rings of [1,2,3,4-Ph_4Cp]$_2$Co (71.1º, 46.0º).[165] Two of the external C_6F_5 rings are i nvolved in an intramolecular stacking interaction defined by a long centroid-centroid distance of 4.20 Å. The dihedral angles of the two stacking C_6F_5 rings (49.4º, 45.4º) represent the largest angles ever found for an intramolecular C_6F_5/C_6F_5 stacking interaction in a metallocene. An additional intermolecular C_6F_5/C_6F_5 stacking interaction was found and has a centroid-centroid distance of 3.89 Å.

NMR Spectroscopic Analysis

As shown at the top of Figure 5.11, the room temperature ^{1}H NMR spectrum of **22Fe** (in THF-d_8) exhibits a single Cp resonance at 5.61 ppm suggesting that rotation about the Cp-Fe axis is fast. Upon lowering the temperature, the signal decoalesces into a two signals of equal intensity. This feature is attributed to slowing Cp-Fe rotation and will be explained in detail below. A lineshape analysis for this process yields a free energy of activation ($\Delta G^{\ddagger}$) of 10 kcal/mol. Table 5.6 compares this value to Cp-Fe rotational barriers in other ferrocene

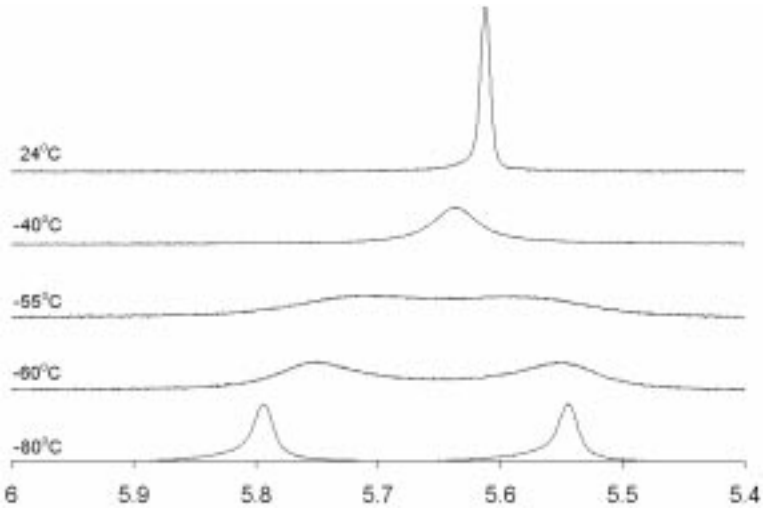

Figure 5.11. Stacked plot of ^{1}H NMR spectra of **22Fe** obtained at several temperatures in THF-d_8 at 500 MHz.

complexes.[166,168-171,180,182,183] The rotational barrier is roughly 8 kcal/mol larger than that of ferrocene but similar to several $SiMe_3$-substituted ferrocenes.

A variable temperature ^{19}F NMR analysis (Figure 5.12) of **22Fe** further supports the ^{1}H NMR observations. The room temperature spectrum suggests fast Cp-Fe rotation with two fluorine signals (2:1) in the *para* region (–153 to –158 ppm) representing the four equivalent

Table 5.6. Cp rotational barriers in ferrocene derivatives.

complex	$\Delta G^{\ddagger}$ (kcal/mol)[a]
Cp_2Fe	1.8-2.3
[4-(^{t}Bu)-1,2-$(Me_3Si)_2Cp]_2Fe$	9.7
[1,2,4-$(C_6F_5)_3Cp]_2Fe$ (**22Fe**)	10.0
[1,3-$(Me_3Si)_2Cp]_2Fe$	11.0
[1,2,4-$(Me_3Si)_3Cp]_2Fe$	11.0
[1,3-(^{t}Bu)$_2$Cp]$_2$Fe	13.1-13.3
[1,2,3,4-(^{i}Pr)$_4$Cp]$_2$Fe	13.6

a.values from literature cited in the text except for **22Fe**; at 298 K; uncertainties are 15% or less

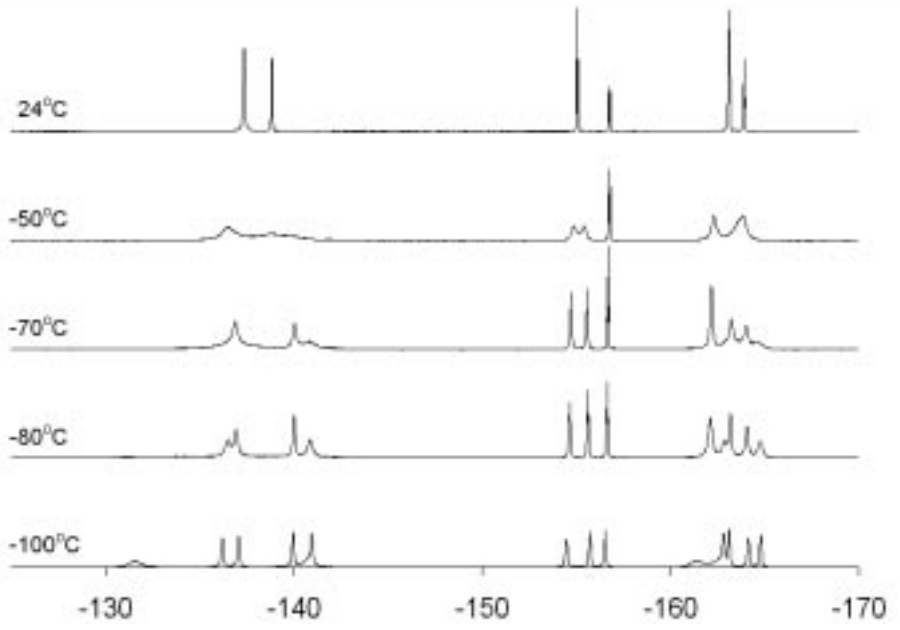

Figure 5.12. Stacked plot of ^{19}F NMR spectra of **22Fe** obtained at several temperatures in THF-d_8 at 470 MHz.

vicinal C_6F_5 groups and the two equivalent isolated C_6F_5 groups. As the temperature is lowered, the vicinal C_6F_5 signal (–155 ppm) decoalesces into two equally integrating signals signifying the loss of time-averaged C_{2h} symmetry. The additional broadening of the vicinal *ortho* signal at –137 ppm and the vicinal *meta* signal at –163 ppm is attributed to slowing rotation about the Cp-C_6F_5 bonds as was previously described in the piano stool complexes **18Mn** and **18Re**.

The loss of time-averaged C_{2h} symmetry in **22Fe** is explained with the aid of the rotamer dia gram shown in Figure 5.13. Of the ten rotamers, **a** and **f** are eliminated as possible ground state structures since neither would be expected to possess two ^{1}H NMR signals. The four remaining enantiomeric pairs would all display two Cp signals. The arbitrary enthalpic units suggest that the ground state structures are **c**/**c′** and this is indeed the case for [1,2,4-$(SiMe_3)_3Cp]_2Fe$.[180] However, the crystal structure of **22Fe** (Figure 5.8) suggests that rotamers **e**/**e′** are the ground state structures. There are two possible explanations for this discrepancy. First, unlike the spherical $SiMe_3$ substituent, the ellipsoidal C_6F_5 groups can rotate in a gear-like fashion to reduce vicinal and transannular steric strain. As one C_6F_5 group lowers its dihedral angle to avoid a transannular contact, the vicinal C_6F_5 group's dihedral angle can increase to facilitate this process by lowering vicinal steric strain. Secondly, the rotamer diagram does not

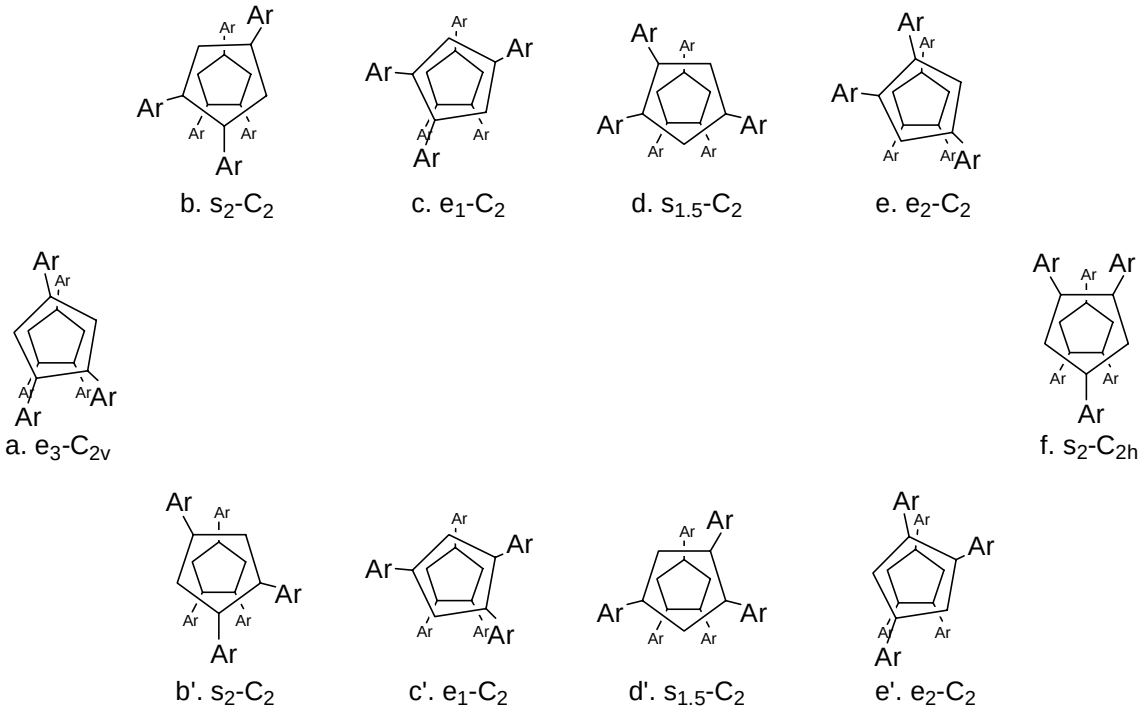

Figure 5.13. Rotamer diagram for **22Fe**. Notation is described in the text.

account for any stabilization incurred from aryl stacking interactions. Of the four enantiomeric pairs, only **e**/**e′** allows the formation of two intramolecular stacking interactions.

The variable temperature ^{19}F NMR spectra of **23Fe** are presented in Figure 5.14 and, as with **22Fe**, reveal two dynamic processes. First, the broadening and decoalescence of the *ortho* signal at –137 ppm and the *meta* signal at –164 ppm indicate the slowing rotation of the four external C_6F_5 groups. Similar spectral features were observed for piano stool complexes **17Mn** and **17Re** (chapter 3). Lineshape analysis of the *ortho* signal yields an Arrhenius activation energy (E_a) of 9(1) kcal/mol which is similar to the barriers calculated for piano stool complexes possessing the same Cp ligand (see chapter 4).

The para signal (–155 ppm) representing the four external C_6F_5 groups broadens at –100˚C and suggests that the second dynamic process involves slowing Cp-Fe rotation. Unfortunately, the solvent (THF-d_8) freezes before the slow-exchange data needed to calculate $\Delta G^{\ddagger}$ can be obtained. Analysis of the rotamer diagram in Figure 5.15 provides some rationale for the observed signal broadening. Rotamers **g** and **l** can not be the ground state structures since neither would produce the observed external C_6F_5 *para* signal broadening. The remaining four enantiomeric pairs would lead to signal broadening because the external C_6F_5 groups on an

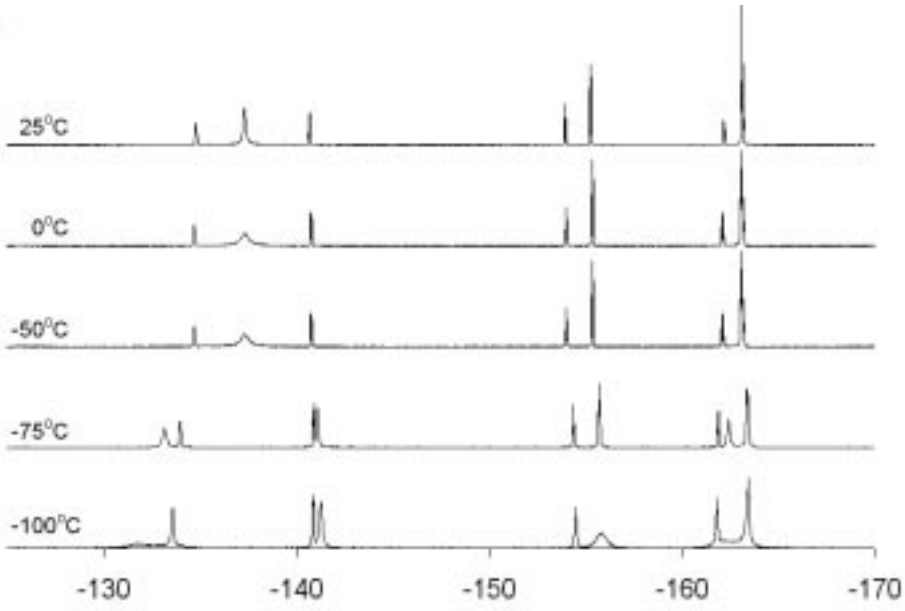

Figure 5.14. Stacked plot of ^{19}F NMR spectra of **23Fe** obtained at several temperatures in THF-d_8 at 470 MHz.

individual Cp ring have different transannular neighbors. The enthalpic units suggest that **k**/**k′** are the ground state structures because they possess the minimal amount of transannular steric strain. While an X-ray crystal structure for **23Fe** was not obtained, the crystal structure of **23Co** was found to adopt a conformation similar to **k′** in agreement with the qualitative enthalpic energy units predicted by the rotamer diagram. The variable ^{1}H NMR spectra exhibited no broadening attributable to chemical exchange.

Conclusion

With the aid of electrochemistry, X-ray crystallography, and NMR spectroscopy, several electronic and steric implications of the C_6F_5 substituent were characterized. Ferrocene oxidation potentials showed the C_6F_5 group to be as electron-withdrawing as several halo substituents but not as much as cyano, trifluoromethyl, or carbonyl-based substituents. Each C_6F_5 substituent raises the ferrocene oxidation potential by approximately 0.165 V. X-ray crystallography suggests that a C_6F_5 steric effect does lengthen the Cp-M bond but not enough to perturb oxidation potentials. Finally, the ellipsoidal shape and stacking tendency of the C_6F_5 substituent contributes to the dynamic rotational behavior observed in the variable temperature NMR spectroscopy experiments.

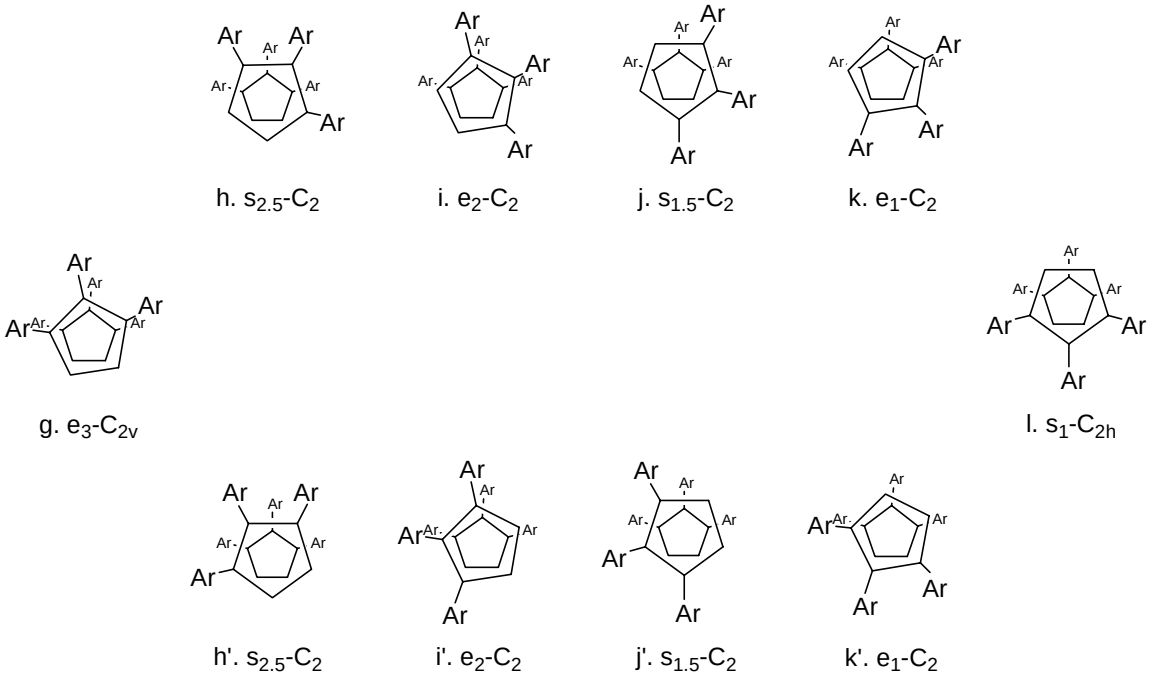

Figure 5.15. Rotamer diagram for **23Fe**. Notation is described in the text.

Experimental Section

General Procedures. Standard inert-atmosphere techniques were used for all reactions. $FeBr_2$ was used as received from Aldrich. Anhydrous $CoBr_2$ was prepared by heating the red commercial hydrate (Fisher) under vacuum to obtain a bright green powder. Complexes **20Fe**, **20Co**, **21Fe**, and **21Co** were prepared as previously reported.[91,93] NMR experiments used JEOL ECP500 or Varian U400 instruments. THF-d_8 was vacuum-transferred from Na/K alloy. ^{19}F NMR spectra were referenced to external C_6F_6 at –163.00 ppm in $CDCl_3$. All metallocenes were insufficiently soluble for ^{13}C NMR analysis. Elemental analyses were performed by Desert Analytics (Tucson, AZ).

Electrochemical Studies. Single-sweep cyclic and Osteryoung square-wave voltammetric data were obtained for the sparingly soluble substituted ferrocenes **22Fe** and **23Fe** at nominal concentrations of about 2 μM in CH_2Cl_2 using 0.10 M [*n*-Bu_4N][PF_6] as the electrolyte and activated alumina as an internal desiccant. Sample voltamograms are presented in Figure 5.16. The apparatus was a BioAnalytical Systems BAS-100B automated digital potentiostat with a Pt-disk working electrode, a Pt wire auxiliary electrode, and a Ag/AgCl reference electrode. Cyclic voltammetric (CV) sweeps for substituted ferrocenes were typically initialized at +100 mV, scanned to +1100 mV, and reversed to +100 mV, at a scan rate 100 mV s^{-1}. $|E_{ox} - E_{red}|$ were less than 80 mV, and I_c/I_a ratios were within 15% of unity, both indicators of substantially reversible couples. Shifts in oxidation potential of substituted ferrocenes were obtained by Osteryoung square-wave voltammetry (OSWV) using ferrocene as an internal standard. The cell voltage was

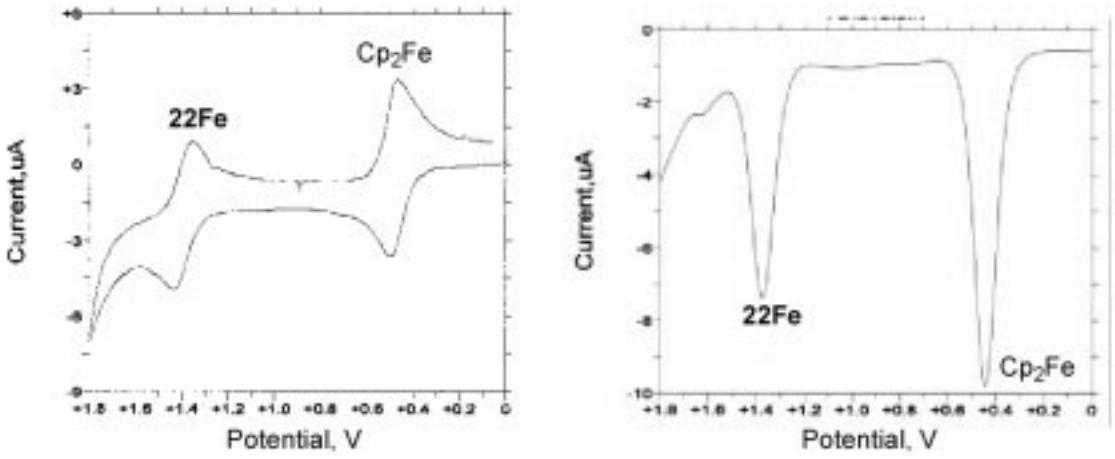

Figure 5.16. Sample cyclic and Osteryoung square-wave voltamograms.

typically swept from -200 to +1100 mV with a step resolution of 4 mV, a square wave-amplitude of 25 mV, and frequency of 15 Hz.

Crystallographic Studies. Crystallography was performed by Carla Slebodnick (Virginia Tech) for **23Co** or Frank Fronczek (Louisiana State University) for **22Fe**. Crystals of **22Fe** were grown from benzene by slow evaporation. Crystals of **23Co** were obtained by slow evaporation of an *n*-octane solution at 25 ºC. No unusual procedures were required in the preparation of any of these crystals, except that the benzene solvate of **22Fe** must be handled quickly after removal from the mother liquor. The single-crystal X-ray diffraction analyses (data collection, solution, and refinement) were unremarkable.

Bis[η ^{5}-1,2,4-tris(pentafluorophenyl)cyclopentadienyl]iron(II) (22Fe). A mixture of sodium 1,2,4-tris(pentafluorophenyl)cyclopentadienide (**4Na**, 0.493 g, 0.841 mmol), $FeBr_2$ (0.095 g, 0.44 mmol), and THF (50 mL) was refluxed for 1 day, and then the solvent was evaporated. The residue was extracted with hot toluene (50 mL) and filtered, and the filtrate was evaporated. The resulting orange solid was washed with pentane (50 mL) on a fritted filter to afford 0.284 g (0.24 mmol, 57%) of an orange solid. ^{1}H NMR (THF-d_8): δ 5.61 (s, 4 H). ^{19}F NMR (THF-d_8): δ -137.36 (br s, 8 F), -138.84 (d, ^3J = 16 Hz, 4 F), -155.08 (t, ^3J = 20 Hz, 4 F), -156.78 (t, ^3J = 20 Hz, 2 F), -163.11 (m, 8 F), -163.92 (m, 4 F). Anal. Calcd for $C_{46}H_4F_{30}Fe$: C, 46.73; H, 0.34. Found: C, 46.62; H, 0.16.

Bis[η ^{5}-1,2,3-tris(pentafluorophenyl)cyclopentadienyl]iron(II) (23Fe). A mixture of sodium 1,2,3-tris(pentafluorophenyl)cyclopentadienide (**3Na**, 0.305 g, 0.520 mmol), $FeBr_2$ (0.052 g, 0.243 mmol), and THF (25 mL) was refluxed for 1 day. The THF was then evaporated. The residue was extracted with hot toluene (25 mL), filtered, and cooled to room temperature to afford 0.100 g (0.084 mmol, 35%) of orange crystals. ^{1}H NMR (THF-d_8): δ 5.63 (s, 4 H). ^{19}F NMR (THF-d_8): δ -134.82 (s, 2 F), -137.33 (br s, 8 F), -140.69 (d, ^3J = 24 Hz, 2 F), -153.96 (t, ^3J = 21 Hz, 2 F), -155.27 (t, ^3J = 20 Hz, 4 F), -162.17 (m, 2 F), -163.14 (m, 10 F). Anal. Calcd for $C_{46}H_4F_{30}Fe$: C, 46.73; H, 0.34. Found: C, 46.50; H, 0.24.

Bis[η^5-1,2,4-tris(pentafluorophenyl)cyclopentadienyl]cobalt(II) (22Co). A mixture of **4Na** (0.494 g, 0.843 mmol), $CoBr_2$ (0.093, 0.425 mmol), and THF (25 mL) was refluxed for 1 day, cooled, and filtered. Evaporation of the filtrate afforded a violet solid, which was triturated with toluene, collected on a filter, and dried under vacuum to afford 0.337 g (0.284 mmol, 67%) of a

purple solid. ^{1}H NMR (THF-d_8): δ 1.7 (br s). ^{19}F NMR (THF-d_8): δ -84.60 (br s, 4 F), -100.76 (br s, 10 F), -129.73 (s, 4 F), -163.09 (s, 8 F), -179.62 (s, 4 F). Anal. Calcd for $C_{46}H_4F_{30}Co$: C, 46.73; H, 0.34. Found: C, 46.58; H, 0.05.

Bis[η ^{5}-1,2,3-tris(pentafluorophenyl)cyclopentadienyl]cobalt(II) (23Co). A mixture of **3Na** (0.265 g, 0.422 mmol), $CoBr_2$ (0.047 g, 0.215 mmol), and THF (50 mL) was refluxed for 1 day, cooled, and filtered. Evaporation of the filtrate afforded a violet solid, which was triturated with hexanes, collected on a filter, and dried to afford 0.086 g (0.072 mmol, 34%) of a purple solid. ^{1}H NMR (THF-d_8): δ -20.5 (br s). ^{19}F NMR (THF-d_8): δ -43.3 (s, 2 F), -84.4 (br s, 8 F), -125.8 (s, 4 F), -142.5 (s, 2 F), -144.0 (s, 2 F), -146.2 (t, ^{3}J = 21 Hz, 2 F), -160.3 (br s, 8 F), -163.0 (s, 2F). Anal. Calcd for $C_{46}H_4F_{30}Co$: C, 46.73; H, 0.34. Found: C, 46.58; H, 0.05.

Chapter 6: Electronic Effects in Metallocene-Catalyzed Olefin Polymerization

Introduction

Metallocenes were first used to polymerize olefins in the late 1950s. Originally, these complexes were studied as homogenous models for the heterogenous Ziegler-Natta catalysts still used by industry. The earliest studies found poor to moderate ethylene polymerization activity when Cp_2TiX_2 (X = Cl, Me, Et) was used in conjunction with alkylaluminum cocatalysts.[184-186] It was eventually discovered that the controlled addition of water to trimethylaluminum afforded a better cocatalyst known as methylalumoxane (MAO).[187-189] In the early 1980s, Kaminsky and Sinn were the first to report the use of a MAO/Cp_2ZrX_2 (X = Me, Cl) polymerization catalyst for which the polymerization activities were comparable to those obtained with heterogenous Ziegler-Natta catalysts.[190-193] Since these early studies, the research in the field of metallocene-catalyzed olefin polymerization has expanded tremedously.[190,194-203]

Figure 6.1 illustrates the simplified and generally accepted olefin polymerization mechanism.[1] After methylating Cp_2ZrCl_2, the MAO abstracts a methide ligand to form the active metallocenium polymerization catalyst. Next, ethylene monomer coordinates to the electron-deficient metal. In the rate-limiting step, ethylene inserts into the Zr-alkyl bond, beginning polymer chain growth. Chain propagation involves subsequent ethylene insertion into the Zr-polymer bond. Chain termination can occur by chain transfer (to monomer or aluminum) or β-hydride elimination pathways. The resultant Zr(IV) products can also insert ethylene into their metal alkyl and hydride bonds thus beginning new polymer chains.

Altering the catalyst activity and polymer properties through ligand modification is one of the more thoroughly studied and reviewed areas of metallocene-catalyzed olefin polymerization.[42,43,195,196] To make the review manageable, this chapter will specifically focus on the study of Cp substituent effects within the nonbridged derivatives of zirconocene dichloride, Cp_2ZrCl_2.

Substituent Effect Examples

Of the many polymerization substituent effect studies, only a few are complete enough to allow the elucidation of steric and electronic effects. Often, researchers attempt to compare their polymerization data with results obtained by others. Unfortunately, these comparisons are poor at best since the catalyst and polymer properties are highly dependent on subtle aspects of the

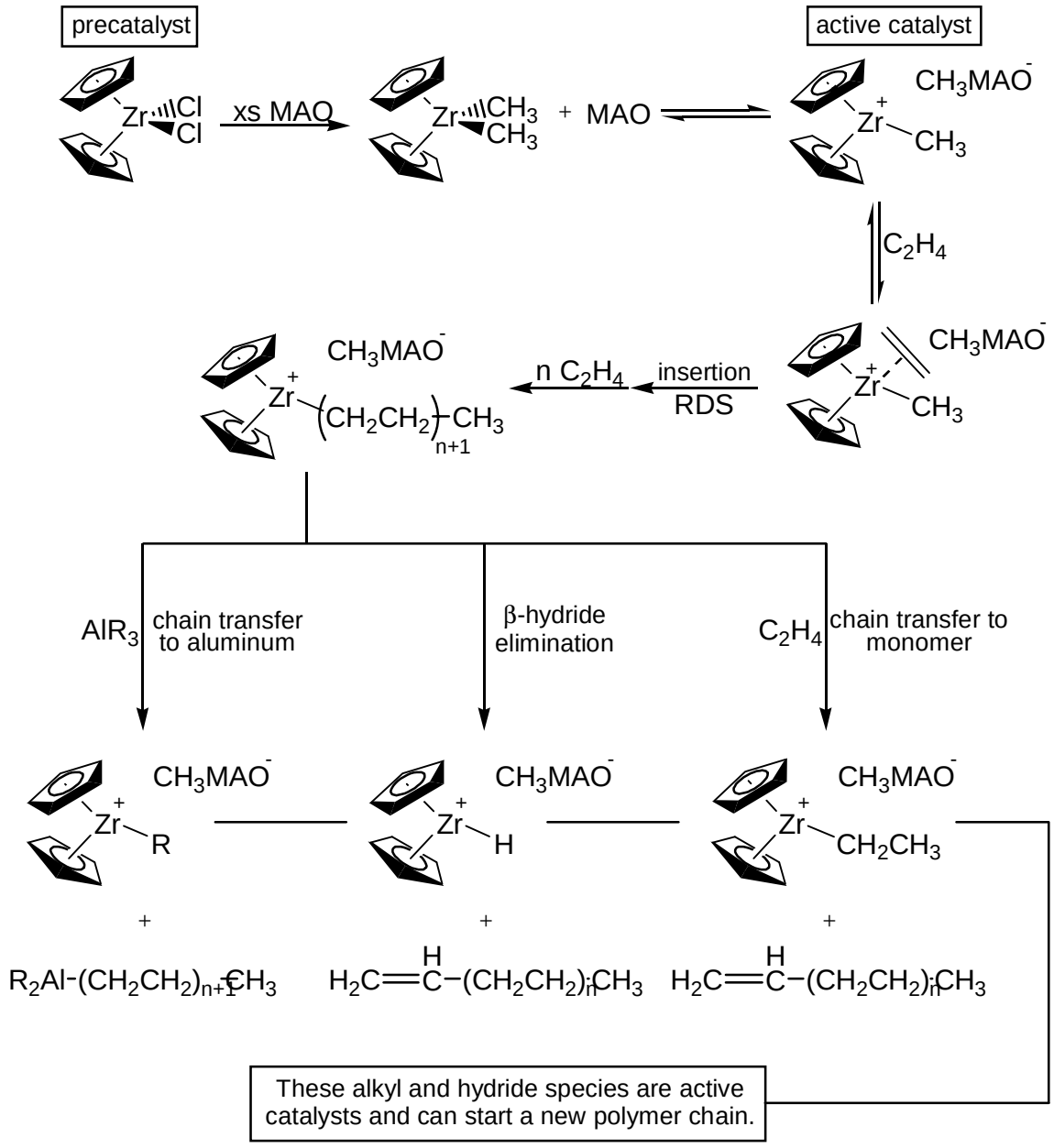

Figure 6.1. Simplified ethylene polymerization mechanism.

polymerization (reactor geometry, stirring, monomer introduction, catalyst activation, etc.). The following examples of substituent effects were chosen because several substituents varying in size and electron-donating ability were surveyed under uniform polymerization conditions. Ethylene homopolymerizations will be addressed initially followed by ethylene/1-hexene copolymerizations.

In 1992, Möhring and Coville used a combination of Hammett constants and substituent cone angles to assess substituent effects for a series of 1,1′-disubstituted zirconocene dichloride precatalysts.[204] Table 6.1 lists the ethylene polymerization activities, substituent cone angles, and Hammett constants for several substituents. The authors conclude that both steric and electronic effects control catalyst activity. However, from the data, it is apparent that steric effects are minor, as the bulkier substituents (^{t}Bu, $SiMe_3$, ^{i}Pr) are present in the more active catalysts. However, heavily substituted complexes like $Cp^{*}_2ZrCl_2$ do exhibit lower catalytic activities that are attributed to the bulky Cp ligands impeding monomer coordination.[205-207] Electronic effects on catalyst activity appear more significant, as the three most active catalysts are substituted with the three most electron-donating groups.

Studies by Piccolrovazzi[208] and by Collins[209] look more exclusively at substituent electronic effects by examining a series of bis(indenyl)zirconium dichloride precatalysts in which the substituents are located in positions distant from the catalytic reaction site. Piccolrovazzi studied catalysts that were functionalized in the 4- and 7-positions of the indenyl ligand and examined the effect on ethylene polymerization activity and molecular weight. The results are shown in Table 6.2 and indicate little change in catalyst activity or polymer molecular

Table 6.1. Ethylene polymerization data for substituted Cp_2ZrCl_2 complexes.

$(CpR)_2ZrCl_2$[a] R	Activity[b]	CpR cone angle, θ (deg.)	F[c]
^{t}Bu	860000	139	-0.02
$SiMe_3$	490000	144	0.01
Et	480000	132	0.0
^{i}Pr	320000	135	0.04
H	190000	116	0.03
Me	170000	128	0.01
CMe_2Ph	170000	145	0.05

a. 70 ^{o}C, 45 min, $P(C_2H_4)$ = 10 bar, [Al]/[Zr] = 42,500
b. units = (g PE)/[(mol Zr)(h)]
c. linear combination of Hammett constants (σ_m and σ_p)

Table 6.2. Ethylene polymerization data for substituted $(Ind)_2ZrCl_2$ complexes.

$(Ind')_2ZrCl_2$[a] Ind'	Activity[b]	M_n
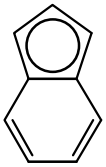	43000	320000
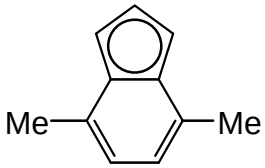	40000	310000
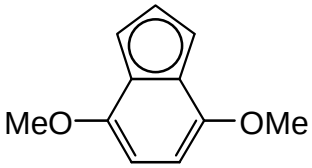	18000	88000
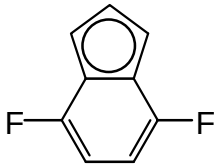	2300	29000

a. 33 ^oC, 1 h, $[C_2H_4]$ = 0.032 mol/L, [Al]/[Zr] = approx. 500
b. units = (g PE)/[(g Zr)(bar)(h)]

weight when methyl substituents are incorporated. The electron-withdrawing flouro substituents drastically reduce the catalyst activity and polymer molecular weight. This effect is almost entirely electronic since there is little difference in the Van der Waals radii of hydrogen (1.20 Å) and fluorine (1.47 Å).[210] The fluoro substituents lower catalytic activity by strengthening the Zr-polymer bond, thus reducing the rate of olefin insertion. Finally, the peculiar results for the electron-donating methoxy groups are explained by oxygen coordination with the Lewis acidic aluminum cocatalyst (MAO). This interaction transforms the substituent into an electron-withdrawing group and accounts for the lowered activity and polymer molecular weight.

Alt and coworkers further minimized steric effect contributions by incorporating substituents into the more distant 2- and 7-positions of the fluorenyl ligand in $Cp(Flu')ZrCl_2$ precatalysts.[211] The ethylene polymerization activities are shown in Table 6.3 and illustrate the enhancement of catalyst activities by electron-donating groups. The electron-withdrawing

Table 6.3. Ethylene polymerization results for substituted $(Flu)_2ZrCl_2$ complexes.

$Cp(Flu')ZrCl_2$[a]	
Flu'	Activity[b]
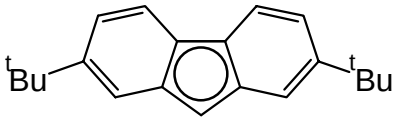	21.9
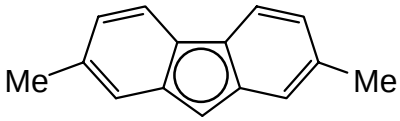	21.3
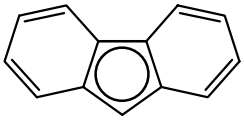	16.1
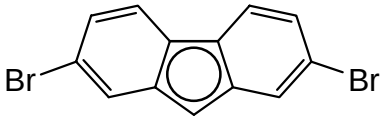	5.5
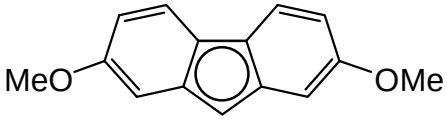	4.0

a. 30 °C, 1 h, $P(C_2H_4)$ = 10 bar
b. units = (t PE)/[(mol Zr)(h)]

bromo and methoxy (when coordinated with MAO) groups lower the catalytic activity as expected.

In an ethylene/1-hexene copolymerization study, Rytter and coworkers demonstrated the effect of increasing methyl substitution.[212] Table 6.4 compares the catalyst activities, copolymer molecular weights, and extent of hexene incorporation into the copolymer for several substituted zirconocene dichlorides. As anticipated from the previously described ethylene homopolymerization studies, the electron-donating methyl group initially increases catalyst activity and copolymer molecular weight. However, when eight or ten methyl groups are present, steric effects overcome the electronic effects resulting in lowered activities and molecular weights. The hexene incorporation data suggest that the more heavily substituted catalysts exhibit a steric effect which lowers the amount of hexene incorporation. A low degree of methyl substitution seems to enhance comonomer incorporation, however, the electronic effect is not straightforward.

Table 6.4. Ethylene/1-hexene copolymerization data for substituted Cp_2ZrCl_2 complexes.

$(Cp')_2ZrCl_2$[a] Cp' Ligand	Activity[b]	M_n	1-hexene incorp.[c]
C_5H_5	22	11000	2.7
C_5H_4Me	88	25500	2.5
$C_5H_3(1,3\text{-}Me)_2$	29	34100	4.0
$C_5H_3(1,2\text{-}Me)_2$	314	57200	1.8
$C_5H_2(1,2,4\text{-}Me)_3$	361	51600	5.5
$C_5H_2(1,2,3\text{-}Me)_3$	334	65200	1.7
C_5HMe_4	99	73000	1.4
C_5Me_5	31	47300	0.3

a. 80 ^oC, 1 h, $P(C_2H_4)$ = 2 bar, [Al]/[Zr] = 3000
b. (t PE)/[(mol Zr)(h)(bar)
c. mol %

Karol and Kao also examined substituent effects in ethylene/1-hexene copolymerizations and their findings (relative to Cp_2ZrCl_2) are summarized in Table 6.5.[213] They conclude that the electronic effect of two electron-donating methyl groups increases catalyst activity while the steric effect of ten methyl groups lowers the activity. The most crowded catalysts ($Cp^*_2ZrCl_2$, $[CpBu]_2ZrCl_2$) incorporate the least comonomer while bridged metallocenes ($Me_2Si(Cp)_2ZrCl_2$, $Ph_2C(Cp)_2ZrCl_2$) incorporate the most comonomer. The later effect occurs because the bridging group ties back the Cp ligands making the zirconium coordination sphere more accessible to the bulky hexene comonomer.

The above homo- and copolymerization examples illustrate how catalyst activity and polymer molecular weight generally increase with electron-donating group functionalization. Electron-withdrawing groups are shown to lower catalyst activity and polymer molecular weight. When a highly substituted catalyst is used, steric effects tend to lower the catalyst activity and polymer molecular weight. In copolymerizations, the extent of comonomer incorporation is also dependent on steric effects as illustrated with examples of crowded and bridged metallocenes which incorporate the least and most amounts of comonomer. Unfortunately, the electronic effect on comonomer incorporation is not very clear. Some studies suggest that electron-

Table 6.5. Relative ethylene/1-hexene copolymerization data for substituted Cp_2ZrCl_2 complexes.

Catalyst[a]	Activity[b]	1-hexene incorp.[c]	Catalyst[a]	Activity[b]	1-hexene incorp.[c]
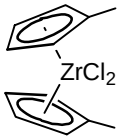	2.08	1.39	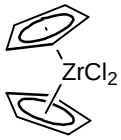	1.00	1.00
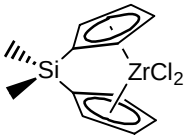	1.03	1.97	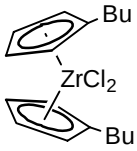	0.50	0.14
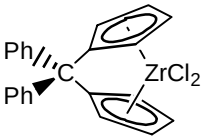	0.60	1.42	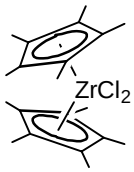	0.50	0.14

a. 85 ^oC, $P(C_2H_4)$ = 100 psi; b. (g PE)/[(mol Zr)(h)]; c. mol %

donating groups slightly increase comonomer incorporation[214,215] while others show that the electronic effect is not so straightforward.[212] Clearly, a definitive study is needed to determine the extent that substituent electronic effects impact comonomer incorporation.

Measuring Electronic Effects

Comparing two substituents that are similar in size but different in electron-donating ability is the simplest method for elucidating electronic effects without contributions from steric effects. While this has not been undertaken for a copolymerization, three studies of this type have appeared for ethylene homopolymerizations using unbridged Cp_2ZrCl_2 precatalysts. As was previously shown in Table 6.1, the Cp ligands possessing the ^{t}Bu and $SiMe_3$ are similar in size as shown by their respective cone angles (139º and 144º) while a ^{91}Zr NMR study shows that the ^{t}Bu group is slightly more electron-donating than the $SiMe_3$ group.[216] Table 6.6 compares the actual and relative ethylene polymerization activities obtained by Möhring[204] (A), Nekhaeva[217] (B), and Bravaya[218] (C) for catalysts possessing these two substituents. Unfortunately, the differences in activity are small and contradictory. The different polymerization conditions and the similar electron-donating abilities of the ^{t}Bu and $SiMe_3$ groups

Table 6.6. Comparison of ethylene polymerization activities obtained in seperate studies.

$(CpR)_2ZrCl_2$	**A**[a,b]		**B**[a,c]		**C**[a,d]	
R	Actual	Relative	Actual	Relative	Actual	Relative
^{t}Bu	860	4.5	29900	0.9	959	1.4
$SiMe_3$	490	2.6	38100	1.2	2049	2.9
H	190	1.0	31500	1.0	706	1.0

a. units = (kg PE)/[(mol Zr)(h)]
b. 70 ^{o}C, P(C_2H_4) = 10 bar, [Al]/[Zr] = 42500
c. 70 ^{o}C, P(C_2H_4) = 7 atm, [Al]/[Zr] = 11000
d. 30 ^{o}C, P(C_2H_4) = 0.54 atm, [Al]/[Zr] = 2000

prevent an effective estimation of substituent electronic effects in this example. Similarly, Brintzinger and Beck have shown that the $SiMe_3$ and ^{t}Bu substituents produce statistically equivalent equilibrium constants for methylation reactions with aluminum trialkyls.[219]

In order to effectively elucidate electronic effects, it is necessary to use substituents that differ substantially in their electron-donating abilities, yet still remain virtually isosteric. To date, copolymerization substituent effect studies have focused only on electron-donating substituents (Me, Et, ^{i}Pr, ^{t}Bu, $SiMe_3$, CMe_2Ph) while leaving electron-withdrawing substituents unexplored.

Chapter Overview

This chapter addresses electronic effects in metallocene catalyzed olefin polymerization involving catalysts substituted with the structurally similar Ph and C_6F_5 aryl groups. While both the Ph[220-223] and the C_6F_5[92] groups have appeared in studies of ethylene homopolymerization studies, the two substituents have never been compared in an ethylene/α-olefin copolymerization. First the syntheses and characterization of Ph and C_6F_5-substituted complexes will be described. An analysis of ^{1}H NMR spectra will show that the Ph substituent is electron-donating while the C_6F_5 substituent is electron-withdrawing. Finally, these two substituents will allow the elucidation of electronic effects in ethylene/1-hexene copolymerizations.

Results & Discussion

Complex Synthesis

As shown in Figure 6.2, Ph and C_6F_5-substituted Cp ligands are reacted with $ZrCl_4$ or $CpZrCl_3$ to afford the corresponding metallocenes in moderate yields (23 – 77%). The syntheses and characterizations of **24**, **25**, and **26** are reported elsewhere.[91,224] The synthesis of **31** was hampered by low product yields and uncharacterized byproducts which dominated at temperatures above 25 ºC. When the synthesis and work up of **31** was conducted below room temperature, clean product could be isolated in a 44% yield. The thermal instability of **31** could be a consequence of the triarylated ligand's poor electron donation ability and steric bulk which strain the metallocene structure.

Table 6.7 lists the ^{1}H NMR chemical shifts of the unsubstituted Cp rings (δ_{Cp}) in Cp_2ZrCl_2, **28**, **29**, **30**, and **31**. The values provide a comparative measurement of zirconium electron density in these unsymmetrical complexes. Excluding any steric perturbations, the electron-donating Ph substituents in **30** are expected to increase the electron density at Zr. When compared to the Cp_2ZrCl_2 (δ_{Cp} = 6.49 ppm), the Cp signally is substantially shifted upfield

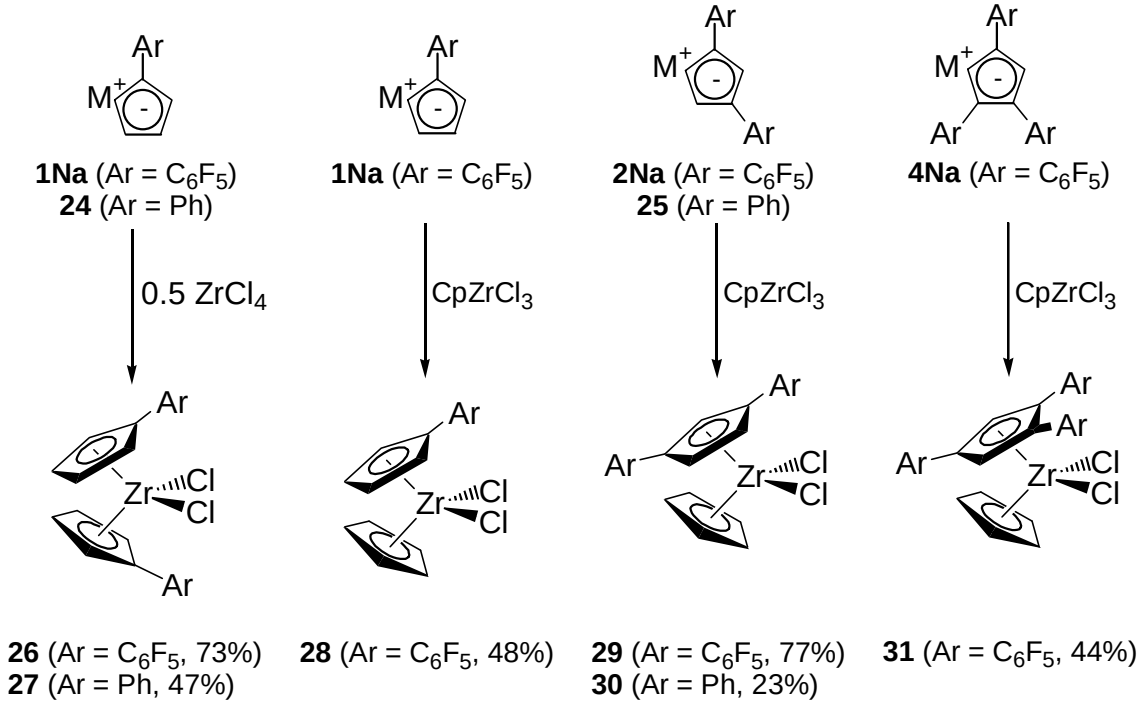

Figure 6.2. Synthetic scheme for aryl-substituted Cp_2ZrCl_2 complexes.

Table 6.7. ^{1}H NMR data of aryl-substituted Cp_2ZrCl_2 complexes.

complex	^{1}H NMR Data (ppm)	
	δ_{Cp}	$\Delta\delta_{Cp}$ (per group)
Cp_2ZrCl_2	6.49	0
$(Ph_2Cp)CpZrCl_2$ (**30**)	6.16	-0.16
$[(C_6F_5)Cp]CpZrCl_2$ (**28**)	6.53	0.04
$[1,3\text{-}(C_6F_5)_2Cp]CpZrCl_2$ (**29**)	6.55	0.03
$[1,2,4\text{-}(C_6F_5)_3Cp]CpZrCl_2$ (**31**)	6.42	-0.02

(about 0.16 ppm per phenyl substituent) confirming the electron-donating nature of the Ph group. The electron-withdrawing C_6F_5 substituents in compounds **28**, **29**, and **31** should decrease the electron density at Zr and shift the δ_{Cp} signal downfield and, as expected complexes **28** and **29** do exhibit a downfield shift (0.04 ppm and 0.03 ppm per C_6F_5 group, respectively). Suprisingly, **31** does not produce the anticipated δ_{Cp} downfield shift. Instead, an upfield shift of 0.02 ppm per C_6F_5 group is observed. This deviation is attributed to the steric strain associated with the bulky triarylated Cp ligand and will be described more thoroughly in the following discussion of its crystal structure.

Crystal Structures of Metallocenes

The X-ray crystal structures of **27** and **30** are shown in Figures 6.3 and 6.4. Crystallographic data are presented in Table 6.8. Some important bond distances are presented in Table 6.9 along with those of other Cp_2ZrCl_2 derivatives for comparison.[221-223,225-227] The Cp ligands in both **27** and **30** are bonded in a typical pentahapto fashion and their structures exhibit no significant distortions. The Zr-Cp distances for **27** (2.215 Å) and **30** (2.211, 2.194 Å) are close to those found in Cp_2ZrCl_2 (2.200 – 2.208 Å). The Cp-Zr-Cp angles in **27** (129.3˚) and **30** (129.9˚) are also similar those in Cp_2ZrCl_2 (129.5˚, 129.1˚).

The Ph rings in **27** and **30** do not participate in any intramolecular or intermolecular stacking interactions. The Cp-Ph dihedral angles in both structures are listed in Table 6.10 and are compared with other Cp_2ZrCl_2 derivatives.[222,223,228] The angles in **27** (5.0º) and **28** (3.4º, 15.2º) show that the aryl rings are virtually coplanar with the Cp ligand. These angles are

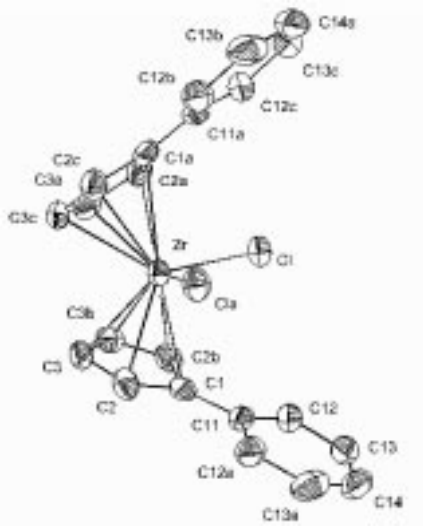

Figure 6.3. Thermal ellipsoid plot of **27** shown at 50% probability. Hydrogen atoms were omitted for clarity.

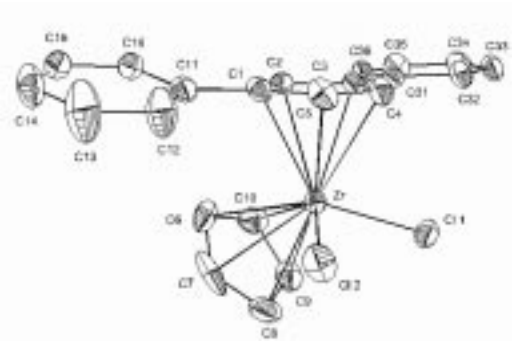

Figure 6.4. Thermal ellipsoid plot of **30** shown at 50% probability. Hydrogen atoms were omitted for clarity.

slightly more coplanar than those found in $(1,2\text{-}Me_2\text{-}4\text{-}PhCp)_2ZrCl_2$ (13.6º, 18.8º). The dihedral angles in Table 6.10 are much larger (31.2º – 56.9º) when a vicinal substituent is present.

The X-ray crystal structure of **31** is shown in Figure 6.5. Relevant crystallographic data are presented in Table 6.8. Some important bond distances are presented in Table 6.9 along with those of other Cp_2ZrCl_2 derivatives for comparison.[221-223,225-227] Complex **31** possesses a long Zr-Cp distance (Ar_3Cp = 2.294 Å) which indicates steric strain between the C_6F_5 rings and the $CpZrCl_2$ moiety. Only $(Ph_5Cp)CpZrCl_2$ exhibits a longer Zr-C(centroid) distance (2.302 Å). The bulkiness of the C_6F_5 rings is also apparent in the Cp-Zr-Cp angle (131.7˚) which is larger than the angles in Cp_2ZrCl_2 (129.5˚, 129.1˚) but not as large as those in the more heavily substituted $[1,2,4\text{-}(SiMe_3)_3Cp]_2ZrCl_2$ (135.4˚) and $(Ph_5Cp)CpZrCl_2$ (132.9˚). The strain in the molecular structure of **31** is a potential contributor to its thermal instability.

The C_6F_5 rings in **31** do not participate in intermolecular stacking interactions. The Cp-C_6F_5 dihedral angles are listed in Table 6.11 where they are compared with other C_6F_5-substituted complexes which also possess no stacking interactions. Surprisingly, the isolated C_6F_5 dihedral angle (39.6˚) is larger than the more crowded vicinal C_6F_5 dihedral angles (36.9˚, 38.6˚). This isolated dihedral angle is also larger than the angles measured in $[(C_6F_5)Cp]_2HfMe_2$ (3.4˚, 24.2˚) but similar to the isolated angle in **18Re** (41.5˚). The two vicinal dihedral angles in **31** (36.9˚, 38.6˚) are small compared to those in **18Re** (66.3˚, 51.0˚). These smaller angles

Table 6.8. Crystallographic data for C_6F_5-substituted zirconocene dichlorides.

compound	**31**	**27**	**30**
empirical formula	$C_{28}H_7Cl_2F_{15}Zr$	$C_{22}H_{18}Cl_2Zr$	$C_{22}H_{18}Cl_2Zr$
fw	790.46	444.48	444.48
diffractometer	Nonius Kappa	Nonius Kappa	Nonius Kappa
cryst dimens (mm)	0.20 × 0.23 × 0.28	0.03 × 0.08 × 1.00	0.10 × 0.25 × 0.35
cryst system	monoclinic	orthorhombic	monoclinic
a (Å)	11.2970(2)	11.5690(13)	14.8140(2)
b (Å)	14.0810(3)	23.3310(18)	29.8600(9)
c (Å)	16.4470(4)	6.755(3)	8.6230(3)
α (deg)			
β (deg)	90.6920(14)		99.7980(14)
γ (deg)			
V $(Å)^3$	2616.08(10)	1823.3(8)	3758.71(18)
space group	$P2_1/n$ (No. 14)	Fmm2 (No. 42)	$P2_1/n$ (No. 14)
Z	4	4	8
D_{calc} (Mg m^{-3})	2.007	1.619	1.571
abs coeff (mm^{-1})	0.8	0.9	0.9
F_{000}	1536	896	1792
λ (Mo K_α) (Å)	0.71073	0.71073	0.71073
temp (K)	150	150	120
range for collection	2.6 - 35.0	3.5 - 30.3	2.6 - 30.0
no. of reflns colld	20309	9620	18512
no. of indep reflns	11399	1308	10906
abs corr method	multi-scan	multi-scan	multi-scan
data / restrs / params	11399 / 0 / 415	1308 / 0 / 64	10906 / 0 / 451
R [$I > 2\sigma(I)$]	0.032	0.061	0.033
R_w [$I > 2\sigma(I)$]	0.081	0.160	0.074
GoF on F^2	0.98	1.09	0.87
peak, hole (e $Å^{-3}$)	0.48, 0.84	0.94, 1.07	0.75, 0.73

Table 6.9. Selected bond distances and angles in Cp_2ZrCl_2 derivatives.

	bond distances and angles (Å)[a]	
complex	Zr-Cp	Cp-Zr-Cp
Cp_2ZrCl_2[b]	2.200, 2.208 2.201, 2.202	129.5, 129.1
$(PhCp)_2ZrCl_2$ (**27**)	2.215	129.3
$(1,3\text{-}Ph_2Cp)CpZrCl_2$ (**30**)	2.211 (Ph_2Cp) 2.194 (Cp)	129.9
$(^tBuCp)_2ZrCl_2$	2.217	128.6
$(1,2,3\text{-}Ph_3Cp)_2ZrCl_2$	2.226 2.230	130.8
$(1,2,4\text{-}Ph_3Cp)_2ZrCl_2$	2.245	129.3
$[1,2,4\text{-}(SiMe_3)_3Cp]_2ZrCl_2$	2.246	135.4
$[1,2,4\text{-}(C_6F_5)_3Cp]CpZrCl_2$ (**31**)	2.294 (Ar_3Cp) 2.202 (Cp)	131.7
$(Ph_5Cp)CpZrCl_2$	2.302 (Ph_5Cp) 2.211 (Cp)	132.9

a. from literature cited in the text except for **27**, **30**, and **31**; b. two independent molecules in unit cell

probably aid in minimizing the steric strain between the C_6F_5 substituents and the $CpZrCl_2$ moiety.

Polymerization Studies

An ethylene homopolymerization study was conducted with precatalysts **26**, **27**, and Cp_2ZrCl_2 using an MAO cocatalyst. The catalysts activities and polymer molecular weights are presented in Table 6.12. Significant substituent electronic effects are notable when comparing the structurally similar precatalysts **26** and **27**. The electron-withdrawing C_6F_5 group lowers

Table 6.10. Cp-Ph dihedral angles in phenyl-substituted zirconocene dichlorides.

complex	dihedral (deg)[a]
$(PhCp)_2ZrCl_2$ (**27**)	5.0 (iso)
$(1,3\text{-}Ph_2Cp)CpZrCl_2$ (**30**)	15.2 (iso) 3.4 (iso)
$(1,2\text{-}Me_2\text{-}4\text{-}PhCp)_2ZrCl_2$	18.8 (iso) 13.6 (iso)
$(1,2\text{-}Ph_2Cp)_2ZrCl_2$	50.1 (vic), 39.6 (vic) 32.9 (vic), 31.2 (vic)
$(1,2,4\text{-}Ph_3Cp)_2ZrCl_2$	56.9 (vic) 33.3 (vic) 24.1 (iso)

a. from literature cited in the text except for **27** and **30**; aryl group abbreviations (vic = vicinal; iso = isolated; int = internal; ext = external)

both the catalyst activity and the polymer molecular weight relative the electron-donating Ph substituent. The above findings are in agreement with several other substituent effect studies.[42,204,208,209,211,229]

MAO activated ethylene/1-hexene copolymerizations were performed using precatalysts **26 – 30** and Cp_2ZrCl_2. Compound **31** was not tested due to its thermal instability at the copolymerization temperature (50 °C). The catalyst activities, copolymer molecular weights,

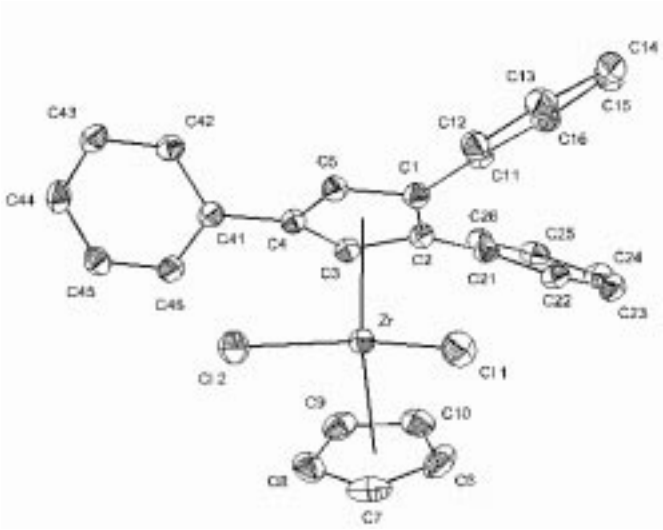

Figure 6.5. Thermal ellipsoid plot of **31** shown at 50% probability. Fluorine and hydrogen atoms are omitted for clarity.

Table 6.11. Cp-C_6F_5 dihedral angles in C_6F_5-substituted Cp complexes.

complex	dihedral (deg)[a]
$[(C_6F_5)Cp]_2HfMe_2$[b]	24.2 3.4
[1,2,4-$(C_6F_5)_3$Cp]$CpZrCl_2$ (**31**)	36.9 (vic) 38.6 (vic) 39.6 (iso)
[1,2,4-$(C_6F_5)_3$Cp]$Re(CO)_3$ (**18Re**)	66.3 (vic) 51.0 (vic) 41.5 (iso)

a. aryl group abbreviations (vic = vicinal; iso = isolated; int = internal; ext = external); b. unpublished structure from our laboratory

comonomer incorporation (mol %), and reactivity ratios are presented in Table 6.13. Similar to the ethylene homopolymerization results, the activities and polymer molecular weights decrease with increasing C_6F_5 functionalization. The Ph-substituted catalysts (**27** and **30**) produce higher mole cular weight polymers than the other catalysts but have the same activity as Cp_2ZrCl_2. The degree of 1-hexene incorporation (mol %, measured by ^{13}C NMR[230,231]) and the ethylene reactivity ratios (r_E, measured by ^{13}C NMR[231,232]) for precatalysts **27**, **28**, **30**, and Cp_2ZrCl_2 are similar and reveal no significant substituent effects. The copolymers created by these catalysts are all white, fluffy solids.

Complexes **26** and **29** exhibit different comonomer incorporations and reactivity ratios compared to their phenyl-substituted analogues. Precatalyst **26** incorporates 11.3% hexene

Table 6.12. Ethylene polymerization data for aryl-substituted Cp_2ZrCl_2 complexes.

Complex[a]	Activities[b]	M_w
Cp_2ZrCl_2	53 (10)	730,000
$(PhCp)_2ZrCl_2$ (**27**)	53 (10)	524,000
$[(C_6F_5)Cp]_2ZrCl_2$ (**26**)	14 (2)	432,000

a. 50(2)°C, 5 min, $P(C_2H_4)$ = 1 atm, [Al]/[Zr] = 2000
b. (kg PE)/[(mmol Zr)(h)]

Table 6.13. Ethylene/1-hexene copolymerization data for aryl-substituted Cp_2ZrCl_2 complexes.

Complex[a]	Activities[b]	M_w	% 1-hexene[c]	r_E[d]	r_H[d]
Cp_2ZrCl_2	26 (4)	130,000	4.7	78	-
$(PhCp)_2ZrCl_2$ (**27**)	26 (4)	230,000	5.9	58	-
$(1,3\text{-}Ph_2Cp)CpZrCl_2$ (**30**)	26 (6)	265,000	5.4	68	-
$[(C_6F_5)Cp]CpZrCl_2$ (**28**)	12 (6)	114,000	6.0	60	-
$[(C_6F_5)Cp]_2ZrCl_2$ (**26**)	10 (3)	37,500	11.3	27	0.01
$[1,3\text{-}(C_6F_5)_2Cp]CpZrCl_2$ (**29**)	7 (1)	17,000	19.0	16	0.08

a. 50(2)^{o}C, 5 min, $P(C_2H_4)$ = 1 atm, [Al]/[Zr] = 2000, [1-hexene] = 0.4 mol/L; b. units = (kg PE)/[(mmol Zr)(h)]; c. mol % determined by ^{13}C NMR; uncertainty = 1%; d. determined by ^{13}C NMR.

comonomer producing a w hite, rubbery copolymer while **29** incorporates 19.0% comonomer resulting in a translucent, sticky copolymer. These changes in polymer properties are consistent with increased polymer branching which is known to produce a less crystalline, lower melting polymer (T_m).[215,233] The ethylene reactivity ratios for **26** and **29** are substantially lower than the other values in Table 6.13 while the hexene reactivity ratios (r_H) are large enough to measure. We propose that the C_6F_5 groups increases hexene copolymer content by generating a more electrophilic catalyst which should exhibit enhanced coordination with the more electron-rich comonomer (1-hexene). As shown in Figure 6.6, the equilibrium constants for hexene coordination (K_{eq}(EH) and K_{eq}(HH)) should increase relative to the equilibrium constants for ethylene coordination (K_{eq}(EE) and K_{eq}(HE)). This decreases the ratio $K_{eq}(EE)/K_{eq}(EH)$ and increases the ratio $K_{eq}(HH)/K_{eq}(HE)$ which accounts for the observed decrease in r_E and increase in r_H. Interestingly, the single C_6F_5 group in **28** does not produce a significant change in monomer reactivity ratios or hexene incorporation.

The similar structures of **26** and **27** or **29** and **30** reveal the magnitude of the electronic effect on comonomer incorporation. Upon switching the Ph group for the C_6F_5 group, the change in hexene content is substantial (5.4% for **26** and **27**; 13.6% for **29** and **30**). This large increase in comonomer incorporation rivals those generated upon tying back the Cp ligands with a bridging functionality. For example, Quijada and coworkers used similar copolymerization conditions to study the impact of a bridging group on comonomer incorporation and their results are highlighted in Table 6.14.[234] They detected an approximate 5% increase in hexene content

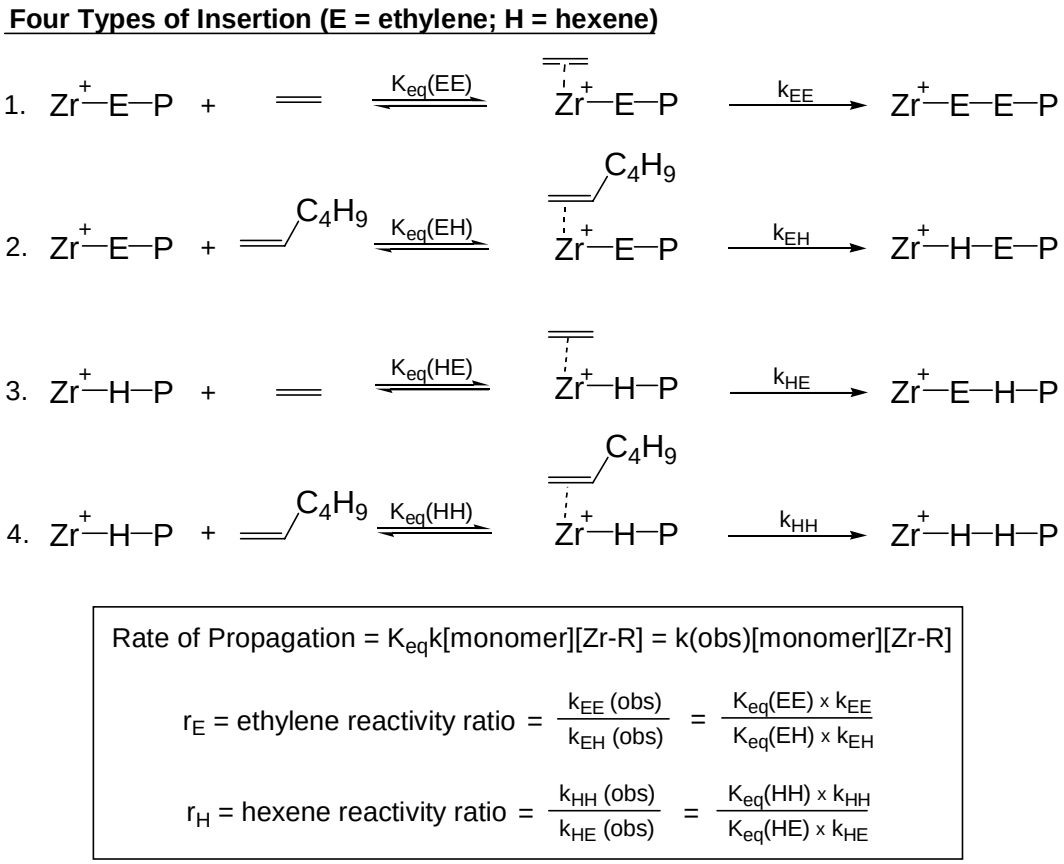

Figure 6.6. Definition of reactivity ratios for an ethylene/1-hexene copolymerization.

upon incorporating a bridging functionality. The change in comonomer incorporation for **26** and **27** (5.4%) is similar while the change measured for **29** and **30** (13.6%) is substantially larger. However, a more reliable comparison requires that these catalysts be tested under analogous polymerization conditions.

Conclusion

This chapter describes a breakthrough in the study of electronic effects in transition-metal catalyzed olefin polymerization. Previous copolymerization studies have shown that changes in catalyst and polymer properties are minimal when substituent electronic effects are varied. Hence, the tailoring of catalyst structure currently dominates much of the focus in olefin polymerization research. Contrary to past research, this copolymerization study has shown that substituent electronic effects can affect catalyst and copolymer properties. Substantial changes in both copolymer molecular weight and comonomer incorporation are possible by a simple modification of a substituent's electron-donating ability.

Table 6.14. Effect of bridging group in ethylene/1-hexene copolymerizations.

Complex[a]	Activities[b]	% hexene[c]
Cp_2ZrCl_2	18.2	7.9
$(CH_3)_2SiCp_2ZrCl_2$	17.2	13.4
$(Ind)_2ZrCl_2$	7.8	6.3
$C_2H_4(Ind)_2ZrCl_2$	17.2	11.6

a. 60(2)^{o}C, 30 min, P(C_2H_4) = 1.6 bar,
[Al]/[Zr] = 1750, [hexene] = 0.5 mol/L
b. (kg PE)/[(mmol Zr)(h)(bar)]
c. mol %

Experimental Section

General Procedures. Standard inert-atmosphere techniques were used for all reactions. Cp_2ZrCl_2 and $CpZrCl_3$(DME) were used as received from Aldrich. 1-Hexene was distilled from CaH_2. Complexes **24**, **25**, and **26** were prepared as previously reported.[91,224] All NMR experiments used a Varian Unity (400) instrument. ^{19}F NMR spectra were referenced to external C_6F_6 in $CDCl_3$ at -163.00 ppm. All metallocenes were insufficiently soluble for ^{13}C NMR analysis. Elemental analyses were performed by Desert Analytics (Tucson, AZ).

Crystallographic Studies. Crystallography was performed by Frank Fronczek (Louisiana State University) for **27**, **30**, and **31**. Crystals of **27** were grown from a cooling toluene solution and the structure's resulting data set was of marginal quality. An ambiguity arose in the assignment of the space group. Our collaborator (F. R. Fronczek) initially solved the structure in C2 (monoclinic), but the systematic absences were equally consistent with Fmm2 (orthorhombic), so he defaulted to the higher symmetry. Thermal ellipsoids looked about the same in both solutions. Thus, even if **27** does not have crystallographic mm2 symmetry, the molecular geometry must still be very close to C_{2v}. Crystals of **30** were grown from a slowly cooling toluene/hexane mixture. An initial structure of **30** obtained at 173 K showed only one molecule per asymmetric unit, but some of the ellipsoids for the carbon atoms of the unsubstituted Cp ligand were elongated, suggesting a positional disorder. A superior data set was subsequently obtained at 120 K, showing two molecules per independent unit. Low-temperature phase changes in which small positional disorders are "resolved" are becoming increasingly commonly observed with the advent of high-throughput diffractometers which enable data collections at two or more temperatures to be obtained within a day with small molecules such as these. Crystals of **31** were grown from a slowly cooling toluene/hexane mixture; crystallographic analysis was routine.

Polymerization studies. Catalyst cocktail preparations and polymerizations were conducted as described in the following example for the Cp_2ZrCl_2 precatalyst. In a glove box, 17.2 mg of Cp_2ZrCl_2 is weighed into a 10-mL volumetric flask which is filled with toluene to give a 0.00588 mol/L precatalyst stock solution. In a separate 10-mL volumetric flask, 300 mg of solid MAO is weighed. Into this flask is injected 0.44 mL of stock precatalyst solution along with additional toluene to give a 0.00026 mol/L catalyst cocktail solution. After 20 minutes of activation time, 0.98 mL (2.5×10^{-7} mol Zr) of the catalyst cocktail is injected into the polymerization reactor.

Injection volumes generating less than 2 ˚C exotherms were used. The polymerizations are conducted in a 1-L glass reactor fitted with a thermal resistor, motorized stir bar, condensor, gas dispersion tube, and septum. The reactor is baked out for at least 12 hours prior to use after which it is evacuated (50 mtorr) and backfilled with nitrogen. Under a nitrogen flow, 400 mL of dry, deoxygenated toluene is added from a pressurized solvent column. The reactor is placed in a temperature regulated water bath and stirring is begun until the reactor temperature equilibrates to 50 ˚C. Under a nitrogen purge, 20 mg of solid MAO is added to the reactor. During a copolymerization, 20 mL of freshly distilled 1-hexene would be syringed into the reactor through the septum at this time. Ethylene is then bubbled through the stirring solution and out to an oil bubbler. Once the reactor temperature stabilizes at 50 ˚C, the catalyst cocktail is injected. The polymerization is terminated after 5 minutes by injecting 20 mL of a methanol solution (5% HCl). The polymerization mixture is then roto-evaporated until 20 mL of liquid remain. Subsequently, 150 mL of methanol (5% HCl) is added to precipitate any dissolved polymer. The mixture is stirred vigorously for 30 minutes and then filtered. The polymers are dried for 24 hours in a vacuum oven (50 mTorr) at 80 ˚C. The ^{13}C NMR spectra of the copolymer samples were obtained at 120 ºC in 10-mm tubes using a trichlorobenzene/1,1,2,2-tetrachloroethane-d_2 (95:5) solvent mixture. Chromium(II) acetylacetonate (5×10^{-2} mol/L) was used to reduce relaxation times. NMR conditions and calculations (mol %, reactivity ratios) are described by Randall[230] and Galland.[231]

Dichlorobis[η^5-(phenyl)cyclopentadienyl]zirconium(IV) (27). A mixture of $ZrCl_4$ (0.29 g, 1.2 mmol), **24** (0.40 g, 2.4 mmol), and THF (50 mL) was stirred at room temperature for 24 h. The THF was stripped and the crude green product was dissolved in hot toluene, filtered, and cooled to room temperature. The product crystallized upon standing and 0.25 g (0.56 mmol, 47 %) of greenish yellow needles were filtered off. ^{1}H NMR ($CDCl_3$) δ 7.53 (m, 4 H), 7.15 (tm, $^3J_{HH}$ = 7.6 Hz, 4 H), 7.32 (tt, $^3J_{HH}$ = 7.4 Hz, $^4J_{HH}$ = 1.5 Hz, 2 H), 6.71 (t, $^3J_{HH}$ = 2.8 Hz, 4 H), 6.29 (t, $^3J_{HH}$ = 2.6 Hz, 4 H). ^{13}C NMR ($CDCl_3$) δ 133.0, 129.2, 128.4, 128.3, 126.3, 115.8, 115.6. Anal. Calcd for $C_{22}H_{18}Cl_2Zr$: C, 59.45; H, 4.08. Found: C, 59.33: H, 3.76.

Dichloro(η^5-cyclopentadienyl)[η^5-(pentafluorophenyl)cyclopentadienyl]zirconium(IV) (28). A mixture of $CpZrCl_3$(DME) (1.511 g, 4.28 mmol), **1Na** (1.108, 4.36 mmol), and toluene (50 mL) was stirred at a gentle reflux for 24 h. The hot mixture was filtered through a glass frit. Any filtered product was washed with additional hot toluene and filtered. The toluene solution

was cooled to –78 °C. The product precipitated and was filtered, washed with hexane, and collected to yield 942 mg (2.06 mmol, 48 %) of white solid. ^{1}H NMR ($CDCl_3$) δ 6.87 (tt, ^{3}J = 2.8 Hz, ^{4}J = 1.6 Hz, 2 H), 6.61 (t, $^{3}J_{HH}$ = 2.8 Hz, 2 H), 6.53 (s, 5 H). ^{19}F NMR ($CDCl_3$) δ -139.56 (d, $^{3}J_{FF}$ = 16 Hz, 2 F) , -154.58 (tt, $^{3}J_{FF}$ = 21 Hz, $^{4}J_{FF}$ = 2.5 Hz, 1 F) , -162.25 (m, 2 F). Anal. Calcd for $C_{16}H_9Cl_2F_5Zr$: C, 41.94; H, 1.98. Found: C, 42.05: H, 1.89.

Dichloro(η^5-cylcopentadienyl)[η^5-1,3-bis(pentafluorophenyl)cyclopentadienyl]-zirconium(IV) (29). A mixture of $CpZrCl_3$(DME) (1.043 g, 3.97 mmol), **2Na** (1.720, 4.09 mmol), and toluene (100 mL) was stirred at a gentle reflux for 2 h. The hot mixture was filtered through a glass frit. Any filtered product was washed with additional hot toluene and filtered. The toluene solution was cooled to –78 °C. The product precipitated and was filtered, washed with hexane, and collected to yield 1.911 g (3.06 mmol, 77%) of white solid. ^{1}H NMR ($CDCl_3$) δ 7.35 (s, 1 H), 6.93 (s, 2 H), 6.55 (s, 5 H). ^{19}F NMR ($CDCl_3$) δ -139.65 (d, $^{3}J_{FF}$ = 16 Hz, 4 F) , -153.51 (tt, $^{3}J_{FF}$ = 21 Hz, $^{4}J_{FF}$ = 2.6 Hz, 2 F) , -161.65 (m, 4 F). Anal. Calcd for $C_{22}H_8Cl_2F_{10}Zr$: C, 42.32; H, 1.29. Found: C, 42.55: H, 1.03.

Dichloro(η^5-cylcopentadienyl)[η^5-1,3-(diphenyl)cyclopentadienyl]zirconium(IV) (30). A mixture of $CpZrCl_3$(DME) (0.514 g, 1.46 mmol), **25** (0.30, 1.2 mmol), and toluene (50 mL) was stirred at reflux for 20 h. The reaction mixture was cooled and filtered through a glass frit. The toluene was stripped and the crude solid was crystallized from a toluene/hexane mixture to yield 0.13 g (0.29 mmol, 23%) of gray needles. ^{1}H NMR ($CDCl_3$) δ 7.69 (m, 4 H), 7.46 (tm, $^{3}J_{HH}$ = 7.8 Hz, 4 H), 7.34 (tt, $^{3}J_{HH}$ = 7.4 Hz, $^{4}J_{HH}$ = 1.4 Hz, 2 H), 7.24 (t, $^{4}J_{HH}$ = 2.6 Hz, 1 H), 6.88 (d, $^{4}J_{HH}$ = 2.4 Hz, 2 H), 6.18 (s, 5 H). ^{13}C NMR ($CDCl_3$) δ 133.1, 129.2, 128.5, 127.3, 126.2, 117.2, 113.8, 112.9. Anal. Calcd for $C_{22}H_{18}Cl_2Zr$: C, 59.45; H, 4.08. Found: C, 59.13: H, 3.85.

Dichloro(η^5-cylcopentadienyl)[η^5-1,2,4-bis(pentafluorophenyl)cyclopentadienyl]-zirconium(IV) (31). A mixture of $CpZrCl_3$(DME) (0.138 g, 0.391 mmol), **4Na (**0.222 g, 0.379 mmol), and toluene (25 mL) was stirred at room temperature for 20 h. The reaction mixture was subsequently filtered and the toluene was stripped from the filtrate. The crude product was washed and filtered with 15 mL of cold hexane to yield 0.132 g of tan solid (0.167 mmol, 44 %). An analytically pure sample was obtained by crystallization from a toluene/hexane mixture. ^{1}H NMR ($CDCl_3$) δ 7.35 (s, 2 H), 6.42 (s, 5 H). ^{19}F NMR ($CDCl_3$) δ -134.98 (d, $^{3}J_{FF}$ = 19 Hz, 4 F), -138.96 (d, $^{3}J_{FF}$ = 18 Hz, 2 F), -151.77 (tt, $^{3}J_{FF}$ = 21 Hz, $^{4}J_{FF}$ = 2.8 Hz, 2 F), -152.46 (tt, $^{3}J_{FF}$ = 21

Hz, $^{4}J_{FF}$ = 3.0 Hz, 1 F), -160.50 (m, 2 F), -160.93 (m, 4 F). The thermal instability of **31** prevented us from obtaining a satisfactory elemental analysis.

Works Cited

1. Togni, A.; Halterman, R. L., ed. *Metallocenes: Synthesis, Reactivity, Applications*; Wiley-VCH: New York, 1998.
2. Long, N. J. *Metallocenes*; Blackwell Science Ltd: Oxford, 1998.
3. Jutzi, P.; Burford, N. *Chem. Rev.* **1999**, *99*, 969.
4. Gassman, P. G.; Winter, C. H. *Organometallics* **1991**, *10*, 1592.
5. Ernst, R. D.; Kennelly, W. J.; Day, C. S.; Day, V. W.; Marks, T. J. *J. Am. Chem. Soc.* **1979**, *101*, 2656.
6. Manriquez, J. M.; Fagan, P. J.; Marks, T. J. *J. Am. Chem. Soc.* **1978**, *100*, 3939.
7. Bickley, D. G.; Hao, N.; Bougeard, P.; Sayer, B. G.; Burns, R. C.; McGlinchey, M. J. *J. Organomet. Chem.* **1983**, *246*, 257.
8. Manriquez, J. M.; McAlister, D. R.; Sanner, R. D.; Bercaw, J. E. *J. Am. Chem. Soc.* **1976**, *98*, 6733.
9. Erker, G. *Pure Appl. Chem.* **1992**, *64*, 393.
10. Gassman, P. G.; Deck, P. A.; Winter, C. H.; Dobbs, D. A.; Cao, D. H. *Organometallics* **1992**, *11*, 959.
11. Parsons, E. J.; Gassman, P. G. *J. Coord. Chem.* **1995**, *35*, 41.
12. Wakatsuki, Y.; Yamazaki, H.; Kobayashi, T.; Sugawara, Y. *Organometallics* **1987**, *6*, 1191.
13. Graham, P. B.; Rausch, M. D.; Taschler, K.; von Philipsborn, W. *Organometallics* **1991**, *10*, 3049.
14. Blais, M. S.; Rausch, M. D. *Organometallics* **1994**, *13*, 3557.
15. Ryan, M. F.; Siedle, A. R.; Burk, M. J.; Richardson, D. E. *Organometallics* **1992**, *11*, 4231.
16. Finch, W. C.; Anslyn, E. V.; Grubbs, R. H. *J. Am. Chem. Soc.* **1988**, *110*, 2406.
17. Evans, S.; Green, M. L. H.; Jewitt, B.; Orchard, A. F.; Pygall, C. F. *J. Chem. Soc., Faraday Trans. 2* **1972**, 1847.
18. Richardson, D. E.; Ryan, M. F.; Geiger, W. E.; Chin, T. T.; Hughes, R. P.; Curnow, O. J. *Organometallics* **1993**, *12*, 613.
19. Langmaier, J.; Samec, Z.; Varga, V.; Horacek, M.; Mach, K. *J. Organomet. Chem.* **1999**, *579*, 348.
20. Langmaier, J.; Samec, Z.; Varga, V.; Horacek, M.; Choukroun, R.; Mach, K. *J. Organomet. Chem.* **1999**, *584*, 323.

21. Richardson, D. E.; Lang, L.; Eyler, J. R.; Kircus, S. R.; Zheng, X.; Morse, C. A.; Hughes, R. P. *Organometallics* **1997**, *16*, 149.
22. Richardson, D. E.; Ryan, M. F.; Khan, M. N. I.; Maxwell, K. A. *J. Am. Chem. Soc.* **1992**, *114*, 10482.
23. Bönnemann, H.; Brijoux, W.; Brinkmann, R.; Meurers, W.; Mynott, R. *J. Organomet. Chem.* **1984**, *272*, 231.
24. Hoch, M.; Duch, A.; Rehder, D. *Inorg. Chem.* **1986**, *25*, 2907.
25. Meier, E. J. M.; Kozminski, W.; Linden, A.; Lustenberger, P.; von Philipsborn, W. *Organometallics* **1996**, *15*, 2469.
26. Bönnemann, H. *Angew. Chem., Int. Ed. Engl.* **1985**, *24*, 248.
27. Buhl, M.; Hopp, G.; von Philipsborn, W.; Beck, S.; Prosenc, M. H.; Rief, U.; Brintzinger, H. H. *Organometallics* **1996**, *15*, 778.
28. Koller, M.; von Philipsborn, W. *Organometallics* **1992**, *11*, 467.
29. Schuster-Woldan, H. G.; Basolo, F. *J. Am. Chem. Soc.* **1966**, *88*, 1657.
30. Rerek, M. E.; Basolo, F. *J. Am. Chem. Soc.* **1984**, *106*, 5908.
31. Cheong, M.; Basolo, F. *Organometallics* **1988**, *7*, 2041.
32. Kakkar, A. K.; Taylor, N. J.; Marder, T. B.; Shen, J. K.; Hallinan, N.; Basolo, F. *Inorg. Chim. Acta* **1992**, *198-200*, 219.
33. Burger, B. J.; Santarsiero, B. D.; Trimmer, M. S.; Bercaw, J. E. *J. Am. Chem. Soc.* **1988**, *110*, 3134.
34. Hammond, G. S. *J. Am. Chem. Soc.* **1955**, *77*, 334.
35. Arthurs, M. A.; Nelson, S. M. *J. Coord. Chem.* **1983**, *13*, 29.
36. Wakatsuki, Y.; Yamazaki, H. *Bull. Chem. Soc. Jpn.* **1985**, *58*, 2715.
37. Diversi, P.; Ingrosso, G.; Lucherini, A.; Vanacore, D. *J. Mol. Cat.* **1987**, *41*, 261.
38. Diversi, P.; Ermini, L.; Ingrosso, G.; Lucherini, A. *J. Organomet. Chem.* **1993**, *447*, 291.
39. Garrett, C. E.; Fu, G. C. *J. Org. Chem.* **1998**, *63*, 1370.
40. Brinkman, J. A.; Nguyen, T. T.; Sowa, J. R. *Org. Lett.* **2000**, *2*, 981.
41. Costa, M.; Dias, F. S.; Chiusoli, G. P.; Gazzola, G. L. *J. Organomet. Chem.* **1995**, *488*, 47.
42. Möhring, P. C.; Coville, N. J. *J. Organomet. Chem.* **1994**, *479*, 1.
43. Alt, H. G.; Köppl, A. *Chem. Rev.* **2000**, *100*, 1205.

44. Palmer, G. T.; Basolo, F.; Larence, B. K.; Rausch, M. D. *J. Am. Chem. Soc.* **1986**, *108*, 4417.
45. Quindt, V.; Saurenz, D.; Schmitt, O.; Schar, M.; Dezember, T.; Wolmershauser, G.; Sitzmann, H. *J. Organomet. Chem.* **1999**, *579*, 376.
46. Ivchenko, N. B.; Ivchenko, P. V.; Nifant'ev, I. E. *Rus. J. Org. Chem.* **2000**, *36*, 609.
47. Rausch, M. D.; Hart, W. P.; Atwood, J. L.; Zaworotko, M. J. *J. Organomet. Chem.* **1980**, *197*, 225.
48. Nesmeyanov, A. N.; Perevalova, E. G.; Yur'eva, E. P. *Chem. Ber.* **1960**, *93*, 2729.
49. Webster, O. W. *J. Am. Chem. Soc.* **1966**, *88*, 3046.
50. Stahl, K. P.; Boche, G.; Massa, W. *J. Organomet. Chem.* **1984**, *277*, 113.
51. Cais, M.; Narkis, N. *J. Organomet. Chem.* **1965**, *3*, 269.
52. Conway, B. G.; Rausch, M. D. *Organometallics* **1985**, *4*, 688.
53. Laganis, E. D.; Lemal, D. M. *J. Am. Chem. Soc.* **1980**, *102*, 6633.
54. Gassman, P. G.; Winter, C. H. *J. Am. Chem. Soc.* **1986**, *108*, 4228.
55. Gassman, P. G.; Mickelson, J. W.; Sowa, J. R. *J. Am. Chem. Soc.* **1992**, *114*, 6942.
56. Hughes, R. P.; Trujillo, H. A. *Organometallics* **1996**, *15*, 286.
57. Rogers, R. D.; Atwood, J. L.; Rausch, M. D.; Macomber, D. W.; Hart, W. P. *J. Organomet. Chem.* **1982**, *238*, 79.
58. Jones, S. S.; Rausch, M. D.; Bitterwolf, T. E. *J. Organomet. Chem.* **1990**, *396*, 279.
59. Rausch, M. D.; Fischer, E. O.; Grubert, H. *J. Am. Chem. Soc.* **1960**, *82*, 76.
60. Bruce, M. I.; Skelton, B. W.; Wallis, R. C.; Walton, J. K.; White, A. H.; Williams, M. L. *J. Chem. Soc., Chem. Comm.* **1981**, 428.
61. Paprott, G.; Seppelt, K. *J. Am. Chem. Soc.* **1984**, *106*, 4060.
62. Hedberg, F. L.; Rosenberg, H. *J. Am. Chem. Soc.* **1970**, *92*, 3239.
63. Hedberg, F. L.; Rosenberg, H. *J. Organomet. Chem.* **1971**, *28*, C14.
64. Hedberg, F. L.; Rosenberg, H. *J. Am. Chem. Soc.* **1973**, *95*, 870.
65. Curnow, O. J.; Hughes, R. P. *J. Am. Chem. Soc.* **1992**, *114*, 5895.
66. Hughes, R. P.; Zheng, X.; Ostrander, R. L.; Rheingold, A. L. *Organometallics* **1994**, *13*, 1567.
67. Hughes, R. P.; Zheng, X.; Morse, C. A.; Curnow, O. J.; Lomprey, J. R.; Rheingold, A. L.; Yap, G. P. A. *Organometallics* **1998**, *17*, 457.

68. Day, V. W.; Stults, B. R.; Reimer, K. J.; Shaver, A. *J. Am. Chem. Soc.* **1974**, *96*, 4008.
69. Reimer, K. J.; Shaver, A. *Inorg. Chem.* **1975**, *14*, 2707.
70. Reimer, K. J.; Shaver, A. *J. Organomet. Chem.* **1975**, *93*, 239.
71. Lei, Y. X.; Cerioni, G.; Rappoport, Z. *J. Org. Chem.* **2000**, *65*, 4028.
72. Baschky, M. C.; Sowa, J. R.; Gassman, P. G.; Kass, S. R. *J. Chem. Soc., Perkin Trans. 2* **1996**, 213.
73. Boev, V. I.; Dombrovskii, A. V. *Zh. Obshch. Khim.* **1977**, *47*, 727.
74. Winter, C. H.; Han, Y. H.; Heeg, M. J. *Organometallics* **1992**, *11*, 3169.
75. Winter, C. H.; Han, Y. H.; Ostrander, R. L.; Rheingold, A. L. *Angew. Chem., Int. Ed. Engl.* **1993**, *32*, 1161.
76. Bunz, U. H. F.; Enkelmann, V.; Rader, J. *Organometallics* **1993**, *12*, 4745.
77. Han, Y. H.; Heeg, M. J.; Winter, C. H. *Organometallics* **1994**, *13*, 3009.
78. Kur, S. A.; Heeg, M. J.; Winter, C. H. *Organometallics* **1994**, *13*, 1865.
79. Bruce, M. I.; Walton, J. K.; Skelton, B. W.; White, A. H. *J. Chem. Soc., Dalton Trans.* **1982**, 2227.
80. Bruce, M. I.; Walton, J. K.; Williams, M. L.; Patrick, J. M.; Skelton, B. W.; White, A. H. *J. Chem. Soc., Dalton Trans.* **1983**, 815.
81. Bruce, M. I.; White, A. H. *Aust. J. Chem.* **1990**, *43*, 949.
82. Bruce, M. I.; Humphrey, P. A.; Skelton, B. W.; White, A. H. *J. Organomet. Chem.* **1989**, *361*, 369.
83. Christopher, R. E.; Venanzi, L. M. *Inorg. Chim. Acta* **1973**, *7*, 489.
84. Rausch, M. D.; Lewison, J. F.; Hart, W. P. *J. Organomet. Chem.* **1988**, *358*, 161.
85. Wahren, R. *J. Organomet. Chem.* **1973**, *57*, 415.
86. Lindsell, W. E. *J. Chem. Soc., Dalton Trans.* **1975**, 2548.
87. Roloff, A.; Meier, K.; Riediker, M. *Pure Appl. Chem.* **1986**, *58*, 1267.
88. Klingert, B.; Roloff, A.; Urwyler, B.; Wirz, J. *Helv. Chim. Acta* **1988**, *71*, 1858.
89. Imrie, C.; Nonhebel, D. C.; Pauson, P. L. *J. Chem. Soc., Perkin Trans. 1* **1991**, 2555.
90. Ivushkin, V. A.; Sazonov, P. K.; Artamkina, G. A.; Beletskaya, I. P. *Rus. J. Org. Chem.* **1999**, *35*, 1640.
91. Deck, P. A.; Jackson, W. F.; Fronczek, F. R. *Organometallics* **1996**, *15*, 5287.
92. Maldanis, R. J.; Chien, J. C. W.; Rausch, M. D. *J. Organomet. Chem.* **2000**, *599*, 107.

93. Thornberry, M. P.; Slebodnick, C.; Deck, P. A.; Fronczek, F. R. *Organometallics* **2000**, *19*, 5352.
94. Deck, P. A.; Fronczek, F. R. *Organometallics* **2000**, *19*, 327.
95. Deck, P. A.; Lane, M. J.; Montgomery, J. L.; Slebodnick, C. *Organometallics* **2000**, *19*, 1013.
96. Thornberry, M. P.; Slebodnick, C.; Deck, P. A.; Fronczek, F. R. *Organometallics* **2001**, *20*, 920.
97. March, F. C.; Ferguson, G.; Lloyd, D. *J. Chem. Soc., Dalton Trans.* **1975**, 1377.
98. Evrard, G.; Piret, P.; Germain, G.; Van Meerssche, M. *Acta Crystallogr., Sect. B* **1971**, *B27*, 661.
99. Field, L. D.; Hambley, T. W.; Lindall, C. M.; Masters, A. F. *Inorg. Chem.* **1992**, *31*, 2366.
100. Blanchard, M. D.; Hughes, R. P.; Concolino, T. E.; Rheingold, A. L. *Chem. Mater.* **2000**, *12*, 1604.
101. Clare, P.; Sowerby, D. B.; Haiduc, I. *J. Organomet. Chem.* **1986**, *310*, 161.
102. Sommazzi, A.; Masi, F.; Borsotti, G.; Proto, A.; Santi, R. *Eur. Pat. Appl.* **2000**, 30 pp.
103. Cram, D. J. *Fundamentals of Carbanion Chemistry*; Academic Press: New York, 1965.
104. Reutov, O. A.; Beletskaya, I. P.; Butin, K. P. *CH-Acids*; Pergamon Press: Oxford, 1978.
105. Streitwieser, A.; Juaristi, E.; Nebenzahl, L. L. *Comprehensive Carbanion Chemistry*; Elsevier Scientific Publishing Company: New York, 1980.
106. Okuyama, T.; Ikenovchi, Y.; Fueno, T. *J. Am. Chem. Soc.* **1978**, *100*, 6162.
107. Bordwell, F. G.; Bausch, M. J. *J. Am. Chem. Soc.* **1983**, *105*, 6188.
108. Streitwieser, A.; Caldwell, R. A.; Granger, M. R. *J. Am. Chem. Soc.* **1964**, *86*, 3578.
109. Dessy, R. E.; Okuzumi, Y.; Chen, A. *J. Am. Chem. Soc.* **1962**, *84*, 2899.
110. McEwen, W. K. *J. Am. Chem. Soc.* **1936**, *58*, 1124.
111. Applequist, D. E.; O'Brien, D. F. *J. Am. Chem. Soc.* **1963**, *85*, 743.
112. Salinger, R. M.; Dessy, R. E. *Tetrahedron Lett.* **1963**, *11*, 729.
113. Breslow, R.; Washburn, W. *J. Am. Chem. Soc.* **1970**, *92*, 427.
114. Schaeffer, D. J. *J. Chem. Soc., Chem. Comm.* **1970**, 1043.
115. Streitwieser, A.; Nebenzahl, L. L. *J. Am. Chem. Soc.* **1976**, *98*, 2188.
116. Bordwell, F. G.; Drucker, G. E.; Fried, H. E. *J. Org. Chem.* **1981**, *46*, 632.
117. Bordwell, F. G. *Acc. Chem. Res.* **1988**, *21*, 456.

118. Jaun, B.; Schwarz, J.; Breslow, R. *J. Am. Chem. Soc.* **1980**, *102*, 5741.
119. Fraser, R. R.; Bresse, M.; Mansour, T. S. *J. Chem. Soc., Chem. Comm.* **1983**, 620.
120. Fraser, R. R.; Bresse, M.; Offermanns, N. C.; Houk, K. N.; Rondan, N. G. *Can. J. Chem.* **1983**, *61*, 2729.
121. Fraser, R. R.; Bresse, M.; Mansour, T. S. *J. Am. Chem. Soc.* **1983**, *105*, 7790.
122. Miah, M. A. J.; Fraser, R. R. *Indian J. Chem.* **1996**, *35B*, 71.
123. Fraser, R. R.; Mansour, T. S.; Savard, S. *J. Org. Chem.* **1985**, *50*, 3232.
124. Fraser, R. R.; Mansour, T. S. *J. Org. Chem.* **1984**, *49*, 3442.
125. Fraser, R. R.; Mansour, T. S.; Savard, S. *Can. J. Chem.* **1985**, *63*, 3505.
126. Miah, M. A. J.; Fraser, R. R. *Indian J. Chem.* **1990**, *29A*, 588.
127. Taft, R. W.; Levins, P. L. *Analytical Chem.* **1962**, *34*, 436.
128. Boiadjiev, S. E.; Lightner, D. A. *J. Phys. Org. Chem.* **1999**, *12*, 751.
129. Streitwieser, A.; Wang, D. Z.; Stratakis, M.; Facchetti, A.; Gareyev, R.; Abbotto, A.; Krom, J. A.; Kilway, K. V. *Can. J. Chem.* **1998**, *76*, 765.
130. Grutzner, J. B.; Lawlor, J. M.; Jackman, L. M. *J. Am. Chem. Soc.* **1972**, *94*, 2306.
131. Krom, J. A.; Petty, J. T.; Streitwieser, A. *J. Am. Chem. Soc.* **1993**, *115*, 8024.
132. Kaufman, M. J.; Gronert, S.; Streitwieser, A. *J. Am. Chem. Soc.* **1988**, *110*, 2829.
133. Streitwieser, A.; Ciuffarin, E.; Hammons, J. H. *J. Am. Chem. Soc.* **1967**, *89*, 63.
134. Deck, P. A.; Warren, A. D.; Thornberry, M. P. In *220th National Meeting of the American Chemical Society,*: Washington D.C., August 20-24, 2000, Abstract INOR-172.
135. Lokshin, B. V.; Rusach, E. B.; Valueva, Z. P.; Ginzburg, A. G.; Kolobova, N. E. *J. Organomet. Chem.* **1975**, *102*, 535.
136. Lyatifov, I. R.; Gulieva, G. I.; Babin, V. N.; Materikova, R. B.; Petrovskii, P. V.; Fedin, E. I. *J. Organomet. Chem.* **1987**, *326*, 93.
137. du Plooy, K. E.; Ford, T. A.; Coville, N. J. *J. Organomet. Chem.* **1992**, *441*, 285.
138. du Plooy, K. E.; du Toit, J.; Levendis, D. C.; Coville, N. J. *J. Organomet. Chem.* **1996**, *508*, 231.
139. Priebsch, W.; Hoch, M.; Rehder, D. *Chem. Ber.* **1988**, *121*, 1971.
140. Young, K. M.; Wrighton, M. S. *Organometallics* **1989**, *8*, 1063.
141. Khotsyanova, T. L.; Kuznetsov, S. I.; Bryukhova, E. V.; Makarov, Y. V. *J. Organomet. Chem.* **1975**, *88*, 351.

142. Fitzpatrick, P. J.; LePage, Y.; Butler, I. S. *Acta Crystallogr.* **1981**, *B37*, 1052.
143. Fitzpatrick, P. J.; Page, Y. L.; Sedman, J.; Butler, I. S. *Inorg. Chem.* **1981**, *20*, 2852.
144. Rausch, M. D.; Tsai, W.; Chambers, J. W.; Rogers, R. D.; Alt, H. G. *Organometallics* **1989**, *8*, 816.
145. Cowie, J.; Hamilton, E. J. M.; Laurie, J. C. V.; Welch, A. J. *J. Organomet. Chem.* **1990**, *394*, 1.
146. Raptis, K.; Dornberger, E.; Kanellakopulos, B.; Nuber, B.; Ziegler, M. L. *J. Organomet. Chem.* **1991**, *408*, 61.
147. Huang, Y.; Butler, I. S.; Gilson, D. F. R. *Inorg. Chem.* **1992**, *31*, 4762.
148. Sünkel, K.; Stramm, C. *Inorg. Chim. Acta* **2000**, *298*, 33.
149. Macomber, D. W.; Hart, W. P.; Rausch, M. D. *Adv. Organomet. Chem.* **1982**, *21*, 1.
150. Coville, N. J.; du Plooy, K. E.; Pickl, W. *Coord. Chem. Rev.* **1992**, *116*, 1.
151. Janiak, C.; Schumann, H. *Adv. Organomet. Chem.* **1991**, *33*, 291.
152. Okuda, J. *Top. Curr. Chem.* **1991**, *160*, 97.
153. Mason, J. G.; Rosenblum, M. *J. Am. Chem. Soc.* **1960**, *82*, 4206.
154. Benson, R. E.; Lindssay, R. V. *J. Am. Chem. Soc.* **1957**, *79*, 5471.
155. Nesmeyanov, A. N.; Sazonova, V. A.; Drozd, V. N. *Tetrahedron Lett.* **1959**, *17*, 13.
156. Kuwana, T.; Bublitz, D. E.; Hoh, G. L. K. *J. Am. Chem. Soc.* **1960**, *82*, 5811.
157. Hoh, G. L. K.; McEwen, W. E.; Kleinberg, J. *J. Am. Chem. Soc.* **1961**, *83*, 3949.
158. Little, W. F.; Feilley, C. N.; Johnson, J. D.; Sanders, A. P. *J. Am. Chem. Soc.* **1964**, *86*, 1382.
159. Little, W. F.; Reilley, C. N.; Johnson, J. D.; Lynn, K. N.; Sanders, A. P. *J. Am. Chem. Soc.* **1964**, *86*, 1376.
160. Hall, D. W.; Russell, C. D. *J. Am. Chem. Soc.* **1967**, *89*, 2316.
161. Sabbatini, M. M.; Cesarotti, E. *Inorg. Chim. Acta* **1977**, *24*, L9.
162. Okuda, J.; Albach, R. W.; Herdtweck, E. *Polyhedron* **1991**, *10*, 1741.
163. Burkey, D. J.; Hays, M. L.; Duderstadt, R. E.; Hanusa, T. P. *Organometallics* **1997**, *16*, 1465.
164. Freyberg, D. P.; Robbins, J. L.; Raymond, K. N.; Smart, J. C. *J. Am. Chem. Soc.* **1979**, *101*, 892.

165. Castellani, M. P.; Geib, S. J.; Rheingold, A. L.; Trogler, W. C. *Organometallics* **1987**, *6*, 1703.
166. Luke, W.; Streitwieser, A. *J. Am. Chem. Soc.* **1981**, *103*, 3241.
167. Abel, E. W.; Long, N. J.; Orrell, K. G.; Osborne, A. G.; Šik, V. *J. Organomet. Chem.* **1991**, *403*, 195.
168. Holm, C. H.; Ibers, J. A. *Journal of Chem. Phys.* **1959**, *30*, 885.
169. Mulay, L. N.; Attalla, A. *J. Am. Chem. Soc.* **1963**, *85*, 702.
170. Makova, M. K.; Leonova, E. V.; Karimov, Y. S.; Kochetkova, N. S. *J. Organomet. Chem.* **1973**, *55*, 185.
171. Okuda, J.; Herdtweck, E. *J. Organomet. Chem.* **1989**, *373*, 99.
172. Gloaguen, B.; Astruc, D. *J. Am. Chem. Soc.* **1990**, *112*, 4607.
173. Castellani, M. P.; Wright, J. M.; Geib, S. J.; Rheingold, A. L.; Trogler, W. C. *Organometallics* **1986**, *5*, 1116.
174. Britton, W. E.; Kashyap, R.; El-Hashash, M.; El-Kady, M. *Organometallics* **1986**, *5*, 1029.
175. McDaniel, D. H.; Brown, H. C. *J. Org. Chem.* **1958**, *23*, 420.
176. Sheppard, W. A. *J. Am. Chem. Soc.* **1970**, *92*, 5419.
177. Bünder, W.; Weiss, E. *J. Organomet. Chem.* **1975**, *92*, 65.
178. Seiler, P.; Dunitz, J. D. *Acta Crystallogr.* **1979**, *B35*, 1068.
179. Haaland, A. *Acc. Chem. Res.* **1979**, *12*, 415.
180. Okuda, J.; Herdtweck, E. *Chem. Ber.* **1988**, *121*, 1899.
181. Burman, J. A.; Hays, M. L.; Burkey, D. J.; Tanner, P. S.; Hanusa, T. P. *J. Organomet. Chem.* **1994**, *479*, 135.
182. Okuda, J. *Chem. Ber* **1989**, *122*, 1075.
183. Sitzmann, H. *J. Organomet. Chem.* **1988**, *354*, 203.
184. Natta, G.; Pino, P.; Mazzanti, G.; Giannini, U. *J. Am. Chem. Soc.* **1957**, *79*, 2975.
185. Natta, G.; Pino, P.; Mazzanti, G.; Giannini, U.; Mantica, E.; Peraldo, M. *J. Poly. Sci.* **1957**, *26*, 120.
186. Breslow, D. S.; Newburg, N. R. *J. Am. Chem. Soc.* **1957**, *79*, 5072.
187. Reichert, K. H.; Meyer, K. R. *Makromol. Chem.* **1973**, *169*, 163.
188. Long, W. P.; Breslow, D. S. *Liebigs Ann. Chem.* **1975**, 463.

189. Andresen, A.; Cordes, H. G.; Herwig, J.; Kaminsky, W. *Angew. Chem., Int. Ed. Engl.* **1976**, *15*, 630.
190. Sinn, H.; Kaminsky, W. *Adv. Organomet. Chem.* **1980**, *18*, 99.
191. Sinn, H.; Kaminsky, W.; Vollmer, H. J.; Woldt, R. *Angew. Chem., Int. Ed. Engl.* **1980**, *19*, 390.
192. Kaminsky, W.; Miri, M.; Sinn, H.; Woldt, R. *Makromol. Chem., Rapid Commun.* **1983**, *4*, 417.
193. Kaminsky, W.; Külper, K.; Niedoba, S. *Makromol. Chem., Macromol. Symp.* **1986**, *3*, 377.
194. Ewen, J. A. In *Catalytic Polymerization of Olefins*; Keii, T., Soga, K., Eds.; Elsevier: New York, 1986; pp 271-292.
195. Brintzinger, H. H.; Fischer, D.; Mülhaupt, R.; Rieger, B.; Waymouth, R. M. *Angew. Chem., Int. Ed. Engl.* **1995**, *34*, 1143.
196. Kaminsky, W.; Arndt, M. In *Applied Homogenous Catalysis with Organometallic Compounds*; Cornils, B., Herrmann, W. A., Eds.; VCH: New York, 1996; Vol. 1, pp 220-236.
197. Kaminsky, W.; Arndt, M. *Adv. Poly. Sci.* **1997**, *127*, 143.
198. Soga, K.; Shiono, k. T. *Prog. Poly. Sci.* **1997**, *22*, 1503.
199. Janiak, C. In *Metallocenes*; Togni, A., Halterman, R. L., Eds.; Wiley-VCH: New York, 1998; Vol. 2, pp 547-623.
200. Kaminsky, W. *J. Chem. Soc., Dalton Trans.* **1998**, 1413.
201. Hlatky, G. G. *Coord. Chem. Rev.* **1999**, *181*, 243.
202. Hlatky, G. G. *Coord. Chem. Rev.* **2000**, *199*, 235.
203. Rappé, A. K.; Skiff, W. M.; Casewit, C. J. *Chem. Rev.* **2000**, *100*, 1435.
204. Möhring, P. C.; Coville, N. J. *J. Mol. Cat.* **1992**, *77*, 41.
205. Ewen, J. A. *Stud. Surf. Sci. & Catal.* **1986**, *25*, 271.
206. Chien, J. C. W.; Razavi, A. *J. Polym. Sci. Part A: Polym. Chem.* **1988**, *26*, 2369.
207. Chien, J. C. W.; Wang, B. P. *J. Polym. Sci. Part A: Polym. Chem.* **1990**, *28*, 15.
208. Piccolrovazzi, N.; Pino, P.; Consiglio, G.; Sironi, A.; Moret, M. *Organometallics* **1990**, *9*, 3098.
209. Lee, I. M.; Gauthier, W. J.; Ball, J. M.; Iyengar, B.; Collins, S. *Organometallics* **1992**, *11*, 2115.

210. Bondi, A. *J. Phys. Chem.* **1964**, *68*, 441.
211. Schmid, M. A.; Alt, H. G.; Milius, W. *J. Organomet. Chem.* **1995**, *501*, 101.
212. Wigum, H.; Tangen, L.; Støvneng, J. A.; Rytter, E. *J. Polym. Sci. Part A: Polym. Chem.* **2000**, *38*, 3161.
213. Karol, F. J.; Kao, S. C.; Wasserman, E. P.; Brady, R. C. *New J. Chem.* **1997**, *21*, 797.
214. Karol, F. J.; Kao, S. C. *New J. Chem.* **1994**, *18*, 97.
215. Möhring, P. C.; Coville, N. J. *J. Mol. Catal. A: Chem.* **1995**, *96*, 181.
216. Böhme, U.; Thiele, K. H. *Z. Anorg. Allg. Chem.* **1994**, *620*, 1455.
217. Nekhaeva, L. A.; Bondarenko, G. N.; Rykov, S. V.; Nekhaev, A. I.; Krentsel, B. A.; Mar'in, V. P.; Vyshinskaya, L. I.; Khrapova, I. M.; Polonskii, A. V.; Korneev, N. N. *J. Organomet. Chem.* **1991**, *406*, 139.
218. Bravaya, N. M.; Strelets, V. V.; Dzhabieva, Z. M.; Babkina, O. N.; Maryin, V. P. *Russ. Chem. Bull.* **1998**, *47*, 1491.
219. Beck, S.; Brintzinger, H. H. *Inorg. Chim. Acta* **1998**, *270*, 376.
220. Conti, G.; Arribas, G.; Altomare, A.; Mendez, B.; Ciardelli, G. *Z. Naturforsch.* **1995**, *50b*, 411.
221. Lee, B. Y.; Han, J. W.; Chung, Y. K.; Lee, S. W. *J. Organomet. Chem.* **1999**, *587*, 181.
222. Zhang, F.; Mu, Y.; Zhao, L.; Zhang, Y.; Bu, W.; Chen, C.; Zhai, H.; Hong, H. *J. Organomet. Chem.* **2000**, *613*, 68.
223. Zhang, F.; Mu, Y.; Wang, J.; Shi, Z.; Bu, W.; Hu, S.; Zhang, Y.; Feng, S. *Polyhedron* **2000**, *19*, 1941.
224. Farnum, D. G.; Mostashari, A.; Hagedorn III, A. A. *J. Org. Chem.* **1971**, *36*, 698.
225. Howie, R. A.; McQuillan, G. P.; Thompson, D. W.; Lock, G. A. *J. Organomet. Chem.* **1986**, *303*, 213.
226. Corey, J. Y.; Zhu, X. H.; Brammer, L.; Rath, N. P. *Acta Cryst.* **1995**, *C51*, 565.
227. Greene, D. L.; Villalta, O. A.; Macias, D. M.; Gonzalez, A.; Tikkanen, W.; Schick, B.; Kantardjieff, K. *Inorganic Chemistry Communications* **1999**, *2*, 311.
228. Kimura, K.; Takaishi, K.; Matsukawa, T.; Yoshimura, T.; Yamazaki, H. *Chem. Lett.* **1998**, 571.
229. Kamigaito, M.; Lal, T. K.; Waymouth, R. M. *J. Polym. Sci. Part A: Polym. Chem.* **2000**, *38*, 4649.

230. Hsieh, E. T.; Randall, J. C. *Macromolecules* **1982**, *15*, 1402.
231. Galland, G. B.; Quijada, P.; Mauler, R. S.; Menezes, S. C. *Macromol. Rapid Commun.* **1996**, *17*, 607.
232. Krauss, V. W.; Gestrich, W. *Chem-Tech* **1977**, *6*, 513.
233. Böhm, L. L. In *Applied Homogenous Catalysis with Organometallic Compounds*; Cornils, B., Herrmann, W. A., Eds.; VCH: New York, 1996; Vol. 1, pp 236-245.
234. Quijada, R.; Dupont, J.; LMiranda, M. S. L.; Scipioni, R. B.; Galland, G. B. *Macromol. Chem. Phys.* **1995**, *196*, 3991.

Vita

Matthew P. Thornberry

Matthew P. Thornberry was born August 14, 1975 to Gary and Elsie Thornberry in Norfolk, Virginia. He earned a B.S. degree in chemistry at James Madison University (1993-1997) in Harrisonburg, Virginia. While there, he participated in undergraduate research under the guidance of Professor Donna Amenta. In the summer of 1995, he conducted undergraduate research at the University of Florida under the guidance of Professor Russell Drago. He began graduate school at Virginia Polytechnic Institute and State University in the summer of 1997 with Professor Paul Deck as his research advisor. On August 3, 2001 he received a Ph.D. in Chemistry.